UNIVERSIDADE DE LISBOA
FACULDADE DE CIÊNCIAS
DEPARTAMENTO DE FÍSICA

Cubic Galileon theory in the Effective Field Theory formalism: a cosmological study

Inês Sarranito Albuquerque

Mestrado em Física
Especialização em Astrofísica e Cosmologia

Dissertação orientada por:
Doutora Noemi Frusciante
e Doutor Nelson Nunes

2019

Acknowledgments

I would like to take this opportunity to thank everyone whose counsel and support have been indispensable throughout this journey. First and foremost, to my supervisors, Doutora Noemi Frusciante and Doutor Nelson Nunes, for introducing me to the world of scientific research, for all the guidance and helpful discussions and, above all, for never giving up on me. To Noemi, for all the dedication, never-ending patience and fundamental support along the entire project. A huge thank you for always keeping your door open, being there to calm down when needed and for all the fun and interesting conversations. To Nelson, for stealing me away from particle physics, for pushing me to do new and challenging things and for the all around good mood. I am very grateful for everything that I learned from both of you.

I also want to express my gratitude to Doctor Shinji Tsujikawa for the helpful discussions and contributions to formulation of the Scaling Cubic Model.

A very special thank you goes out to my college family, for standing beside me from the beginning and for sharing with me all the highs and lows of academic life. To Rui, Laura, Rafael, Gonçalo, João, Zé, Ana and Daniela for all the memorable moments, inspiring conversations and crazy games that have made the entire experience more than worth it. But above all, for your endless support, helping hand and loving care throughout the years. Your friendship means more to me than I can express.

I would also like to thank my crew back home: Mónica, Daniela, Sérgio, Tiago, Nuno, Rico, Rua e Silva. You are living proof that we can find family in the craziest way possible. Thank you for helping me keep going, for your creative support, for all the late-night hang outs and some of the best laughs of my life. You are the best worst influences that anyone could hope for. I owe you my sanity so, from the bottom of my heart, thank you.

To my best friend Ruben, for being a constant in my life for more than 12 years. Thank you for always being by my side, even if you can be terribly annoying sometimes. Here's to a lot more than another 12 years!

To Rui, in particular, for being a true partner, nerd companion and huge supporter. One can only be so lucky to share this journey with someone like you. Thank you for making me into a better person.

Finally, a heartfelt thank you to my family. Your unconditional love, undying loyalty and incredible faith in me has given me the strength to always put 100% of myself in everything I do. To my parents, in particular, for always being supportive of my choices and giving me the opportunity to complete my education. A very special thank you to my mum, who despite not understanding a single bit of what I was doing was always available to help in any way she could and cheer me up when needed. Your love means everything to me.

Resumo

A Cosmologia é a área de estudo dedicada à descrição do Universo como um todo, lidando com questões relacionadas com o seu início, composição e destino. Estes assuntos sempre foram do interesse humano. Todavia, quando em 1915 Einstein publicou a Teoria da Relatividade Geral (RG), a Cosmologia foi relançada, dando-se início a um período de maior precisão e produtividade dentro da área. A RG revolucionou a visão de gravidade vigente, apresentando uma descrição geométrica da interação gravítica onde a última é consequência direta da curvatura do espaço-tempo. O formalismo matemático desta teoria tem-se mostrado bem-sucedido na descrição do Universo, tanto a pequena como a grande escala, registando sucessos como a correta previsão do desvio do periélio de Mercúrio ou a previsão das recém-detetadas ondas gravitacionais. O rigor matemático oferecido pela RG, em conjunto com o sucesso continuado em testes observacionais, levaram ao seu estabelecimento como a teoria da gravitação em vigor, servindo até hoje de base à prática da Cosmologia.

No entanto, um dos maiores desafios tanto para a RG como para o Modelo Padrão da Física de Partículas viria a surgir em 1998, quando dados provenientes do estudo de supernovas de tipo Ia mostraram que o Universo está a expandir de forma acelerada. O problema reside no facto de nenhum tipo de matéria ou energia conhecida ou detetada até ao momento ser capaz de explicar esta aceleração. Dentro do formalismo da RG, a explicação mais simples para o fenómeno em questão passa pela introdução da constante cosmológica, Λ, para descrever uma componente de matéria/energia caracterizada por uma pressão negativa constante. Sabe-se ainda que esta componente de natureza desconhecida, genericamente considerada como uma forma de Energia Escura (EE), precisa de ser a mais abundante no Universo de modo a ajustar os dados observacionais. Adicionalmente, uma grande quantidade e variedade de observações apoia ainda a existência de um tipo de matéria que aparenta não absorver nem emitir radiação eletromagnética. Esta componente, consequentemente designada de Matéria Escura (ME), é ainda restringida observacionalmente a ser não relativista e de natureza não bariónica. Partículas de ME que se movem lentamente em comparação com a luz são designadas por Matéria Escura Fria (*Cold Dark Matter* - CDM).

Atualmente, as observações apontam para um Universo composto por 68.9% de EE e 31.1% de matéria de entre os quais 26.1% são de ME. Desta forma, as componentes padrão, nomeadamente a matéria bariónica e a radiação, contribuem apenas com cerca de 4.9% e 0.001%, sendo completamente dominadas pelo sector "escuro". De modo a explicar os dados disponíveis, o atual modelo padrão da Cosmologia baseia-se na RG para descrever um Universo com uma componente de EE descrita pela constante cosmológica, Λ, e uma componente de ME fria. Este é conhecido como o modelo ΛCDM.

Apesar de este continuar a ser o modelo que apresenta o melhor ajuste aos dados observacionais, foram-lhe já identificados vários problemas conceptuais. Na sua maioria, as falhas do atual modelo padrão estão relacionadas com a constante cosmológica. A falta de respostas satisfatórias para muitas destas questões levou à formulação de uma grande variedade de modelos alternativos para a expansão acelerada do Universo. Algumas destas propostas continuam a incluir uma componente de EE, podendo esta manter-se constante como no caso de Λ ou então variar no tempo. Por outro lado, existem propostas nas quais as leis que regem a interação gravítica são modificadas a grandes escalas. No primeiro caso as propostas são designadas como modelos de EE, já no segundo caso é comum falar-se em modelos de Gravitação Modificada

(GM).

Hoje em dia existe uma variedade e abundância de propostas alternativas para o fenómeno da aceleração cósmica. Tendo isto em conta, e considerando a atual possibilidade de aceder a novos dados observacionais e de melhor qualidade, tornou-se imperativo que os modelos existentes sejam testados de forma rigorosa na esperança de encontrar a melhor proposta possível. Para estudar um modelo ao nível de grandes escalas (> 100 Mpc) recorre-se à teoria de perturbações lineares. Nesta abordagem, começa-se por considerar e analisar um Universo globalmente homogéneo e isotrópico. Este serve depois de base sobre a qual se consideram pequenas perturbações, necessárias para compreender a formação de estrutura no Universo e o desenvolvimento das pequenas heterogeneidades observadas. O estudo da evolução de perturbações e a consideração de observáveis relacionados com a estrutura de grande escala têm provado ser essenciais na distinção entre modelos concorrentes que apresentem histórias de expansão semelhantes.

O desafio surge, no entanto, do facto de cada modelo ser, geralmente, descrito por um conjunto de equações e parâmetros específicos. Sendo à partida necessário um tratamento individual para cada proposta. De modo a agilizar e simplificar o processo de teste das propostas existentes, procurou-se encontrar um formalismo mais abrangente, sendo capaz de descrever diferentes modelos de EE/GM e que em simultâneo oferecesse uma forma mais prática de os investigar. Várias abordagens foram então desenvolvidas, de entre as quais se destaca a Teoria de Campo Efetivo (*Effective Field Theory* - EFT) por manter uma maior conexão com a teoria de gravitação subjacente. A EFT oferece um formalismo geral, ou seja, sem dependência de um modelo específico, que descreve a evolução de perturbações lineares em modelos que apresentem um único grau de liberdade escalar extra. Esta revela ser uma abordagem englobante uma vez que a maioria dos modelos de EE/GM propostos podem ser descritos como modificações da RG através da adição de um campo escalar extra. Dentro do formalismo da EFT, o comportamento tanto ao nível da história de expansão como ao nível das perturbações passa a ser descrito por um conjunto de coeficientes com dependência temporal, designados por funções EFT, que são introduzidos na formulação da ação que descreve a teoria. Esta construção permite que a EFT tenha uma aplicação dual. Por um lado, é possível investigar o efeito de ligar ou desligar um certo conjunto de coeficientes, sem selecionar nenhum modelo em particular. Por outro lado, é também possível estudar um modelo específico após encontrada a correspondência entre este e o formalismo da EFT, isto é, após serem encontradas as formas correspondentes das funções EFT.

Adicionalmente, é também comum recorrer a códigos Einstein-Boltzmann para resolver numericamente as equações que descrevem a evolução de perturbações. Este tipo de códigos podem ser construídos de forma particular para tratar um único modelo. No entanto, proceder desta maneira implica um enorme esforço de programação para conseguir cobrir um grande número de propostas. Assim sendo, o formalismo da EFT foi implementado no código público `CAMB` com o intuito de construir uma ferramenta numérica capaz de servir um grande número de modelos. Desta implementação resultou o código `EFTCAMB`, o qual pode ser usado para resolver as equações que regem a evolução de perturbações lineares em qualquer modelo que tenha sido previamente traduzido no formalismo da EFT. Desta forma, qualquer modelo que seja abrangido pela EFT pode ser estudado com recurso a um único código de acesso público.

O foco desta dissertação recai sobre um modelo específico de GM, o Galileão Cúbico de Escalamento (*Scaling Cubic Galileon* - SCG), no qual a interação gravítica descrita pela RG

é modificada em grandes escalas através da introdução de um campo escalar. Este modelo, em particular, apresenta uma característica peculiar: durante o período inicial da evolução do Universo, as densidades de energia do campo escalar e da matéria/radiação escalam uma com a outra. Este é um traço interessante pois oferece a possibilidade de aliviar o Problema da Coincidência Cósmica, um dos desafios teóricos que afetam o modelo padrão.

Nesta dissertação investigámos a fenomenologia do modelo SCG, explorando tanto a sua história de expansão como o seu impacto nos observáveis cosmológicos, avaliando a sua viabilidade enquanto descrição do Universo observado. Para tal, começámos por recorrer a ferramentas de análise dinâmica de modo a determinar a história de expansão do modelo, verificando que este é capaz de reproduzir uma época tardia de expansão acelerada. Procedemos depois à tradução do modelo SCG para o formalismo da EFT de modo a implementá-lo no código `EFTCAMB`. Para este efeito criámos um pacote relativo ao nosso modelo para o `EFTCAMB`, que foi usado para evoluir as equações de perturbação e calcular as previsões do modelo para os observáveis cosmológicos. A análise destes resultados revelou a existência de características distinguíveis em relação ao modelo padrão e que podem ser testadas por atuais e futuras observações. Em particular, encontrámos modificações na região de grandes escalas angulares do espectro de potência da Radiação Cósmica de Fundo (RCF), podendo este aparecer suprimido ou aumentado em relação ao modelo padrão. Encontrámos também modificações semelhantes nos espectros de potência da matéria e do efeito de lente gravitacional. Alguns destes traços são de grande interesse cosmológico. Nomeadamente, uma amplitude reduzida na região de grandes escalas angulares do espectro de potência da RCF poderá representar um melhor ajuste aos dados observacionais. Adicionalmente, a supressão do espectro de potência da matéria poderá aliviar a tensão existente entre as medições obtidas a partir da RCF e as provenientes de observações de fenómenos de lente gravitacional. Estas características fazem do modelo SCG um candidato viável a ser investigado pela futura missão Euclid da Agência Espacial Europeia.

Palavras-chave: Energia Escura, Gravitação Modificada, Observáveis Cosmológicos, Teoria de Campo Efetivo, Códigos Einstein-Boltzmann

Abstract

The late-time accelerated expansion of the Universe is one of the most challenging problems of modern Cosmology. Within the framework of General Relativity, the simplest explanation for this phenomenon is via the introduction of the cosmological constant Λ. However, the cosmological constant framework is plagued by a series of shortcomings. These have led cosmologists to explore and propose alternative approaches to cosmic acceleration which can range from models of a dynamical dark fluid known as Dark Energy (DE), to long-scale modifications of the gravitational interaction known as Modified Gravity (MG) models. To investigate these proposals it is useful to resort to a model-independent approach. One of such approaches is the Effective Field Theory (EFT) of DE and MG which provides a framework to describe the evolution of linear perturbations in all gravity theories with a single extra scalar degree of freedom. Additionally, the use of Einstein-Boltzmann solvers such as `EFTCAMB` also simplifies and expedites the testing process. The latter allows one to compute the cosmological observables and make theoretical predictions regarding any model that has been translated into the EFT language.

This dissertation is dedicated to the study of a particular MG model, namely the Scaling Cubic Galileon (SCG), where a scalar field is introduced to modify the gravitational interaction on large scales. We have explored both the background phenomenology of the model and its impact on the cosmological observables, evaluating its viability as a description of the Universe and searching for testable features against observational data. To this purpose, we started by applying dynamical analysis tools to determine the model's expansion history, finding that the SCG is indeed capable of reproducing a late-time period of cosmic acceleration. Following this, we translated the SCG model into the EFT formalism in order to implement it in the `EFTCAMB` solver. We created a new patch for `EFTCAMB` specifically for this model which was used to evolve the perturbation equations and compute the model's predictions for the cosmological observables. From the analysis of these results, we find distinguishable characteristics with respect to the standard model and testable features for both present and future observational surveys. In particular, we find a modified temperature-temperature Cosmic Microwave Background (CMB) power spectra which at low ℓ can be either suppressed or enhanced with respect to the standard scenario. Similarly, we find modifications in the matter and lensing power spectra. These prove to be interesting characteristics. Indeed, a lower Integrated Sachs-Wolfe tail might in principle provide a better fit to data whereas a suppressed matter power spectra might alleviate the existing tension between CMB and weak gravitational lensing measurements. Such features make the SCG model a viable candidate to be investigated by ESA's future mission, Euclid.

Keywords: Dark Energy, Modified Gravity, Cosmological Observables, Effective Field Theory, Einstein-Boltzmann Solver

Contents

List of Tables

List of Figures

Nomenclature

Greek symbols

α_B	Braiding function.
α_K	Kineticity function.
α_M	Running Planck mass function.
α_T	Tensor speed excess function.
η	Gravitational slip parameter.
γ	Baratropic coefficient.
Λ	Cosmological constant.
μ	Effective gravitational coupling.
∇_μ	Covariant derivative.
Ω_i	Density parameter of component i.
ϕ	Scalar field's expectation value.
ρ	Fluid energy density.
Σ	Light deflection parameter.
τ	Conformal time.

Roman symbols

$\bar{A}$	Background value of quantity A.
δA	Linear perturbation of quantity A.
a	Scale factor.
c	Speed of light.
g	Determinant of the metric tensor.
G_N	Newton's gravitational constant.
$G_{\mu\nu}$	Einstein tensor.

$g_{\mu\nu}$ Metric tensor.

$\mathcal{H}$ Hubble function in conformal time.

H Hubble function in proper time.

$h^{\mu\nu}$ Spatial metric on constant-time hypersurfaces.

K Trace of the extrinsic curvature.

$K_{\mu\nu}$ Extrinsic curvature tensor.

m_0 Planck mass.

n_μ Normal vector to a constant-time hypersurface.

p Fluid pressure.

$\mathcal{R}_{\mu\nu}$ Three-dimensional Ricci tensor.

R Ricci scalar.

$R_{\mu\nu}$ Ricci tensor.

t Proper/cosmic time.

$T_{\mu\nu}$ Stress-energy tensor.

w Equation of state parameter.

z Redshift.

Subscripts

μ, ν Four-dimensional indices in vectors and tensors.

i, j Three-dimensional spatial indices in vectors and tensors.

Superscripts

$*$ Complex conjugate.

Glossary

ΛCDM Λ Cold Dark Matter.

ADM Arnowitt-Deser-Misner.

BAO Baryon Acoustic Oscillation.

BBN Big Bang Nucleosynthesis.

BH Black Hole.

C.L. Confidence Level.

CDM Cold Dark Matter.

CMB Cosmic Microwave Background.

DE Dark Energy.

DM Dark Matter.

DoF Degree of Freedom.

EFT Effective Field Theory.

EoS Equation of State.

ESA European Space Agency.

FLRW Friedmann-Lemaître-Robertson-Walker.

GBD Generalized Brans-Dicke.

GG Generalized Galileon.

GLPV Gleyzes-Langlois-Piazza-Vernizzi.

GR General Relativity.

GW Gravitational Wave.

HDM Hot Dark Matter.

ISW Integrated Sachs-Wolfe.

KiDS Kilo-Degree Survey.

LSS Large-Scale Structure.

MCMC Markov-Chain Monte-Carlo.

MDM Mixed Dark Matter.

MG Modified Gravity.

QFT Quantum Field Theory.

QSA Quasi-Static Approximation.

RSD Redshift-Space Distortions.

SCG Scaling Cubic Galileon.

SPT Standard Perturbation Theory.

WEP Weak Equivalence Principle.

Chapter 1

Introduction

The Theory of General Relativity (GR) has stand as the accepted theory of gravitation since Albert Einstein published it in 1915 [1]. Its impressive predictive power and remarkable performance in observational tests along the years quickly established it as one of modern Physics' pillars. Very early on, Einstein's theory gained support by being able to account for the perihelion precession of Mercury and correctly predicting the degree of light deflection for rays passing closely to the Sun. On large scales, GR has served as the basis for Cosmology for more than a hundred years and still continues to experience major successes, such as the detection of Gravitational Wave (GW) events [2, 3] and the recent first direct observation of a Black Hole (BH) [4].

When in 1998 data coming from the study of type Ia supernovae [5, 6] showed that the Universe had recently entered a period of accelerated expansion, both GR and the Standard Model of Particle Physics were thrown into a bit of a predicament, given that none of the known and detected matter components is capable of driving such an evolution. The problem of cosmic acceleration has since been proving itself as one of the most formidable challenges of modern Cosmology. In the framework of GR, the simplest way to explain this late-time period of accelerated expansion is through the introduction of a non-zero cosmological constant (Λ) describing a negative-pressure component of the Universe. The latter is also needed to make up most of the Universe's content ($\sim 68\%$) in order to be consistent with cosmological observations. Therefore, the lack of detection of this essential and seemingly abundant component remains a complete mystery.

Additionally, evidence had already been mounting in favor of the existence of another component of unknown nature. The idea of a non-luminous matter component was first put forward by Zwicky in 1933 to account for the missing mass necessary to explain the high dispersion velocities of galaxies in the Coma Cluster [7]. The fact that this matter component does not appear to emit or absorb light, only interacting gravitationally, has led to its designation as Dark Matter (DM) [8, 9]. Currently, the existence of a DM sector is supported by galactic rotation curves [7, 10, 11], Cosmic Microwave Background (CMB) data [12], gravitational lensing effects [13] and Large-Scale Structure (LSS) observations. Furthermore, it is constrained to only interact gravitationally and, according to Big Bang Nucleosynthesis (BBN) bounds, to be of a non-baryonic nature. Moreover, N-body simulations of LSS show that the observed structure formation scenario is better accounted for when the DM particles are taken to move slowly. DM particles with small velocities are designated as Cold Dark Matter (CDM). Scenarios with Hot Dark Matter (HDM), where the DM particles move with high velocities, are found to not allow

the observed distribution of LSS. Nowadays, HDM is usually only mentioned when in combination with CDM, in what is known as Mixed Dark Matter (MDM). Nevertheless, it is expected that HDM only makes up a few percent of DM, if the amount is even measurable.

In summary, current observations [12] show a Universe composed of about 68.9% of Λ and 31.1% of matter of which 26.1% comes from DM. The standard fluid components, namely, baryonic matter and radiation, only contribute with about 4.9% and 0.001%, respectively, being completely overrun by the dark sector. To account for these observations, the standard cosmological model, which is based on GR, describes a Universe containing a cosmological constant Λ as well as a non-relativistic CDM component. This framework is known as the Λ Cold Dark Matter (ΛCDM) model, which aims to explain both the expansion history and the formation of structure in the Universe.

Even though ΛCDM remains the best fit for cosmological data so far [12, 14], a series of conceptual problems have also been identified, many of them related to the cosmological constant [15]. The lack of satisfying answers for the majority of these problems has motivated a plethora of alternative explanations for the phenomenon of cosmic acceleration. These approaches may include a general Dark Energy (DE) component, keeping it static like the cosmological constant or allowing it to be dynamical instead, i.e., varying in time, or introduce proposals in which the gravitational laws are actually modified. The results of the first approach are usually referred to as DE models [16–19] whereas in the second case one usually talks about Modified Gravity (MG) models [20–24]. By this point in time, the amount of alternative models that have been put forward is extraordinary, making the issue of late-time acceleration also one of the most productive ones in Cosmology.

In light of the overwhelming load of material that is available, combined with the prospect of accessing new and quality observational data, a thorough testing process of theories has become essential in discriminating between competing models and, eventually, identifying the best possible explanation. To study a gravity theory on large scales (> 100 Mpc) one uses linear perturbation theory [25–28]. In this framework, a background analysis is performed in order to probe the homogeneous and isotropic Universe, which is then complemented by the study of small perturbations around such background to understand structure formation and the development of the observed small inhomogeneities. The study of perturbations and LSS observables is essential in discerning between models that present similar evolution histories, helping to break the degeneracy that can exist at background level.

However, given that each model is usually characterized by different sets of parameters that have to be independently investigated, it is easy to understand why going through all of the existing proposals can be a strenuous and lengthy process. In order to simplify this type of undertaking, some effort was put into finding a more encompassing and efficient way of describing and studying DE/MG models. The aim was to construct a general and unifying framework capable of describing several different proposals while offering a smarter approach for model testing and comparison with data. Several of such model-independent frameworks came forward along the years. These include approaches such as the μ, η and Σ parametrization [29–32], the Parametrized Post-Friedmann Framework for Theories of Modified Gravity [33] and the Effective Field Theory (EFT) of DE and MG [34, 35]. The first two introduce functions of time and scale to model MG effects at the level of the equations, having a weak connection with the underlying theory. On the other hand, the EFT framework models the modifications at the level of the action, thus maintaining a stronger link with the underlying gravity theory. Thanks

to this, EFT has taken over the other approaches in the last years.

The EFT provides a model-independent framework to describe the evolution of linear cosmological perturbations in all theories of gravity with a single additional scalar Degree of Freedom (DoF). This is in fact quite encompassing since the majority of DE/MG proposals can be described as a modification of GR's Einstein-Hilbert action through the addition of a single extra scalar DoF. In this framework, the dynamics of both background and perturbations become determined by a set of time-dependent coefficients, known as EFT functions, that are introduced at action level. This allows for a completely model-free analysis where one can test the effect of turning on and off the different functions. Nevertheless, it is also fairly simple to switch to a model-specific approach by mapping the target proposal into the EFT formalism, i.e., by finding the corresponding specific forms of the EFT functions [36].

To further simplify and expedite the study of cosmological perturbations it is useful to resort to Einstein-Boltzmann codes [37, 38] in order to numerically solve the perturbation equations. These can be, of course, model-specific codes designed to evolve the equations of a given model only. However, this approach would require an enormous programming effort to cover a large number of proposals. Thus, with the purpose of having a more unifying and effective approach, the EFT formalism was implemented into the publicly available Einstein-Boltzmann solver Code for Anisotropies in the Microwave Background (`CAMB`) [37, 39]. The result is the `EFTCAMB` code [40–42], which can be employed to evolve the full dynamics of linear cosmological perturbations in a given model provided that it has been mapped into the EFT formalism. This way, one can study the growth of perturbations and the impact on cosmological observables of any model that is encompassed by the EFT formalism using a single general public code.

The aim of this dissertation is to focus on a specific MG proposal: the Scaling Cubic Galileon (SCG) model we proposed in [43]. This is a scalar field model which belongs to the Horndeski/Generalized Galileon (GG) class [22, 44, 45]. This class of models has gained attention due to its ability to describe both an early epoch of Inflation [46–48] and a late-time period of cosmic acceleration [49–55]. The SCG model, in particular, also presents the peculiar feature of having the scalar field density scaling like a standard fluid at early-times, providing an opportunity to alleviate one of the shortcomings of ΛCDM: the Coincidence Problem [56]. Our objective is to investigate the effects of the SCG model on the cosmological observables, allowing us to make concrete theoretical predictions. For this purpose, we start by studying the SCG's background dynamics using a dynamical analysis approach [57, 58], looking to verify if the model is capable of reproducing the proper cosmological evolution. Following this, we study the model's impact on LSS observables resorting to the EFT formalism and the `EFTCAMB` solver, searching for testable features against current and future observational data.

This dissertation is organized as follows. In Chapter 2 we briefly review Einstein's GR and the ΛCDM model. We also use this Chapter to introduce some of the fundamental cosmological concepts that shall be necessary during the rest of the dissertation and that will help in understanding the distinction with respect to a DE/MG model. In Chapter 3 we present the major problems surrounding the cosmological constant which have led cosmologists to construct alternative gravity models for cosmic acceleration. We also discuss the different approaches to modify GR and the different resulting classes of MG models. In addition to this, we review cosmological perturbation theory both in GR and MG and discuss the possible effects of MG theories on the cosmological observables. Chapter 4 contains the building blocks on top of which we constructed the analysis of the SCG model. In this Chapter, we discuss the construction of

the EFT formalism, review the mapping procedure for the study of specific models and explore the mechanics of the `EFTCAMB` solver. Chapter 5 collects the results of this dissertation, focusing on the SCG model and its study. We present the model's construction, background analysis and viability. Following this, we discuss the model's implementation in `EFTCAMB` and analyse in detail the impact of the model's parameters on the cosmological observables. In order to better understand the differences with respect to the standard cosmological model we also include the results of the latter. Finally, we conclude in Chapter 6 by summarizing our main findings and presenting the future prospects regarding the investigation of the SCG model.

Chapter 2

General Relativity

GR was first published in 1915 by Albert Einstein [1] as a generalization of his Theory of Special Relativity [59]. Aiming for a general and accurate theory of gravitation, its publication introduced a revolutionary view on gravity. Rather than keeping the notion of a force mediated by a field acting on space-time, as it is for the electromagnetic field, Einstein's proposal presented gravity as a direct manifestation of space-time's geometry. Thus, GR is a geometrical theory of gravity in which the gravitational interactions felt by an object are seen as a consequence of the curvature of space-time, while in turn the geometry of space-time is shaped by the object's mass.

Einstein's theory surpassed Newton's law of universal gravitation, the reigning gravitational theory for over two hundred years. Many of the shortcomings of Newton's theory were solved by GR. The concept of an invisible force acting over large distances that was present in Newton's formulation is explained as a consequence of a curved space-time. Additionally, the anomaly in Mercury's orbit was also accounted for in GR. Nevertheless, Einstein ensured that Newton's theory could be recovered as the weak limit of GR as the former still offers an accurate description of gravitational phenomena in that regime.

GR's capacity to solve the major problems of the Newtonian formulation combined with its remarkable performance in observational tests [60, 61] and great predictive power, established it as the accepted theory of gravitation with very few alterations to its original form. In fact, it did not take long for GR to achieve its first big success. In 1919, four years after Einstein first published his theory, Eddington confirmed GR's prediction of gravitational deflection of light by the Sun [62]. Then, almost a century later, Einstein's theory continues to make history by having also predicted the recently detected GWs [2].

The publication of GR is also often viewed as the dawn of Modern Cosmology. The latter is the branch of Physics concerned with the description of the Universe, dealing with questions regarding its beginning, composition and fate. Although these topics were always of human interest, it was the rigorous mathematical description of the Universe offered by GR that propelled Cosmology into a more exact and productive era. Currently, the standard model of Cosmology, the so called ΛCDM model, is based on GR's framework.

In this Chapter we present a brief review of the technical and conceptual elements that will be needed throughout this dissertation. We start with a brief review of GR, exploring the construction of the Einstein equations in Section 2.1 and then introduce the cosmological constant and discuss the uniqueness of GR's field equations and action in Section 2.2. In Section 2.3 we review the ΛCDM model and the state of the art of cosmological observations. The main

building principle behind the standard cosmological model is discussed in Section 2.3.1, followed by the discussion of the content of the Universe and how it is included in the field equations in Section 2.3.2. Finally, in Section 2.3.3 we present the cosmological solutions for the ΛCDM model.

2.1 Einstein's Field Equations for Gravitational Interaction

As previously mentioned, GR came from Einstein's wish to generalize Special Relativity to include non-inertial reference frames. To do so, Einstein's quest for a set of descriptive field equations was guided by a series of fundamental principles, namely:

- **Mach's Principle**: it is the matter distribution that determines the geometry of the Universe and the existence of local inertial frames.
- **Equivalence Principle**: there are no local experiments that can distinguish free-falling observers from inertial observers. This is also a translation of the equivalence between an object's inertial and gravitational masses.
- **Principle of Relativity**: the laws of physics should be the same in all reference frames, meaning there should be no preferred frame.
- **Principle of General Covariance**: from the Principle of Relativity, having no preferred reference frame translates into a need that the field equations transform covariantly, preserving their fundamental properties under a coordinate transformation.
- **Correspondence Principle**: the theory should be consistent with previous acceptable theories inside their realms of validity. In this case, GR should recover Special Relativity in the absence of gravity and Newtonian gravity in the limit of weak gravitational field and low velocities.

Additionally, the theory should also be capable to correctly describe observational results. By enforcing these principles as requirements of GR, Einstein built a general and predictive theory capable of naturally describing the gravitational interaction. In this Section we shall see how these guidelines came into play.

Firstly, given GR's view on gravity, it comes as no surprise that the geometrical description of space-time takes a central role in its formulation. The theory is built in a four-dimensional pseudo-Riemannian manifold [26] with one time dimension plus three spatial ones. All necessary geometric information is then contained in a single quantity: the metric tensor $g_{\mu\nu}(x^\mu)$[1]. This quantity is a function of the space-time coordinates x^μ and is crucial for the definition of the notions of time and distance in the manifold.

Then, following the objectives set up by the guiding principles, and after a series of failed attempts, Einstein finally presented the field equations, known as Einstein's equations, mediating gravitational interaction in GR:

$$G_{\mu\nu} = R_{\mu\nu} - \frac{1}{2} g_{\mu\nu} R = \frac{1}{m_0^2} T_{\mu\nu}. \tag{2.1}$$

[1] In this definition, and hereafter, we take the convention of using greek indices to denote four-dimensional quantities, i.e, $\mu = 0, 1, 2, 3$ whereas latin indices, such as $i = 1, 2, 3$, shall be used to denote spatial coordinates.

In this expression $G_{\mu\nu}$ and $R_{\mu\nu}$ are the Einstein and Ricci tensors, respectively, R is the Ricci scalar and $T_{\mu\nu}$ is the stress-energy tensor describing the energy-matter content whose form shall be discussed in Section 2.3.2. The specific form of the m_0^2 factor can be determined by the Correspondence Principle. According to it, we must be able to recover the Poisson equation in the Newtonian limit, a requirement that results in the identification of m_0^2 as the square of the Planck mass, i.e.,

$$m_0^2 = \frac{c^4}{8\pi G_N}, \tag{2.2}$$

where G_N is the universal gravitational constant and c is the speed of light. From this point forward, we choose to set the units such that $c = 1$.

The Ricci tensor and scalar, $R_{\mu\nu}$ and R, are defined in terms of the Riemann curvature tensor $R^{\rho}_{\sigma\mu\nu}$ according to[2]

$$R_{\mu\nu} = R^{\rho}_{\mu\rho\nu} \tag{2.3}$$

and

$$R = g^{\mu\nu} R_{\mu\nu}. \tag{2.4}$$

The Riemann tensor, in turn, is defined using the Levi-Civita connection $\Gamma^{\lambda}_{\mu\nu}$ following

$$R^{\rho}_{\sigma\mu\nu} = \partial_\mu \Gamma^{\rho}_{\nu\sigma} - \partial_\nu \Gamma^{\rho}_{\mu\sigma} + \Gamma^{\rho}_{\mu\lambda}\Gamma^{\lambda}_{\nu\sigma} - \Gamma^{\rho}_{\nu\lambda}\Gamma^{\lambda}_{\mu\sigma}, \tag{2.5}$$

where $\partial_\mu \equiv \partial/\partial x^\mu$ is the partial derivative with respect to the x^μ coordinate component and the connection is uniquely computed from the chosen metric:

$$\Gamma^{\lambda}_{\mu\nu} = \frac{1}{2} g^{\lambda\sigma} \left(\partial_\mu g_{\nu\sigma} + \partial_\nu g_{\sigma\mu} - \partial_\sigma g_{\mu\nu} \right). \tag{2.6}$$

Therefore, given the construction of the last quantities, the geometrical information that was contained in the metric tensor ends up encoded in the Einstein tensor on the left-hand side of the Einstein equations (2.1). Furthermore, from the structure of those equations it becomes very clear that in GR the geometry of space-time, now encoded in $G_{\mu\nu}$, and the Universe's matter content, described by the stress-energy tensor $T_{\mu\nu}$, are closely connected. Any changes that may happen in the geometrical sector have a direct impact on the matter content and vice versa. This accounts for the influence of Mach's Principle.

In practice, by taking the Einstein and the stress-energy tensors as symmetric, Einstein's equations amount to a system of 10 independent second-order differential equations. However, by further considering the contracted Bianchi identity, a property of the pseudo-Riemannian manifold that reads

$$\nabla^\mu G_{\mu\nu} = 0, \tag{2.7}$$

with ∇_μ being the covariant derivative, there are 4 extra constraints placed on the Einstein tensor and the number of independent equations is reduced to 6. Furthermore, since $G_{\mu\nu}$ and $T_{\mu\nu}$ are directly connected by the field equations (2.1), the imposition of the Bianchi identity

[2] In the following definitions and throughout the work we will use Einstein notation. According to this convention, repeated indices are to be summed over all possible index values. For example,

$$a^\mu b_\mu = \sum_{\mu=0}^{3} a^\mu b_\mu.$$

yields a conservation law for the stress-energy tensor

$$\nabla^{\mu} T_{\mu\nu} = 0, \tag{2.8}$$

which can be taken as the generalization of the energy conservation law.

For further details on the geometrical framework of GR we refer the reader to [26, 63, 64].

2.2 The Einstein-Hilbert Action, Lovelock's Theorem and the Cosmological Constant

Einstein first postulated GR's field equations by using differential geometry to translate the base principles that he set out for the theory. However, it is also possible to derive Einstein's equations through the principle of least action: $\delta\mathcal{S} = 0$. In fact, both Einstein and Hilbert were able to independently derive them from the metric variation of the following action:

$$\mathcal{S} = \frac{m_0^2}{2}\int d^4x\sqrt{-g}R \; + \; \mathcal{S}_{\gamma}\left[g_{\mu\nu}, \Psi_{\gamma}\right], \tag{2.9}$$

where g is the determinant of the metric tensor. The first term in (2.9) is known as the Einstein-Hilbert action ($\mathcal{S}_{EH}$), which when varied alone yields the vacuum form ($G_{\mu\nu} = 0$) of Einstein's equations. On the other hand, the addition of $\mathcal{S}_{\gamma}$ as the action describing the matter fields Ψ_{γ} leads to Einstein's equations (2.1) in the presence of matter, where the stress-energy tensor is defined as

$$T_{\mu\nu} = -\frac{2}{\sqrt{-g}}\frac{\delta\mathcal{S}_{\gamma}}{\delta g_{\mu\nu}}. \tag{2.10}$$

Knowing that it is possible to derive Einstein's equations either by following the base physical principles or through the variational principle does not, however, guarantee us that both the field equations and the Einstein-Hilbert action should be the unique choices when constructing a gravity theory. To answer that question we must turn to Lovelock's Theorem [65, 66]. It states that in a four-dimensional space-time the only tensor $B_{\mu\nu}$ that is capable of recovering Einstein's equations, now written as

$$B_{\mu\nu} = \frac{1}{m_0^2}T_{\mu\nu}, \tag{2.11}$$

while verifying the following conditions:

1) constructed only from the metric tensor and its derivatives up to second-order:

$$B_{\mu\nu}(g_{\mu\nu}, g_{\mu\nu,\rho}, g_{\mu\nu,\rho\lambda}); \tag{2.12}$$

2) linear in $g_{\mu\nu,\rho\lambda}$;

3) symmetric: $B_{\mu\nu} = B_{\nu\mu}$;

4) divergence free: $\nabla^{\nu} B_{\mu\nu} = 0$;

is given by

$$B_{\mu\nu} = \eta G_{\mu\nu} - \lambda g_{\mu\nu}, \tag{2.13}$$

where η and λ are two constants. Consequently, the resulting field equations correspond to the ones derived by Einstein in vacuum with the possible addition of a constant term, i.e.

$$\eta G_{\mu\nu} - \lambda g_{\mu\nu} = 0. \tag{2.14}$$

Regarding the uniqueness of the action, it is possible to find that in four dimensions the most general Lagrangian density $\mathcal{L}$ built solely from the metric and its derivatives and that can yield Einstein's field equations is

$$\mathcal{L} = \eta\sqrt{-g}R - 2\lambda\sqrt{-g} + \gamma\epsilon^{\mu\nu\alpha\beta}R^{\rho\sigma}{}_{\mu\nu}R_{\rho\sigma\alpha\beta} + \xi\sqrt{-g}\left(R^2 - 4R^{\mu}{}_{\nu}R^{\nu}{}_{\mu} + R^{\alpha\beta}{}_{\mu\nu}R^{\mu\nu}{}_{\alpha\sigma}\right), \tag{2.15}$$

where γ and ξ are constants and $\epsilon^{\mu\nu\alpha\beta}$ is the Levi-Civita tensor. However, it follows from Lovelock's theorem that in four dimensions the third and fourth terms of (2.15) are boundary terms and therefore do not contribute to the field equations. This reduces the contributing part of the previous Lagrangian only to the necessary terms to build the Einstein-Hilbert action plus a constant term.

In conclusion, one finds that both Einstein's equations and the Einstein-Hilbert action, together with a constant term, correspond to the most general field equations and action describing gravitational interactions in four dimensions.

Additionally, Lovelock's theorem also provides fundamental insight when looking to construct a gravitational theory with field equations differing from those of GR. It tells us that if one wishes to introduce modifications in the gravitational sector, at least one of the following options must be taken:

- include more fields beyond or even instead of the metric tensor;
- allow for higher-order derivatives in the field equations;
- work in a space-time with more than 4 dimensions;
- break the diffeomorphism invariance.

We shall discuss each of the previous options in greater detail in Chapter 3.

Let us also discuss the presence of a constant term in equation (2.14). When GR was first published there was no evidence that the Universe should be either expanding or contracting, instead it was believed to be static. This led Einstein to look for solutions to the field equations that would describe a Universe with a non-zero matter content which would be able to remain static. However, since gravity is an attractive interaction, the matter content of the Universe should eventually lead it to collapse. To prevent this and keep the Universe static, some extra repulsive contribution was needed. Thus, in order to achieve a static solution, Einstein introduced the cosmological constant Λ in 1917 [67], modifying GR's field equations (2.1) to yield:

$$G_{\mu\nu} - g_{\mu\nu}\Lambda = 8\pi G_N T_{\mu\nu}. \tag{2.16}$$

However, not long after his proposal, not only did Eddington find that Einstein's static solution was actually unstable [68], but Edwin Hubble also showed that the Universe was actually expanding [69]. This led Einstein to reject the cosmological constant, even calling it his "greatest blunder". Following that, the constant term remained absent of cosmological models for a long period of time.

Nowadays, Λ is back on the field equations, as we shall see in Section 2.3, to actually explain the phenomena that led Einstein to cast it out in the first place: the accelerated expansion of the Universe.

2.3 The Standard Model of Cosmology

GR served as the catalyst for the development of Modern Cosmology. The formal setting of Einstein's theory, providing a set of governing equations whose solutions track the structure and evolution of the Universe and its matter content, came with several testable predictions ranging from Solar System scales all the way up to cosmological ones. Moreover, with the technological advancements made in the following years, it became possible to directly test a theory against nature through high-quality observational data. This propelled years of great theoretical and observational achievements inside the field.

After the publication of GR, a great number of solutions to the Einstein equations were proposed to describe the evolution of the Universe. Einstein's attempt at a static Universe in 1917 being only one of them. Nevertheless, the following years would also see a lot of groundbreaking observational evidence become available, helping to guide the theoretical efforts. The first milestone came in 1929 when the results of Edwin Hubble's study on the recession velocity of galaxies [69] showed that the Universe was expanding. That focused the attention of the scientific community on proposals where a non-empty Universe could be expanding. Until that day, the most successful proposal to be put forward was the result of the independent works of Friedmann, Lemaître, Robertson and Walker. They proposed a set of expanding cosmological solutions to Einstein's equations that followed from the simplifying assumption that the Universe is homogeneous and isotropic on large scales (> 100 Mpc). Although unfounded at the time, this assumption, known as the Cosmological Principle, would receive observational support years later with Penzias and Wilson's discovery of the CMB in 1964 [70].

In addition to this, a substantial amount of observational data collected in the following decades indicated the existence of a large dark sector in the Universe's matter-energy content. This pointed to the existence of DE (68%) and DM (31%) components dominating over the regular fluid components, i.e., over baryonic matter and relativistic particles. Therefore, the majority of the Universe's content remains mostly unknown to us.

Of course, for a model to translate a successful description of the Universe it has to account for the available observational evidence. Currently, the best fit to observational data [12] and the accepted standard model of cosmology is the ΛCDM model. It is based on both Einstein's GR and the Cosmological Principle to describe the evolution and content of the Universe. To account for the volume of formed structure that is observed, this model includes a non-relativistic DM component, i.e., a CDM component. On the other hand, ΛCDM accounts for the late-time acceleration by including a cosmological constant term Λ in the Einstein equations, describing a negative-pressure fluid responsible for driving the mentioned phenomenon. As a whole, the model offers a description of the Universe's evolution history together with a mechanism for the formation and distribution of the observed LSS.

2.3.1 An Homogeneous and Isotropic Universe

The idea that there should be no preferred observers has been around since Copernicus removed the Earth from the center of the Solar System. It gave birth to the notion that Earth was not a place of privileged observation, an idea that became known as the Copernican Principle. The Cosmological Principle, in turn, extends this idea to a cosmic scale, stating that the Universe is globally homogeneous and isotropic. The requirement of homogeneity is that, on large scales, the Universe should appear uniform in its properties: there is no preferred position. Isotropy, on the other hand, means that when observed from a certain place the Universe should look the same in all directions: there is no preferred direction. In summary, there should be no preferred observational positions and the governing laws should have a uniform action on cosmic scales.

Although the Cosmological Principle has been used from early on to find cosmological solutions to Einstein's equations, there was no actual observational evidence to support it. This would only come with the CMB's discovery in 1964. This remnant radiation from the early Universe was observed to have very small ($\sim 10^{-5}$) deviations from isotropy in its temperature field. Later on, LSS surveys also showed a matter distribution which can, in good approximation, be taken as homogeneous at large enough scales (> 100 Mpc). Therefore, nowadays the Cosmological Principle is very well supported by observations.

The absence of observational evidence did not, however, stop Friedmann, Lemaître, Robertson and Walker from independently adopting the Cosmological Principle in their searches for cosmological solutions undertaken between 1920 and 1940. Since, as we discussed in Section 2.1, the metric tensor is the quantity responsible for describing the Universe's geometry, they found that adhering to the Cosmological Principle would also have direct implications on the form of $g_{\mu\nu}$. Specifically, the metric tensor has to describe a spatially homogeneous and isotropic Universe evolving over time. The mentioned authors then found, by taking the proper geometrical arguments, the most general four-dimensional metric that can be constructed consistently with the Cosmological Principle which is known as the Friedmann-Lemaître-Robertson-Walker (FLRW) metric [71–73]. Written in comoving spherical coordinates, the line element for the FLRW metric reads:

$$ds^2 = -dt^2 + a(t)^2 \left[\frac{dr^2}{1-\kappa r^2} + r^2 d\bar{\Omega} \right], \tag{2.17}$$

where t is the cosmic time, $d\bar{\Omega} = r^2 d\theta^2 + r^2 \sin^2(\theta) d\varphi^2$ is the solid angle and the constant $\kappa \in \{-1, 0, +1\}$ represents the curvature of space. The Universe is said to be spatially open for $\kappa = -1$, flat for $\kappa = 0$ and spatially closed for $\kappa = +1$. Finally, the function $a(t)$, known as the scale factor, is taken to represent the relative size of the Universe and is positively defined ($a(t) > 0$) in such a way that it is normalized to unity ($a = 1$) at present time. In Cosmology it is common to work in a flat ($\kappa = 0$) FLRW metric. Besides being the simplest assumption, the current cosmological constraints coming from the *Planck* Collaboration [12] strongly support such geometry, showing a curvature density parameter of only $\Omega_\kappa = 0.0007 \pm 0.0019$ (68% C.L.). That being said, the line element describing an homogeneous, isotropic and flat FLRW metric, now given in comoving Cartesian coordinates, can be written as

$$ds^2 = -dt^2 + a(t)^2 \delta_{ij} dx^i dx^j. \tag{2.18}$$

When introducing the line elements in equations (2.17) and (2.18), we stated that they were

written in terms of comoving coordinates: the first using the spherical coordinates r, θ and φ while the latter is given in Cartesian coordinates x^i. Nevertheless, regardless of them being spherical or Cartesian, comoving coordinates are the ones that remain constant throughout time. This means that the comoving distance x between two objects, which amounts only to a coordinate difference between the two, also remains constant in time. On the other hand, if the Universe is not static, we know the physical distance d between the objects changes. Since the scale factor gives the relative size of the Universe, it allows us to relate the physical distance with the comoving one through:

$$d(t) = a(t)x. \tag{2.19}$$

In turn, the rate at which this distance changes, known as the recession velocity v, can then be given by

$$v(t) \equiv \dot{d} = \dot{a}x = \left(\frac{\dot{a}}{a}\right) d = Hd, \tag{2.20}$$

where the overdot denotes a derivative with respect to the proper time t and

$$H(t) \equiv \frac{\dot{a}(t)}{a(t)} \tag{2.21}$$

is the Hubble function which gives the rate of expansion of the Universe.

If we choose to evaluate equation (2.20) at present time, we are left with the expression for the known Hubble law:

$$v = H_0 d, \tag{2.22}$$

where the Hubble constant H_0 corresponds to today's value of the Hubble parameter. This relation had been previously derived in 1929 by Edwin Hubble while studying nearby galaxies [69]. He came to the conclusion that each galaxy should be receding from us with a velocity proportional to its distance. This was actually the first solid evidence that the Universe is in fact expanding rather than, as previously believed, being static.

2.3.2 The Stress-Energy Tensor

Once again following Einstein's equations (2.1), we can understand that to find cosmological solutions we require information both on the geometric properties and on the matter content dynamics. In the previous Subsection, the geometrical part was taken care of by the adoption of the Cosmological Principle leading to the FLRW metric. As such, the next step should be to find the appropriate description for the matter-energy sector, which is equivalent to say that we want to find the adequate form for the stress-energy tensor $T_{\mu\nu}$. Geometrically, the stress-energy must be symmetric ($T_{\mu\nu} = T_{\nu\mu}$) by construction since it is obtained from the variation of the matter action with respect to the symmetric metric tensor $g_{\mu\nu}$, as we saw in Section 2.2. Additionally, the Principle of General Covariance requires it to be covariant while from the Equivalence Principle together with the Bianchi identity it follows that the tensor must also verify the conservation law presented in equation (2.8).

Following this, and considering only a background level in which the structure in the Universe can be taken as homogeneously distributed as stated by the Cosmological Principle, we can, in good approximation, consider that matter also shows an homogeneous distribution. This means that, modeling the energy-matter content as a fluid, both the fluid pressure p and the fluid energy density ρ are only time-dependent quantities. On the other hand, isotropy ensures the

absence of anisotropic shear. In summary, at background level and on large enough scales, the matter content is well described as a continuous perfect fluid, for which the stress-energy tensor reads

$$T_{\mu\nu} = (\rho + p)\, u_\mu u_\nu + p g_{\mu\nu}, \tag{2.23}$$

where u_μ is the four-velocity of the fluid defined as

$$u^\mu \equiv \frac{dx^\mu}{ds} \tag{2.24}$$

and verifying $u^\mu u_\mu = -1$. If one then chooses an inertial frame comoving with the fluid, the four-velocity becomes $u^\mu = (-1, 0, 0, 0)$ and we can finally compute the stress-energy tensor

$$T^\mu{}_\nu = \begin{pmatrix} -\rho(t) & 0 & 0 & 0 \\ 0 & p(t) & 0 & 0 \\ 0 & 0 & p(t) & 0 \\ 0 & 0 & 0 & p(t) \end{pmatrix}. \tag{2.25}$$

Since there is a variety of energy sources in the Universe, the fluid is generally decomposed into contributions from several components. Therefore, the stress-energy tensor in (2.25) is in reality a sum of stress-energy tensors for each fluid component i where $\rho(t) = \sum_i \rho_i(t)$ and $p(t) = \sum_i p_i(t)$.

Once we have the form of the stress-energy tensor, the generalization of the energy conservation law given by equation (2.8) with $\nu = 0$ yields the evolution equation for $\rho(t)$:

$$\dot{\rho} + 3H\,(\rho + p) = 0. \tag{2.26}$$

This is known as the continuity equation which is, in general, valid for the total energy density and pressure. Only if there are no interactions between the different fluid components does equation (2.26) also hold independently for each fluid component i. Furthermore, we can also assume that the fluid energy density and pressure can be related through the barotropic Equation of State (EoS)

$$p = w\rho = (\gamma - 1)\,\rho, \tag{2.27}$$

where w is the equation of state parameter and $\gamma = w + 1$ is the constant barotropic coefficient. In the case of the standard fluid components, the value of w or, equivalently, the value of γ, is well-known: for non-relativistic pressureless fluids (baryons and CDM) it follows from $p = 0$ that $w = 0$ ($\gamma = 1$), whereas for relativistic fluids, $p = \rho/3$ leads to $w = 1/3$ ($\gamma = 4/3$). Then, by plugging the EoS (2.27) into the continuity equation (2.26), we can re-write it as

$$\dot{\rho} + 3H(w + 1)\rho = 0, \tag{2.28}$$

and obtain an evolution equation for the energy density ρ. Solving it for ρ then leads to:

$$\frac{\rho}{\rho_0} = a^{-3(w+1)}, \tag{2.29}$$

where the subscript 0 signals that the quantity is evaluated at present time. Thus, if we consider a pressureless fluid and a relativistic or radiation-like fluid, their energy densities, ρ_m and ρ_r

respectively, follow:

$$\begin{cases} \rho_m = \rho_{m,0} a^{-3} \\ \rho_r = \rho_{r,0} a^{-4} \end{cases} . \tag{2.30}$$

From these results, it becomes clear that different fluid species demonstrate different scaling behaviours with the scale factor a.

2.3.3 Cosmological Solutions within the ΛCDM Model

Recent observations show that the Universe is expanding in an accelerated fashion (see Section 2.3). The ΛCDM model accounts for this by considering the cosmological constant term. A term that, according to Lovelock's theorem in Section 2.2, is actually expected in the field equations. The corresponding solutions can then be obtained by applying the FLRW metric (2.18) and the stress-energy tensor (2.25) forms to Einstein's equations (2.16). Such a procedure yields two coupled differential equations, known as the Friedmann Equations, which describe the dynamics of the scale factor $a(t)$:

- From the time-time ($\mu\nu = 00$) component one gets the Friedmann constraint:

$$\left(\frac{\dot{a}}{a}\right)^2 - \frac{\Lambda}{3} = \frac{8\pi G_N}{3}\rho - \frac{\kappa}{a^2}; \tag{2.31}$$

- From the diagonal spatial ($\mu\nu = jj$) components one gets the acceleration or Raychaudhuri equation:

$$\frac{\ddot{a}}{a} - \frac{\Lambda}{3} = -\frac{4\pi G_N}{3}(\rho + 3p). \tag{2.32}$$

To close this system one must also consider the continuity equation together with the barotropic relation (2.27) for the fluid components.

It is, however, rather straightforward to see that the Λ term can be moved to the right-hand side of equations (2.31)-(2.32) and absorbed as a new dark fluid component if we define its energy density as

$$\rho_\Lambda = \frac{\Lambda}{8\pi G_N}. \tag{2.33}$$

In that case, the Friedmann equations simply read

$$\left(\frac{\dot{a}}{a}\right)^2 = \frac{8\pi G_N}{3}\rho - \frac{\kappa}{a^2}, \tag{2.34}$$

and

$$\frac{\ddot{a}}{a} = -\frac{4\pi G_N}{3}(\rho + 3p). \tag{2.35}$$

where the sums $\rho(t) = \sum_i \rho_i(t)$ and $p(t) = \sum_i p_i(t)$ now include ρ_Λ and p_Λ.

Equation (2.35) is known as the acceleration equation because it provides a condition that allows to distinguish between an accelerating and a decelerating Universe. The Universe is taken to be accelerating if $\ddot{a} > 0$. Alternatively, if $\ddot{a} < 0$, the Universe is said to be decelerating. Indeed, since π and G_N are positive constants and the scale factor is positive definite ($a(t) > 0$),

it becomes clear that the Universe has

$$\begin{cases} \text{an accelerated expansion if: } \ddot{a} > 0 \Leftrightarrow \rho + 3p < 0, \\ \text{a decelerated expansion if: } \ddot{a} < 0 \Leftrightarrow \rho + 3p > 0. \end{cases} \tag{2.36}$$

Furthermore, if the barotropic EoS holds, the previous conditions can be transformed into constraints of the equation of state parameter: $w < -1/3$ for acceleration and $w > -1/3$ for deceleration. Given these last conditions, it also becomes clear that the standard fluid components – baryonic matter with $w = 0$ and radiation with $w = 1/3$ – are only capable of driving a decelerated expansion. This result is actually the reason why the cosmological constant was reintroduced. If a perfect fluid description is assumed for the Λ component, its pressure and energy density are related through the barotropic equation of state $p_\Lambda = w\rho_\Lambda$ with a non-dynamical EoS parameter corresponding to $w = -1$. Since it verifies $w < -1/3$, the Λ component gives rise to acceleration. If we plug this value of w in the continuity equation (2.28), we find:

$$\dot{\rho}_\Lambda(t) = 0, \tag{2.37}$$

meaning that the energy density of the cosmological constant remains constant through time. Equivalently, and similar as to what we did in (2.30), for the cosmological constant we can write

$$\rho_\Lambda = \rho_{\Lambda,0}, \tag{2.38}$$

where $\rho_{\Lambda,0}$ is the constant density of Λ.

Finally, it is common when discussing the composition of the Universe to introduce the density parameter of a certain fluid component i:

$$\Omega_i = \frac{\rho_i}{\rho_c}, \tag{2.39}$$

where ρ_c is the critical density defined as

$$\rho_c = \frac{3H^2}{8\pi G_N}. \tag{2.40}$$

Making use of this definition, the Friedmann constraint (2.34) can be re-written in the following form:

$$1 = \Omega_m(t) + \Omega_r(t) + \Omega_\kappa(t) + \Omega_\Lambda(t), \tag{2.41}$$

where Ω_m is the matter density parameter accounting for both the baryonic and the DM contributions, Ω_r and Ω_Λ are the densities of the relativistic component and the cosmological constant, respectively, and Ω_κ is the density parameter for curvature defined as

$$\Omega_\kappa = -\frac{\kappa}{H^2 a^2}. \tag{2.42}$$

The density parameters Ω_i are time-dependent functions, such that they vary throughout the cosmological eras towards their present values $\Omega_{i,0}$. It is possible to re-write the Friedmann constraint once again by using the time evolution of the energy densities found in (2.30) and

(2.38), making the present values of the density parameters explicitly appear

$$H^2 = H_0^2 \left(\Omega_{m,0} a^{-3} + \Omega_{r,0} a^{-4} + \Omega_{\kappa,0} a^{-2} + \Omega_{\Lambda,0} \right), \tag{2.43}$$

where we have also taken the curvature density parameter at present time to be $\Omega_{\kappa,0} = -\kappa/H_0^2$.

The best fit values of the density parameters have recently been determined by the *Planck* Collaboration [12]. From the combination of *Planck* CMB power spectra, CMB lensing reconstruction and Baryon Acoustic Oscillation (BAO) measurements, they obtain:

$$\Omega_{m,0} = 0.3111 \pm 0.0056 \text{ (68\% C.L.)}, \tag{2.44}$$

$$\Omega_{\Lambda,0} = 0.6889 \pm 0.0056 \text{ (68\% C.L.)} \tag{2.45}$$

and for the curvature parameter

$$\Omega_{\kappa,0} = 0.0007 \pm 0.0019 \text{ (68\% C.L.)}, \tag{2.46}$$

as we have previously seen. The last result is strongly supportive of the choice $\kappa = 0$, since $\Omega_{\kappa,0}$ is in fact very close to 0 with great confidence [12]. Furthermore, according to the combination of these results, today's contribution from the relativistic component is negligible.

According to their analysis, ΛCDM remains the best fit model to observational data. However, the unknown nature of both Λ and DM leaves the field open to questioning of the current paradigm and venturing into alternative possibilities. The cosmological constant framework in particular, is still plagued by a number of questions with rather unsatisfying answers, as we shall see in Chapter 3. To answer some of these questions, or even to avoid them entirely, a lot of alternative approaches to late-time cosmic acceleration have been put forward, ranging from invoking a generic DE component to actual modifications of gravity.

Chapter 3

Beyond the Standard Cosmological Model

The latest results from the *Planck* Collaboration [12] favor ΛCDM as the best fit model to available data, making it the currently accepted cosmological model for the description of the Universe. Nevertheless, the description provided by this model remains far from completely satisfying. Besides the still unknown nature of DM, the ΛCDM model even fails in explaining one of its base assumptions, that of homogeneity and isotropy, without invoking fine-tuning of initial conditions.

Even so, it is the late-time acceleration that causes the greatest damage in the standard model. The cosmological constant framework remains plagued by conceptual and practical dilemmas to which the ΛCDM model has yet to provide satisfying answers [15], namely the *Cosmological Constant* and *Coincidence* problems [56, 74–79]. This has led, at a first level, to the proposition of alternative explanations for the acceleration phenomenon, originating several models where a dynamical DE component is invoked. However, the fact that it has also not been possible to reconcile GR with quantum gravity so far, given that the theory breaks down around the Planck scale, has raised the question as to if GR really is the most accurate gravity theory. The cosmological constant problems together with the latter shortcoming have, in turn, motivated the search for viable modifications of the laws of gravity in what is known as MG theories [20–24].

The overwhelming load of theories that exists by now needs to be tested against new and quality observational data in hopes of discriminating between competing models. To study a gravity theory on large scales (> 100 Mpc) one uses standard linear perturbation theory [25–28]. In this framework, a background analysis is used to probe the homogeneous and isotropic universe, which is then complemented by the study of small perturbations on top of such background that are necessary for structure formation and to account for the inhomogeneities that can be observed on smaller scales.

In this Chapter we shall discuss some of the cosmological constant shortcomings and introduce both the proposed alternatives and the necessary formalism to study them. Therefore, in Section 3.1 we start by presenting some of the problems affecting the ΛCDM model. Then, in Section 3.2 we explore the basic features of the proposed alternatives to deal with the problem of cosmic acceleration, with special attention given in Section 3.2.1 to the MG model class we shall work within. Finally, in Section 3.3 we introduce the necessary tools to study a gravity

theory on large scales by reviewing both the formalism of linear perturbation theory and the essential aspects of the cosmological observables together with the possible impact of DE/MG on them.

3.1 The Shortcomings of the Cosmological Constant

The ΛCDM model assumes the Cosmological Principle. Therefore, at background level ΛCDM describes a globally homogeneous and isotropic Universe complemented by a CDM component and a DE sector characterized by Λ. This framework, however, has been found to be plagued by a set of conceptual problems that often require fine-tuning of the initial conditions in order to still account for the current observed state of the Universe.

Some of these problems affect the very theoretical basis where the ΛCDM model stands, as it happens, for example, with the *Horizon* and *Flatness* problems. These concern the model's inability to explain the observed homogeneity, isotropy and flatness of the Universe, simply assuming that they were already encoded in the initial conditions for the Universe's evolution. Nowadays, to avoid invoking self-tuning, the ΛCDM model relies on the existence of an early period of exponential acceleration $\left(a \sim e^{Ht}\right)$ called Inflation [80–83]. Although it was not its original purpose, it was later understood that the inflationary mechanism could also offer a solution to the horizon and flatness problems [80].

Nevertheless, the most puzzling questions plaguing the standard cosmological model surround the late-time acceleration phenomenon and the cosmological constant framework. Among them, the most troubling and generally more discussed issues can be posed under the *Cosmological Constant* and *Coincidence* problems.

Let us start with the Cosmological Constant Problem. More than just a cosmological problem, this is also a concern for Quantum Field Theory (QFT). This happens because according to QFT the cosmological constant can be interpreted as a measure of the vacuum energy density, receiving non-negligible contributions from quantum fluctuations of the Standard Model fields. This makes QFT capable of providing a theoretical expectation for the value of the cosmological constant which, given in terms of the Planck mass m_0, is [84]

$$\Lambda_{th} \sim 10^{-60} m_0^4. \tag{3.1}$$

However, the problem arises when we turn to observations looking for Λ. The observationally inferred value of the cosmological constant is [84]

$$\Lambda_{obs} \sim 10^{-120} m_0^4, \tag{3.2}$$

which represents a deviation of about 60 orders of magnitude. The significant discrepancy that exists between the theoretical and observational values for Λ is generally referred to as the Cosmological Constant Problem [74–79].

So far, no explanation has been found for the discrepancy between theory and observation. It has yet to be found any viable mechanism that could lead to a suppression of the cosmological constant to its observed small value. Because of that, anthropic arguments have often been summoned to explain the smallness of Λ. According to the anthropic principle, some of the Universe's parameters are not defined by fundamental laws. Instead we see them take on their

specific values because they need to be compatible with the existence of intelligent observers for us to be making observations at all. Thus, according to this principle, we observe Λ as having such a specifically small value because it is the one compatible with an Universe where we can exist.

In addition to questioning the tension between observations and theoretical predictions regarding Λ, one can also wonder about the remarkable fact that we happen to be living in the precise epoch of transition into an accelerated expansion phase. Since the energy densities of matter and Λ scale differently, as we saw in Section 2.3, it is a rather stunning coincidence that we would catch the period where Ω_m and Ω_Λ are of comparable magnitude. In fact, according to recent observational data we have $\Omega_\Lambda \sim 68\%$ and $\Omega_m \sim 31\%$ [12]. It is the rather fortuitous character of this issue that has led it to become known as the Coincidence Problem [56].

In summary, although the introduction of the cosmological constant appears to be a simple way to account for the cosmic acceleration, it is also accompanied by some disquieting theoretical shortcomings. Consequently, ΛCDM is left as an incomplete model until such a time as a solution has been found. This has served as motivation for the search of an alternative description, aiming mainly to remove the Cosmological Constant Problem.

3.2 Dark Energy and Modified Gravity Models

The discussed shortcomings of the cosmological constant framework have inspired an exploration of alternative approaches to the cosmic acceleration problem. These are, in general, divided into two possible categories: if the model is constructed through the addition of a DE fluid component parametrized by either a static or dynamical equation of state w_{DE}, one talks about a DE Model; in case the modification happens in the gravitational sector itself, resulting in different field equations from those of GR, one refers to it as a MG Theory. Nevertheless, this division is not strict. In fact, there are some MG models in which the modifications can be recast in fluid form and thus treated as in a DE model.

In the case of DE models the modification occurs on the right-hand side of Einstein's equations (2.1), as another matter component is added to the stress-energy tensor, i.e.

$$G_{\mu\nu} = T^{(m)}_{\mu\nu} + T^{(DE)}_{\mu\nu}. \tag{3.3}$$

This means that GR is left untouched as the accepted gravity theory while the added fluid component, characterized by an equation of state parameter verifying $w_{DE} < -1/3$, is introduced as the responsible entity for the late-time acceleration. The main difference between these models and the cosmological constant framework resides in the possibilities for the form of the equation of state parameter. In DE models w_{DE} can be taken either as a constant, usually with $w_{DE} \neq -1$, or as a dynamical function $w_{DE}(t)$. In that sense, the cosmological constant can be regarded as a specific model of DE with $w_{DE} = -1$.

Conversely, MG theories are the somewhat more radical approach. They represent an actual modification of the gravitational sector, meaning that now the changes are introduced in the left-hand side of Einstein's equations, i.e.

$$G^{(GR)}_{\mu\nu} + G^{(MG)}_{\mu\nu} = T^{(m)}_{\mu\nu}, \tag{3.4}$$

which does in fact produce different field equations with respect to GR. To understand how we can achieve this, we recall Lovelock's theorem, which we saw in Section 2.2, and briefly discuss the options it offers to modify the gravitational sector:

a) Introducing new fields in the Lagrangian:

This option translates into a large selection of possibilities. The added fields can be scalar $\phi(t,x)$, vector $v_\mu(t,x)$ or tensor $A_{\mu\nu}(t,x)$ in nature and one can choose to introduce just one or several of them to modify gravity. As examples of MG theories where vector and tensor fields are added we have the Einstein-Æther theory [85] and Massive Gravity [86], respectively. Representing models where a scalar field is introduced, usually known as scalar-tensor theories, we have the simplest case of Quintessence [87]. More complex formulations include Brans-Dicke theory [88] and the most general second-order scalar-tensor theory corresponding to the Horndeski/Galileon theory [22, 23, 89]. The latter shall be the subject of this dissertation.

b) Allowing higher-order field equations:

While Einstein's equations only contain derivatives up to second order, in MG we can look for theories which present higher-order derivatives in their field equations. However, besides being harder to manipulate mathematically, higher-order theories are often plagued by the Ostrogradski's instability [90] which results in an unstable Hamiltonian. Nevertheless, some of them manage to avoid the presence of ghosts, as is the case of $f(R)$ theory [24] whose field equations are fourth-order. In fact, it is possible to show that in some cases higher-order derivative theories can be recast into formulations with second-order field equations plus an extra scalar field, thus evading the Ostrogradski's instability. Such is the case of $f(R)$, which can be re-written as a Brans-Dicke theory [91].

c) Considering a space-time with more than 4 dimensions:

Going to a higher-dimensional space-time might be necessary for a theory to justify some of its characteristics that may appear unnatural when considered in four dimensions. Nonetheless, since so far we can only detect and test four, a four-dimensional effective description should be sufficient to discuss low-energy phenomena. Examples of higher-dimensional theories include the Kaluza-Klein [92] and Dvali-Gabadadze-Porrati (DGP) [93] theories. Galileon theory also possesses an N-dimensional extension [94].

d) Breaking the diffeomorphism invariance:

This option consists of giving up on the diffeomorphism invariance. However, this symmetry can be easily restored by applying the Stückelberg trick [95]. This procedure, which we shall revisit later on, restores the invariance through an infinitesimal time-coordinate transformation that introduces an extra field. Therefore, theories in which the diffeomorphism invariance is broken can simply be viewed as diffeomorphism invariant theories with an extra field, falling back on option a).

To build a MG theory one just needs to adopt at least one of these possibilities. In this dissertation, we shall focus on a specific MG proposal constructed from the introduction of a scalar field, i.e., by choosing to work within option a). Additionally, as we will use the EFT formalism, option d) will also come into play. Nevertheless, as stated, once we restore the diffeomorphism

invariance we end up falling back on option a) all the same. For a more detailed review of these options and models we refer the reader to [18, 20, 21, 84, 96–103] and references therein.

Whatever option (or options) of the above that one decides to work with, one thing is guaranteed: additional Degrees of Freedom (DoFs) will be introduced in the gravitational sector. Since the new DoFs may couple to Standard Model fields, they end up mediating a fifth force between matter sources [84]. However, in laboratory and Solar System scales, where GR has been very well tested [60], no extra DoFs have been detected. Consequently, MG models must have some sort of mechanism capable of locally suppressing the effect of the extra DoFs in order to be compatible with gravity tests. The former are known as *screening mechanisms* [21, 84, 99], and one can classify them according to the nature of the DoF interaction ruling the screening criterion. Following that, we have [84]:

1) Screening controlled by the local properties of the field: this class of screening mechanisms uses the environmental dependence of some properties to suppress the fifth force in high density regions. This is the case for the Chameleon mechanism [104–107], where the scalar field's mass depends on the environment's matter density. In highly dense regions, such as the Solar System, the field's mass becomes very large causing the suppression of the fifth force and actively concealing the field in the local environment. On the other hand, in regions where the density is low, the field becomes lighter and the fifth force is active. This mechanism acts, for example, in $f(R)$ theory. In addition to the Chameleon mechanism, one can also consider the Symmetron mechanism [108, 109]. In the latter, it is the strength of the field's coupling to matter that presents an environmental dependence. In high density regions the coupling becomes very weak, hiding the field's presence.

2) Screening controlled by first derivatives: this screening class relies on self interactions of first-order derivatives of the field becoming important near massive sources, leading to the suppression of the fifth force in such environments. An example of this mechanism is k-mouflage [110].

3) Screening controlled by second derivatives: much like the previous class, it relies on derivative self interactions. This time, however, it is the second-order derivatives that become important near massive sources. This class includes the Vainshtein mechanism [111], which is the one responsible for screening in Massive Gravity and Galileon theory.

Thus, theories that exhibit a screening mechanism are capable of concealing the extra DoF(s) on scales where GR has been well tested, while still providing important modifications of gravity on cosmological scales. This allows for the construction of theories capable of further explanatory and predictive power at large scales that are also able to recover GR at local scales, always aiming for the best possible agreement with observational data.

3.2.1 Galileon Theory

As we have just discussed, there are several options that one can consider when looking to build a MG theory. One of such options is to modify the standard gravitational interaction by introducing an extra scalar DoF. Most often this additional DoF can be described by a scalar field [21, 84], in which case we talk about scalar field theories. This class is among the most explored and well studied alternatives to GR due to the fact that they often produce simple

field equations which admit new solutions that prove useful for the description of both Inflation and late-time cosmic acceleration.

Among the scalar field class we find Galileon theory. First proposed by Nicolis *et al.* in [23], it represents a long distance modification of GR on Minkowski space through the addition of the Galileon scalar field ϕ. The field's designation is born from the fact that the Lagrangian that results from its introduction remains invariant under a generalization of the Galilean invariance given by

$$\phi \to \phi + b_\mu x^\mu + c, \tag{3.5}$$

where b_μ is a vector and c is a constant. This is a hugely attractive feature because it guarantees that the field equations only contain derivatives up to second order, thus avoiding Ostrogradski's ghosts [90] that are known to arise in higher-order theories.

Nevertheless, given that the original formulation of Galileon theory modifies gravity on a Minkowski background, which is suitable for a flat space-time, the theory is not fully covariant. However, during the first attempts at finding a covariant extension for the theory it was also noticed that such an achievement would not be possible while maintaining all of its desired properties, namely the Galilean invariance and the second-order nature of the field equations. As a result, the proposed covariant extension [89] focused on keeping the field equations up to second-order at the cost of losing the Galilean symmetry (3.5).

The covariant formulation of Galileon theory has been generalized [44, 45] to yield the most general scalar field theory with second-order field equations known as GG. Additionally, it has been shown [48] that the GG formulation is equivalent to the most general four dimensional scalar-tensor theory with second-order field equations which had been previously deduced by Horndeski in [22]. For this reason, in literature it is common to find this formulation referred to as both Horndeski and GG theory.

The action describing the GG class can be written as [48]

$$\mathcal{S} = \int d^4x\sqrt{-g}\sum_{i=2}^{5}\mathcal{L}_i \tag{3.6}$$

with the following Lagrangian terms:

$$\mathcal{L}_2 = G_2(\phi, X), \tag{3.7}$$

$$\mathcal{L}_3 = -G_3(\phi, X)\Box\phi, \tag{3.8}$$

$$\mathcal{L}_4 = G_4(\phi, X)R + G_{4,X}\left[(\Box\phi)^2 - (\nabla_\mu\nabla_\nu\phi)^2\right], \tag{3.9}$$

$$\mathcal{L}_5 = G_5(\phi, X)G_{\mu\nu}\nabla^\mu\nabla^\nu\phi - \frac{G_{5,X}}{6}\left[(\Box\phi)^3 - 3(\Box\phi)(\nabla_\mu\nabla_\nu\phi)^2 + 2(\nabla_\mu\nabla_\nu\phi)^3\right], \tag{3.10}$$

where $\Box \equiv \nabla^\mu\nabla_\mu$ is the d'Alembert operator, G_i are arbitrary functions of the scalar field's expectation value ϕ and $X \equiv -\partial_\mu\phi\partial^\mu\phi/2$, and their derivatives are represented as $G_{i,X} \equiv \partial G_i/\partial X$. Specific models are then selected by fixing the functional dependence of the G_i functions. Variations of the action (3.6) with respect to the metric and the scalar field yield the equations of motion for the metric and the scalar field, respectively. Since the complete equations of motion are quite long we shall not present them here, instead referring the reader to [48].

Besides maintaining the attractive property of having second-order field equations, and hence avoiding ghosts, GG models have also been proved capable of driving periods of self-accelerated

expansion. This has led to the consideration of Galileon theory both in the context of the early epoch of Inflation [46–48] and in the period of late-time acceleration [49–55]. Additionally, Galileon theory exhibits the Vainshtein screening mechanism [111, 112], allowing it to hide the presence of the scalar field on small scales. In this case, the scalar field decouples from matter on high density environments due to the growing importance of its non-linear derivative self-interactions in those circumstances.

In Chapter 5, we shall focus on a particular model belonging to the GG class, exploring its implications on the cosmological observables.

3.3 The Discerning Power of Large-Scale Structure Observables

The puzzling challenge posed by late-time acceleration has motivated an enormous scientific effort to explain it. An overwhelming number of DE and MG models have been put forward in search of a viable and complete description of this phenomenon. Nevertheless, in light of the abundance of alternatives proposed and the prospect of accessing new and better quality observational data, thorough testing of the available material has become paramount.

As we have mentioned before, proposed models have to fit observational data in order to be considered as acceptable alternatives to ΛCDM. This needs to be verified both at the background level, where the expansion history must be consistent with distance measurements from geometric probes, and regarding the model's structure formation predictions. The latter has been proving to be vital when trying to discern among competing models [102, 113–116], due to the fact that many of them are practically indistinguishable at the background level. The growth of perturbations and the subsequent structure formation history, however, tend to change from model to model even if they predict a similar background evolution. Thus, the analysis of the perturbation dynamics can offer fundamental information in the process of discerning among alternative models by breaking the degeneracy that exists at the background level.

To study a gravity theory on large scales one uses standard linear perturbation theory. In this framework, the background analysis is complemented by the study of small perturbations on top of an homogeneous and isotropic background. The objective is to obtain a set of evolution equations capable of describing the growth of small inhomogeneities into the observed LSS distribution. Then, the obtained predictions can be compared with the LSS observables, providing important constraints on the parameter space of the model. This treatment is as much valid and useful for the study of DE/MG models as it is for GR.

In this Section we shall review the formalism of linear perturbation theory, compare the evolution equations obtained for GR with those of MG and, finally, discuss the necessary cosmological observables and DE/MG models' impact on them. Therefore, in Section 3.3.1 we walk through the major points of the general procedure of perturbation theory, which we follow with a discussion of the modified forms of the perturbation equations in Section 3.3.2. In Section 3.3.3 we introduce cosmological observables such as the matter power spectrum, the lensing power spectrum and the CMB on which we then consider the effects of DE/MG models in Section 3.3.4.

3.3.1 Standard Perturbation Theory: Formalism

The fundamental objective of Standard Perturbation Theory (SPT), whatever the scientific area to which it is applied, is to find an approximate solution to problems which do not admit an exact one. To that purpose, one takes a known exact solution to a similar problem and considers small deviations around it. The solution to the original problem is then constructed as a series of small perturbative terms of growing order around the known solution for the simpler problem. For example, for a given quantity Z we can write

$$Z = Z_0 + \epsilon Z_1 + \epsilon^2 Z_2 + \epsilon^3 Z_3 + ... + \epsilon^N Z_N + \mathcal{O}\left(\epsilon^{N+1}\right), \tag{3.11}$$

where Z_0 is the known exact solution and ϵ is a small variable quantifying the deviations from Z_0. Then, according to this construction, the bigger the order of a corrective term the smaller its contribution is. Meaning that the terms have progressively smaller impact as the order grows. Therefore, the usual approach is to take the approximate solution by truncating the series at the last order considered to provide an important contribution to the problem at hand.

In the particular case of Cosmology, SPT's objective is to describe the evolution of small perturbations away from homogeneity and isotropy in order to explain structure formation and account for the small existing inhomogeneities that we see, for example, in the CMB. To do so, we must start by understanding to which order in perturbations it might be necessary to go. This will mostly depend on the scale at which we wish to study perturbations. When looking at large enough scales (> 100 Mpc) linear perturbation theory has proven to be highly adequate. However, in smaller local scales, density fluctuations are no longer small and non-linear effects become important. Since we are concerned with studying theories at large scales, we shall limit our review to linear perturbations, i.e., to first order in perturbations.

Now, as previously stated, we are looking to consider small perturbations around an homogeneous and isotropic background. As we saw in Section 2.3, assuming homogeneity and isotropy means that our background metric tensor ($\bar{g}_{\mu\nu}$) and stress-energy tensor ($\bar{T}_{\mu\nu}$) shall be described, respectively, by the FLRW metric (2.18) and the perfect fluid form (2.23). Our first step must then be to perturb the metric tensor by introducing a small perturbation $\delta g_{\mu\nu}$ around the background, i.e.,

$$g_{\mu\nu} = \bar{g}_{\mu\nu} + \delta g_{\mu\nu}, \tag{3.12}$$

where $g_{\mu\nu}$ is the metric tensor for the perturbed space-time. By defining the perturbations as

$$\delta g_{\mu\nu} = \begin{pmatrix} h_{00} & a(t)\tilde{h}_{0i} \\ a(t)\tilde{h}_{i0} & a^2(t)\tilde{h}_{ij} \end{pmatrix}, \tag{3.13}$$

where h_{00}, $\tilde{h}_{0i}$, $\tilde{h}_{i0}$ and $\tilde{h}_{ij}$ are functions of both time and position, the line element for the perturbed FLRW space-time can be explicitly written as

$$ds^2 = -\left(1 - h_{00}\right) dt^2 + 2a(t)\tilde{h}_{i0} dx^i dt + a^2(t)\left(\delta_{ij} + \tilde{h}_{ij}\right) dx^i dx^j, \tag{3.14}$$

where δ_{ij} is the Kronecker delta function which verifies

$$\begin{cases} 0 & \text{if } i \neq j, \\ 1 & \text{if } i = j. \end{cases} \tag{3.15}$$

Next, we consider a further decomposition of the introduced perturbations into scalar, vector and tensor components. This technique, first proposed by Lifshitz in [117], is known as the Scalar-Vector-Tensor (SVT) Decomposition and makes use of the mathematical properties of vectors and tensors. In this case, performing the SVT decomposition leads to

$$h_{00} = -2\psi, \tag{3.16}$$

$$\tilde{h}_{0i} = \partial_i A + B_i, \tag{3.17}$$

$$\tilde{h}_{ij} = -2\phi\delta_{ij} + \partial_i\partial_j C + \partial_i D_j + \partial_j D_i + E_{ij}, \tag{3.18}$$

where $\partial_i B^i = \partial_i D^i = \partial_i E^{ij} = E^i{}_i = 0$. Thus, the 10 DoFs of the metric tensor become divided into: 4 scalar DoFs corresponding to the four scalars $\{\psi, A, \phi, C\}$; 4 vector DoFs coming from the two divergence-less 3-vectors $\{B_i, D_i\}$ and finally 2 tensor DoFs from the transverse and traceless tensor E_{ij}.

Performing the SVT decomposition brings several advantages. On one hand, the evolution equations for each perturbation type do not mix at first order, which means that the different perturbation types evolve independently of each other. Consequently, each perturbation mode can be studied individually without the need to be concerned with the other two. Furthermore, the scalar, vector and tensor perturbations have different origins and physical interpretations. Scalar perturbations are connected to the energy density and pressure perturbations and are also responsible for seeding structure formation. Vector perturbations arise from rotational velocity fields and are expected to fade away with the expansion of the Universe, becoming negligible. Finally, tensor modes are connected with the gravitational DoFs, corresponding to GWs. It is also known that while scalar and tensor perturbations can be produced during Inflation, vector perturbations cannot.

Since in metric theories of gravity the geometry of the Universe is closely related to its matter-energy content, the next step is to perturb the matter-energy sector. To do so, we proceed as we did for the metric tensor: by considering small deviations around the perfect fluid background form of the stress-energy tensor

$$T^\mu{}_\nu = \bar{T}^\mu_\nu + \delta T^\mu{}_\nu, \tag{3.19}$$

where the perturbation is taken to have the following form

$$\delta T^\mu{}_\nu = (\delta\rho + \delta p)\,\bar{u}^\mu\bar{u}_\nu + (\bar{\rho} + \bar{p})\,(\delta u^\mu \bar{u}_\nu + \bar{u}^\mu \delta u_\nu) + \delta p\,\delta^\mu_\nu + \Pi^\mu{}_\nu. \tag{3.20}$$

In the previous expression, the $\bar{\rho}$ and $\bar{p}$ quantities are the background energy density and pressure of the fluid components whereas $\delta\rho$ and δp are their respective perturbations. Additionally, $\bar{u}_\mu$ is the background four-velocity defined in (2.24). By using the normalization condition $g_{\mu\nu}u^\mu u^\nu = -1$ one can deduce that $\delta u^0 = -\psi$. Then, by writing $\delta u^i = v^i/a$ with $v \equiv dx^i/dt$ the peculiar velocity, we get

$$u_\mu = \left(1 - \psi, v^i/a\right) \qquad \text{and} \qquad u^\mu = \left(-1 - \psi, a\left(v^i + \tilde{h}_{0i}\right)\right). \tag{3.21}$$

Moreover, the anisotropic stress tensor $\Pi^\mu{}_\nu$ can be chosen to be orthogonal to u_μ and traceless – $\Pi^0{}_0 = \Pi^0{}_i = 0$ – without any loss of generality. The process of imputing all of the previous results in (3.20) yields the components of the perturbed stress-energy tensor:

$$T^0{}_0 = -(\bar{\rho} + \delta\rho), \tag{3.22}$$

$$T^i{}_0 = -(\bar{\rho} + \bar{p})\, v^i/a, \tag{3.23}$$

$$T^0{}_i = (\bar{\rho} + \bar{p})\left(a\left(v^i + \tilde{h}_{0i}\right)\right), \tag{3.24}$$

$$T^i{}_j = (\bar{p} + \delta p)\,\delta^i_j + \Pi^i{}_j. \tag{3.25}$$

The next step must be, of course, to relate the metric and stress-energy perturbations through Einstein's equations, finally obtaining the perturbed evolution equations. However, before doing this we first draw attention to some of the definitions made so far. We have been perturbing quantities by introducing small deviations from their background values. This means that, implicitly, we have been defining perturbations as the difference between the values of the same quantity in two distinct space-times, for example,

$$\delta g_{\mu\nu} = g_{\mu\nu} - \bar{g}_{\mu\nu}. \tag{3.26}$$

Nevertheless, for such definition to be valid, it has to be done with respect to the same space-time point. In order to ensure that, we need a mapping between the background and the perturbed space-times, i.e., we need to make a *gauge* choice. However, due to GR's covariant nature, there is no preferred way for this correspondence to be made, meaning that there is no preferred gauge choice and the defined perturbations are in fact gauge dependent.

To deal with the ambiguity introduced by gauge freedom one usually has two options: to find and work in gauge invariant quantities or to choose a gauge from the start. A set of gauge-invariant quantities, known as the Bardeen potentials, was found by Bardeen in [118]. If one only considers the scalar perturbation modes, these are given by

$$\Psi = \psi - \frac{d}{dt}\left[a^2\left(\frac{\dot{C}}{2} - \frac{A}{a}\right)\right] \qquad \text{and} \qquad \Phi = \phi - a^2 H\left(\frac{\dot{C}}{2} - \frac{A}{a}\right). \tag{3.27}$$

Regarding the second option, there are several possible gauge choices. Here we shall opt to work in the conformal Newtonian gauge. This choice is equivalent to setting $A = C = 0$ in the previously defined perturbation terms, which according to (3.27) also means that the remaining scalar perturbations coincide with the Bardeen potentials: $\Psi = \psi$ and $\Phi = \phi$. As per the objective of this dissertation, we focus our investigation on scalar perturbations only, therefore, from this point onward we shall limit our discussion to the scalar perturbation modes. Taking all of this into consideration, the perturbed FLRW line element in the Newtonian gauge finally reads

$$ds^2 = -(1 + 2\Psi)\, dt^2 + a^2(t)\,(1 - 2\Phi)\,\delta_{ij} dx^i dx^j. \tag{3.28}$$

We further note that, since the remaining metric perturbations are in fact gauge invariant quantities, the solutions are not affected by any coordinate effects, making it a convenient gauge choice.

Finally, with the metric and stress-energy perturbations computed, one just has to combine them to obtain the linear evolution equations. In GR this means taking Einstein's equations (2.1) and computing its different components. Following this procedure, the perturbed Einstein equations yield 4 constraint equations for the gravitational potentials Ψ and Φ. A system that

is usually complemented by the two conservation equations obtained from the conservation law of the perturbed stress-energy tensor. Besides being quite a lengthy process, the complete derivation of all of the perturbed equations sits beyond the purpose of this dissertation. As such, we shall simply focus on presenting the equations that will be needed in what follows. For a more complete derivation and discussion of the perturbed conservation and Einstein equations we refer the reader to [27, 28, 119, 120].

The first-order perturbed Einstein equations yield 4 evolution equations for the metric potentials. From these we can construct two independent equations relating the metric potentials to the matter perturbations: the Poisson and anisotropy equations. The first results from the combination of the 00 and $0i$ components of the perturbed Einstein equations, and in Fourier space can be written as:

$$-\frac{k^2}{a^2}\Phi = 4\pi G_N \rho \Delta, \tag{3.29}$$

where k is the comoving wavenumber and Δ is the comoving density contrast given by

$$\Delta \equiv \delta + 3H\frac{v}{k}, \tag{3.30}$$

with $\delta = \delta\rho/\bar{\rho}$ the density contrast and v the irrotational component of the peculiar velocity. The choice to work in Fourier space arises from the fact that, in the linear regime, each Fourier mode k evolves independently.

The anisotropy equation, on the other hand, comes from the ij component of the perturbed Einstein equations and translates the difference between the two gravitational potentials:

$$(\Psi - \Phi) = 8\pi G_N a^2 \Pi. \tag{3.31}$$

This means that the difference between the two potentials is related to the anisotropic stress $\Pi^{\mu}{}_{\nu}$. In GR, anisotropic stress can generally be considered negligible at times relevant for structure formation, meaning the two potentials are equal $\Psi = \Phi$. Capitalizing on this last result, it is possible to re-write the Poisson equation into a constraint equation for the lensing potential $\Psi + \Phi$:

$$-\frac{k^2}{a^2}(\Psi + \Phi) = 8\pi G_N \rho \Delta. \tag{3.32}$$

Additionally, the conservation law for the stress-energy tensor – $\nabla_{\mu} T^{\mu}{}_{\nu} = 0$ – provides two extra evolution equations: with $\nu = 0$ one obtains the continuity equation whereas the Euler equation can be derived for $\nu = i$. By combining the Euler, continuity and Poisson equations, it is possible to obtain a second-order differential expression describing either the density contrast δ or the velocity perturbation v. For the density contrast this equation is given by

$$\ddot{\delta} + 2H\dot{\delta} + \frac{k^2}{a^2}\Psi = 0. \tag{3.33}$$

Furthermore, if one uses the Poisson equation to relate Ψ with the density contrast δ, the previous expression can be written completely in terms of the latter, yielding

$$\ddot{\delta} + 2H\dot{\delta} - 4\pi G_N \rho \delta = 0. \tag{3.34}$$

Equations (3.29), (3.31), (3.32) and (3.34) describe the evolution of perturbations in GR. Therefore, if one aims to study the evolution of perturbations in MG models, one has to find

their analogues in MG scenarios.

3.3.2 Modified Evolution Equations

In MG models, where additional DoFs enter in the gravitational interaction, the evolution equations for perturbations can be modified with respect to those of GR. For any given model, the specific forms of these equations can generally be obtained by following the same procedure as the one in Section 3.3.1 but using the respective model's field equations. Nonetheless, when studying the evolution of perturbations in a certain model, it is common to resort to a more practical approach by directly parametrizing the deviations of (3.29), (3.31) and (3.32) from their GR forms [29–32].

For MG models with a single extra scalar DoF, this parametrization is done by introducing three phenomenological functions: $\mu(t,k)$, $\Sigma(t,k)$ and $\eta(t,k)$. These are defined in Fourier space as follows:

$$-\frac{k^2}{a^2}\Phi = 4\pi G_N \mu(t,k)\,\rho\Delta, \tag{3.35}$$

$$\Phi = \eta(t,k)\,\Psi, \tag{3.36}$$

$$-\frac{k^2}{a^2}(\Psi+\Phi) = 8\pi G_N \Sigma(t,k)\,\rho\Delta. \tag{3.37}$$

The $\mu(t,k)$ function is known as the *effective gravitational coupling* and it describes the modifications of the matter clustering through the changes in the Poisson equation. $\Sigma(t,k)$ is known as the *light deflection parameter* and it characterizes the modifications introduced in the paths travelled by photons on cosmological scales via the modification of the lensing potential $\Psi+\Phi$. Finally, the *gravitational slip parameter* $\eta(t,k)$ quantifies the difference between the two gravitational potentials. Each one of these functions parametrizes deviations of the evolution equations from their GR forms, which can be recovered when $\mu=\Sigma=\eta=1$. Thus, any departure from unity is taken as a signature of MG and a signal of deviation from the standard growth scenario.

Given their definitions, it is easy to find the relation between the three functions

$$\Sigma(t,k) = \frac{\mu(t,k)}{2}\left[1+\eta(t,k)\right]. \tag{3.38}$$

Since they are related, one just needs to specify two of them in order to be able to solve for the evolution of perturbations. The problem is that, in general, it is not possible to find exact analytic expressions for these functions. It is, however, possible to obtain functional forms for μ, Σ and η in a specific model if one takes the Quasi-Static Approximation (QSA). By undertaking it, one restricts to perturbation modes below the sound horizon ($c_s^2k^2 \gg a^2H^2$) and ignores the time derivatives of both the scalar field perturbation and the metric potentials in detriment of their spatial gradients. In this regime, one can find analytical expressions for the phenomenological functions describing large model classes [32, 121–123]. We shall return to this point in the next Chapter.

Finally, we also note that the presence of the effective gravitational coupling modifying the Poisson equation (3.35) alters the linear growth equation (3.34) as well:

$$\ddot{\delta} + 2H\dot{\delta} - 4\pi G_N \mu(t,k)\,\rho\delta = 0. \tag{3.39}$$

3.3.3 Cosmological Observables

In the previous subsections we have introduced the necessary quantities to characterize perturbations and their evolution. They include the two gravitational potentials Ψ and Φ and the matter density contrast δ. However, none of these is a direct cosmological observable. Thus, to study and connect them with observations, we analyze their impact on observable quantities such as the matter and lensing power spectra and the CMB. Then, one can compare these predictions with the observational data and perform a statistical analysis over the model's parameters. Therefore, in what follows we shall take the opportunity to review some of the major aspects of the targeted LSS observables in this dissertation.

The Matter Power Spectrum

To study fluctuations in the matter distribution we use the previously defined density contrast $\delta(\vec{x},t)$. However, since by definition the average of all linear perturbations is zero, their statistics are done using two-point auto- or cross-correlation functions and their Fourier transform – the power spectrum. For the case of the density contrast, the power spectrum can be defined as

$$\left\langle \delta(\vec{k},t)\delta^*(\vec{k'},t)\right\rangle = (2\pi)^3\,\delta^{(3)}\left(\vec{k}-\vec{k'}\right)P(k), \tag{3.40}$$

where $\delta^*(\vec{k},t)$ is the complex conjugate of $\delta(\vec{k},t)$ which, in turn, is the Fourier transform of $\delta(\vec{x},t)$ defined as

$$\delta(\vec{k},t) = \int d^3x \delta(\vec{k},t) e^{-i\vec{k}\cdot\vec{x}}, \tag{3.41}$$

where $\vec{k}\cdot\vec{x}$ corresponds to the dot product of the two vectors and the scale k is related to physical length by $k = 2\pi/x$.

The shape of the power spectrum of matter density fluctuations describes the structure forming power as a function of scale. Observationally, it can be probed by surveys of galaxies or galaxy clusters, whose clustering properties can be related to the amplitude of fluctuations in the matter field after taking into account the proper bias factors[1], and the CMB. Only after dealing with the bias can the matter power spectrum be extrapolated. Mathematically it can be computed following [41]

$$P(k) = \frac{2\pi^2}{k^3}\mathcal{P}(k)\Delta_T^2(k), \tag{3.42}$$

where $\mathcal{P}(k) \equiv \Delta^2_{\mathcal{R}}(k)$ is the primordial power spectrum of curvature perturbations and the matter transfer function $\Delta_T(k)$, describing the evolution of matter density perturbations, is defined as

$$\Delta_T(k) = \frac{\delta(k, z=0)\delta(0, z=\infty)}{\delta(k, z=\infty)\delta(0, z=0)} \tag{3.43}$$

with $z \equiv a_0/a(t) - 1$ the redshift.

[1] DM is estimated to be about 84% of the total matter content of the Universe and luminous galaxies are considered biased tracers of the underlying distribution of this dark component. The relation between the spatial distribution of the biased tracer δ_b and the underlying matter density field δ_m can be defined through the bias factor $b \equiv \delta_b/\delta_m$, in a relation known as bias. The real bias is very complicated as it depends on galaxy formation, galaxy types and it might also be influenced by the redshift. In GR and at very large scales the bias has been shown to be scale independent, allowing one to write it as a constant. In MG it is no longer a constant since it depends on both time and scale. However, this is still an open issue because of the complexity of MG models and so a final prescription for the bias does not yet exist.

Cosmic Microwave Background Radiation

The Cosmic Microwave Background (CMB) is a remnant radiation field from the early stages of the Universe predicted by Big Bang theory. According to the latter, in its early stages the Universe was at a high enough temperature to be completely ionized and capable of efficiently thermalizing the radiation field. However, given the ionized state of the Universe, the mean free path of photons before they would suffer Thomson scattering by electrons was very small. Light was incapable of travelling significant distances, i.e., the Universe was opaque. Only later, when the Universe had sufficiently cooled down for protons and electrons to combine and form neutral Hydrogen, would the photons become free to propagate. This is known as the epoch of recombination and it is said that the photons were released from the *last scattering surface*.

As the Universe expands, these photons would have progressively lost energy. This means that nowadays we should expect to detect a signal exhibiting a black body spectrum at a low temperature. The first aware detection of the CMB happened in 1964 when Penzias and Wilson, working at the Bell Telephone Laboratories, recognized it as an excess of antenna temperature [70]. Since then, several measurements of the CMB radiation field have shown it as having a nearly perfect uniform and isotropic black body spectrum with an average temperature of $T \simeq 2.73$ K. Serving, as we have seen, as a supportive argument of the Cosmological Principle. Nevertheless, the largest amount of information provided by the CMB actually comes from its small temperature anisotropies.

The presence of small deviations from the average temperature was first detected by the COBE satellite in 1992 [124]. Since then, missions such as NASA's WMAP [125] and ESA's *Planck* satellite [126] have aimed to map and measure the CMB anisotropies with great precision. The characterization of the existing anisotropies is usually done using the temperature fluctuations $\Delta T(\hat{n})$ around the average in a given direction in the sky $\hat{n}$. These can be expanded on the sphere by using the spherical harmonics basis following

$$\frac{\Delta T(\hat{n})}{T} = \sum_{\ell m} a_{\ell m} Y_{\ell m}(\hat{n}), \tag{3.44}$$

where $Y_{\ell m}(\hat{n})$ are the spherical harmonic functions and ℓ is the multipole which is related to the angular separation, θ, by $\theta = 180^\circ/\ell$. The statistics of the CMB anisotropies are then well described by the temperature-temperature (TT) angular power spectrum C_ℓ^{TT} defined as

$$C_\ell^{TT} = \frac{1}{2\ell+1} \sum_m \langle a_{lm} a_{lm}^* \rangle. \tag{3.45}$$

Given its primordial origins, it comes as no surprise that the CMB contains information about the early stages of the Universe. For example, the smallness of its temperature fluctuations, dating back to the recombination epoch, tells us that perturbations must have started very small before evolving into the structures we now observe. Nevertheless, the CMB anisotropies also receive contributions from redshifts smaller than that of recombination. To analyze this, let us split the anisotropies according to their sources:

$$\frac{\Delta T(\hat{n})}{T} = \left.\frac{\Delta T(\hat{n})}{T}\right|_{\text{LS}} + \left.\frac{\Delta T(\hat{n})}{T}\right|_{\text{ISW}} + \left.\frac{\Delta T(\hat{n})}{T}\right|_{\text{SE}}, \tag{3.46}$$

and describe each of them:

1) Last Scattering (LS): The first term accounts for all the effects acting at the surface of last scattering. This includes the Sachs-Wolfe effect which explains the presence of hotter and colder spots in the CMB as a result of gravitational potential fluctuations at the time of recombination. Photons located at denser regions, where the potential well is consequently bigger, would lose more energy while climbing out after recombination than those located at less dense regions, originating a colder spot on the CMB map. Furthermore, the CMB power spectrum is also observed to have peaks and troughs. These are the result of gravity-driven acoustic oscillations of the photon-baryon plasma before recombination, where the photons' phase differences at the moment of decoupling cause visible temperature oscillations in the CMB.

2) Integrated Sachs-Wolfe (ISW) Effect: The second term of (3.46) accounts for the contribution of the Integrated Sachs-Wolfe (ISW) effect [127]. The latter is rather similar to the regular Sachs-Wolfe effect, the major difference being that it happens along the photons' path from last scattering. In fact, along their trajectories photons might still fall inside potential wells created by structures nearby. If the well's depth remains constant, the energy gain experienced by the photons as they fall inside will be exactly balanced by the loss of energy as they climb out. The net energy of the photons would remain unchanged. On the other hand, if the well either decays or deepens while the photons are inside, there will be either a net gain or loss of energy, creating temperature anisotropies. At linear order, the gravitational potential remains constant when matter dominates the energy budget of the Universe. However, after recombination photons still provide an important contribution to the energy density and the potential evolves in time. This period originates the so called early-ISW effect. Later on, when the DE component becomes dominant, the gravitational potential resumes its evolution in time and gives rise to the late-ISW effect.

3) Secondary Effects (SE): The last term accounts for secondary effects that the CMB radiation might suffer along its way to us. This includes gravitational lensing and the Sunyaev-Zel'dovich effect where the photons receive an energy boost when scattered by hot gas.

These and other effects must be accounted for when estimating the shape of the CMB power spectrum. Here we shall use the convention of [41] for the computation of the temperature-temperature (TT) angular power spectrum which corresponds to:

$$C_\ell^{TT} = (4\pi)^2 \int \frac{dk}{k} \mathcal{P}(k) \left|\Delta_\ell^T(k)\right|^2 \tag{3.47}$$

where the radiation transfer function is given by

$$\Delta_\ell^T(k) = \int_0^{\tau_0} d\tau e^{ik\mu(\tau-\tau_0)} S_T(k,\tau) j_\ell\left[k(\tau_0-\tau)\right]. \tag{3.48}$$

In the previous expression τ is the conformal time, μ is the angular separation, j_ℓ is the spherical Bessel function and S_T is the source for the anisotropies. In particular, the contribution of the

ISW effect to the source function is of the form

$$S_T(k,\tau) \sim \left(\dot{\Phi} + \dot{\Psi}\right), \tag{3.49}$$

translating the effect's dependence on the time evolution of the gravitational potentials.

The CMB has proven to be a fundamental tool of precision Cosmology. Besides shedding light into the conditions of the primordial Universe, the positions of the acoustic peaks also provide important constraints on both the Universe's geometry and the energy densities of the fluid components.

Weak Lensing Power Spectrum

The lensing effect concerns the deflection of light rays by gravitational sources placed along their path. This means that structures throughout the Universe have the power to bend light trajectories, distorting images of distant objects. This makes lensing surveys powerful probes of the matter distribution, especially regarding DM.

As for the study of perturbations, lensing surveys act as probes of the lensing or Weyl potential which, in Newtonian gauge, can be written as $\phi_{len} = (\Phi + \Psi)/2$, because all concerning observables involve spatial gradients of the sum of gravitational potentials: $\nabla_\perp(\Phi + \Psi)$. Then, to describe lensing effects we use the angular lensing power spectrum $C_\ell^{\phi\phi}$. This can be computed using the line of sight integration method, yielding [41]

$$C_\ell^{\phi\phi} = 4\pi \int \frac{dk}{k} \mathcal{P}(k) \left[\int_0^{\chi_*} d\chi S_\phi(k;\tau_0 - \chi) j_\ell(k_\chi)\right]^2, \tag{3.50}$$

where the source term S_ϕ is given as a function of the transfer function $T_\phi(k,\tau) = k\phi_{len}$ as follows:

$$S_\phi = 2T_\phi(k;\tau_0 - \chi)\left(\frac{\chi_* - \chi}{\chi_* \chi}\right). \tag{3.51}$$

In this expression χ is the comoving distance and χ_*, in particular, denotes the comoving distance to the last scattering surface.

3.3.4 The Impact of Dark Energy and Modified Gravity Models on the Cosmological Observables

Different DE and MG models can produce distinct changes at both background and perturbative levels. In turn, these can propagate to the cosmological observables which then show signatures of modifications with respect to GR. Let us list some of the possible effects of DE/MG models on the cosmological observables introduced in the previous Section [128]:

- changes in the growth of structure due to modifications of the Poisson equation (3.29) which then source the density perturbation equation (3.34). These manifest themselves on the matter power spectrum and can cause a mismatch between the amplitude of fluctuations that one infers from the CMB with respect to the one obtained from late-time measurements [129, 130];
- changes on the low-ℓ tails of the CMB TT power spectrum caused by the decay of the gravitational potentials at late-times, i.e., due to modifications on the late-ISW effect;

- shifting of the CMB peaks provoked by a modified expansion history which, subsequently, changes the distance to the last-scattering surface [131];
- modifications on the damping tail (large-ℓ) of the CMB TT power spectrum which can serve as a probe of the abundance of DE at different redshifts [132];
- the ratio between odd and even peaks can be affected if the modifications of gravity treat baryons and CDM differently [133];
- changes on the lensing potential that are connected with the possible modifications of structure growth and distribution, through equation (3.35), as well as modifications on the evolution of the gravitational potentials through equation (3.37) [134, 135].

Each of these modifications constitutes a potentially distinguishable feature to be constrained by observational data, offering the possibility of disentangling MG from GR. In fact, when compared to observations, some of these characteristics can even offer the necessary evidence for discarding some proposals or to explore some others in greater detail. They also constitute a null-test of GR, in the sense that if no modifications are found, this constitutes evidence in favor of Einstein's theory.

In Chapter 5, we will investigate a specific MG model and illustrate how the above features can show up on the concerning LSS observables.

Chapter 4

Effective Field Theory of Dark Energy and Modified Gravity

The theoretical shortcomings of ΛCDM and, in particular, of the cosmological constant framework have fueled the proposal of a large amount of alternative theories. This, in turn, has called for rigorous testing of the available alternatives aiming to get a better grasp on the mechanism behind late-time acceleration. For this task, one calls upon SPT in the hope of discerning between competing models using both background and perturbative arguments.

However, the fact that generally each model is described by a specific set of equations tends to complicate the testing process since every proposal needs to be treated individually. Only after this individual treatment can they be compared, on a performance basis, against one another or, as is usual, against the best fit model available, which so far is ΛCDM. Of course, to proceed like this would be to embark on a lengthy and strenuous enterprise. Therefore, finding more encompassing and model-independent approaches became paramount.

The goal is to find a unifying description capable of embracing the maximum number possible of models, while also allowing for a more efficient method of comparison against observational data. Among different proposals to deal with these necessities, the formulation of the Effective Field Theory (EFT) of Dark Energy and Modified Gravity [34, 35] is the one with the strongest connection with the underlying physics. The EFT framework had previously achieved success in Particle Physics, inspiring its cosmological applications first to Inflation [136, 137] and then later to the problem of cosmic acceleration.

The EFT of DE/MG provides a model-independent framework to describe the evolution of linear cosmological perturbations in all theories of gravity with a single additional scalar DoF. Its formulation happens at the level of the action which is written in terms of perturbed quantities. The latter must be at most of second-order in perturbations and, as a consequence of choosing to work in unitary gauge, must also remain invariant under time-dependent spatial diffeomorphisms. The result is a general action composed by all operators that respect the imposed symmetries and that appear organized according to their perturbative order and accompanied by time-dependent coefficients. These coefficients, known as the EFT functions, are all that one then needs to describe both the background and the perturbation dynamics.

Thanks to its construction, the EFT framework constitutes a powerful tool for studying gravity theories. On a first level, one can capitalize on its model-independent language and investigate the impact of the various EFT operators on the cosmological observables [41, 138].

In this case, all one has to do is to choose which of the EFT functions to set to zero and what functional forms to give to the ones associated with the operators of interest. Alternatively, one can focus on a specific model covered by the EFT framework after it is mapped into the EFT language [34, 36, 139]. This *mapping* procedure basically entails computing the specific forms of the EFT functions for the model in question.

To further simplify and expedite the study of cosmological perturbations it is also quite useful and common to resort to Einstein-Boltzmann codes. These are numerical tools capable of evolving the linear perturbation equations. Before the development of EFT, the publicly available codes were almost exclusively directed at the investigation of GR, with the two major players in the game being the Code for Anisotropies in the Microwave Background (`CAMB`) [37, 39] and the Cosmic Linear Anisotropy Solving System (`CLASS`) [38, 140]. As a consequence, any time that one wished to explore a different model a specific numerical code had to be built for the occasion which would then, most of the times, be kept private. Thus, studying DE/MG models was frequently a tiresome and complicated process.

To make this type of studies globally easier and faster, the full potential of both the EFT framework and the Einstein-Boltzmann solvers can be exploited by implementing the former in some of these numerical tools, thus combining the unifying power of the first with the practical utility of the second. The result is a collection of Einstein-Boltzmann codes such as the Effective Field Theory for `CAMB` (`EFTCAMB`) [41, 42], Horndeski in `CLASS` (`hi_class`) [141], Cosmology Object Oriented Package (`COOP`) [142] and Equation of State for `CLASS` (`EoS_class`) [143].

Since the aim of this dissertation is to investigate the phenomenology of a specific GG model which is encompassed by the EFT framework, we shall take advantage of the former by mapping our model into the EFT language in order to use the `EFTCAMB` solver. This code is the result of the implementation of the EFT approach into `CAMB` and it can be employed to evolve the full dynamics of linear cosmological perturbations. The use of this solver will expedite our analysis since instead of going through the lengthy process of computing and implementing the specific perturbation equations of our model, we can simply map it into the EFT language and use the general perturbation equations computed for the EFT action which are already implemented in the code. `EFTCAMB`'s output will then include the computed expectations for cosmological observables such as the ones presented in Section 3.3.3, which in our case can be used to evaluate the impact of the model on LSS.

In this Chapter we shall go over the EFT formalism and the basic workings of `EFTCAMB`, organizing it as follows. We start by reviewing the EFT formulation in Section 4.1. Following this, in Section 4.2 we take advantage of this language to explore the modified forms of the background Friedmann equations in DE/MG models. In Section 4.3 we present the Stückelberg trick as the necessary step to obtain the evolution equation for the scalar DoF of the theory. Then, to allow for model-specific studies using the EFT formalism, we review the mapping procedure in Section 4.4. In Sections 4.5 and 4.6 we briefly present the enforced stability conditions that guarantee a viable evolution and an alternative parametrization for the GG class, respectively. We revisit the μ, η and Σ parametrization in Section 4.7, presenting their analytical forms under the QSA for the GG model class. Finally, in Section 4.8 we explore the purpose and structure of `EFTCAMB`.

4.1 Action and Formulation

The EFT formulation for DE/MG models, introduced in [34, 35], occurs at the action level. The goal was to build the most general action in unitary gauge capable of describing perturbations around a FLRW background of a gravity theory with a single extra scalar DoF and a matter sector assumed to verify the Weak Equivalence Principle (WEP) [21]. In what follows we shall review the main steps taken in the construction of the EFT action.

Firstly, we start by discussing the choice of unitary gauge. This corresponds to the gauge in which the perturbation of the scalar field vanishes, being "eaten" by the metric. Effectively, if we define the scalar field perturbation $\delta\phi$ as

$$\delta\phi(t,\vec{x}) = \phi(t,\vec{x}) - \bar{\phi}(t), \tag{4.1}$$

where $\bar{\phi}$ is the field's background value, working in unitary gauge is, in practice, choosing the time-coordinate such that $\delta\phi = 0$. The selection of this gauge has two major implications for the EFT action. The first is that the extra scalar DoF will not be explicitly present. The second is that the full diffeomorphism invariance is broken, only the subgroup of time-dependent spatial diffeomorphisms survives.

As a consequence, the operators figuring in the EFT action must be constructed from quantities that remain invariant under the residual symmetries of unbroken time-dependent spatial diffeomorphisms. The different operators can then be constructed from quantities such as the metric tensor $g_{\mu\nu}$, the unit vector perpendicular to the time-slicing n_μ defined as

$$n_\mu = \frac{\partial_\mu\phi}{\sqrt{-(\partial_\mu\phi)^2}}, \tag{4.2}$$

the extrinsic curvature $K_{\mu\nu}$ and its trace K, the Ricci scalar R and any other curvature invariants and contractions of tensors with $g_{\mu\nu}$, n_μ and covariant derivatives ∇_μ. Furthermore, the action's symmetry also allows the presence of a time-dependent coefficient accompanying each of the operators. These coefficients are usually known as EFT functions.

Working in unitary gauge has yet another attractive feature: the operators that enter in the EFT action can be organized in powers of perturbations. Thanks to this, it becomes easy to identify which of the operators contribute at what level, be it the background level, at linear order in perturbations or even higher.

In addition to the choice of unitary gauge, the EFT formulation assumes the validity of the WEP. This is done to ensure that matter fields (Ψ_γ) only appear in the corresponding matter action ($\mathcal{S}_\gamma$) and that all of them couple to the same metric $g_{\mu\nu}$. Once this imposition is made, it is possible to choose a conformal frame in which the matter couples only to the metric and not the scalar field: the Jordan frame. Therefore, the matter action in the Jordan frame is a functional of the matter fields and the metric only: $\mathcal{S}_\gamma[\Psi_\gamma, g_{\mu\nu}]$.

As a result of the previous choices we can expect the final EFT action to be written in unitary gauge and Jordan frame, containing all operators that remain invariant under time-dependent spatial diffeomorphisms and which will appear ordered in powers of perturbations. However, even after imposing the previous conditions, there is still a substantial number of operators capable of meeting the requirements. Thus, when writing the action it helps to understand which of the operators are going to be truly relevant. In our review, we shall limit the EFT action up to second

order in perturbations, keeping in sight our desire to focus on linear perturbation theory, and consider the necessary operators to cover most of the DE/MG models of cosmological interest. These include the Horndeski/GG class, Gleyzes-Langlois-Piazza-Vernizzi (GLPV) [144, 145] and low-energy Hořava [146, 147].

Following this, the EFT action reads [36, 148]:

$$\mathcal{S} = \int d^4x\sqrt{-g}\Bigg[\frac{{m_0}^2}{2}\left(1+\Omega(t)\right)R + \Lambda(t) - c(t)\delta g^{00} + \frac{M_2^4(t)}{2}\left(\delta g^{00}\right)^2 - \frac{\bar{M}_1^3(t)}{2}\delta g^{00}\delta K \\ - \frac{\bar{M}_2^2(t)}{2}\left(\delta K\right)^2 - \frac{\bar{M}_3^2(t)}{2}\delta K^\mu_\nu \delta K^\nu_\mu + \frac{\hat{M}^2(t)}{2}\delta g^{00}\delta\mathcal{R} + m_2^2(t)h^{\mu\nu}\partial_\mu g^{00}\partial_\nu g^{00}\Bigg] + \mathcal{S}_\gamma \qquad (4.3)$$

where $h^{\mu\nu} = (g^{\mu\nu} + n^\mu n^\nu)$ is the spatial metric on constant-time hypersurfaces and δg^{00}, δK^μ_ν, δK and $\delta\mathcal{R}$ are the perturbations of the time-time metric component, the extrinsic curvature, its trace and the trace of the 3-dimensional Ricci tensor $\mathcal{R}_{\mu\nu}$, respectively. We can also identify a set of time-dependent coefficients accompanying each operator. These are the so-called EFT functions. In the case of action (4.3) we can find the following nine:

$$\Omega,\ \Lambda,\ c,\ M_2^4,\ \bar{M}_1^3,\ \bar{M}_2^2,\ \bar{M}_3^2,\ \hat{M}^2 \text{ and } m_2^2\ . \qquad (4.4)$$

Furthermore, we previously mentioned that one of the advantages of working in unitary gauge is the possibility to organize operators according to their order in perturbations. Thanks to this feature, we can easily split the operators in the action into two categories: those which affect both the background and perturbation equations and those which only contribute to the perturbative sector. Only the operators that are up to linear order in perturbations belong to the first group. Thus, only the associated EFT functions $\Omega(t)$, $\Lambda(t)$ and $c(t)$ will enter both the background and perturbation equations. The others only enter at the level of perturbations.

Finally, we note that so far the constructed formalism remains completely model-independent. In fact, by varying the action (4.3) with respect to the metric and the matter fields, one can obtain the equations of motion describing several cosmological models just in terms of the EFT functions. It is then possible to study different observables purely in terms of the impact that selected operators have on them, without any model specification. On the other hand, it is also easy to switch to model-specific investigations simply by finding the specific form of the EFT functions in the desired model. The latter procedure goes by the name of *mapping* and we shall explore it in Section 4.4.

The four major classes encompassed by the EFT action (4.3) are:

- Generalized Brans-Dicke (GBD) theories which are described only by the background functions Ω, Λ and c;
- Horndeski/GG theories for which the EFT function m_2^2 is not present and the relation $\bar{M}_2^2 = -\bar{M}_3^2 = 2\hat{M}^2$ is verified;
- GLPV theories which also verify $m_2^2 = 0$ and $\bar{M}_2^2 = -\bar{M}_3^2$;
- the general class of Lorentz violating theories in which the m_2^2 function is present. In the specific case of low-energy Hořava the functions $\bar{M}_1^3$ and $\hat{M}^2$, however, are absent.

4.2 Modified Background Friedmann Equations

Back in Section 2.3.3 we obtained the Friedmann equations describing the background evolution of ΛCDM on a FLRW Universe. Now, we can make use of the model-independent formalism provided by EFT to obtain the background Friedmann equations for DE/MG models. We start by remembering that only operators up to first order in perturbations will affect the background dynamics, meaning that for our current purpose it is sufficient to consider the following action:

$$\mathcal{S}_0 = \int d^4x\sqrt{g}\left[\frac{m_0^2}{2}\left(1+\Omega(t)\right)R + \Lambda(t) - c(t)\delta g^{00}\right] + \mathcal{S}_\gamma\left[g_{\mu\nu}, \Psi_\gamma\right]. \tag{4.5}$$

Then, to obtain the modified Friedmann equations we vary the previous action with respect to the metric. Assuming a FLRW metric with spatial curvature κ this yields:

$$H^2 + \frac{\kappa}{a^2} = \frac{1}{3m_0^2(1+\Omega)}\left(\bar{\rho}_\gamma + 2c - \Lambda\right) - H\frac{\dot{\Omega}}{1+\Omega}, \tag{4.6}$$

$$\dot{H} + H^2 - \frac{\kappa}{a^2} = -\frac{1}{6m_0^2(1+\Omega)}\left(\bar{\rho}_\gamma + 3\bar{p}_\gamma\right) - \frac{c+\Lambda}{3m_0^2(1+\Omega)} - \frac{\ddot{\Omega} + H\dot{\Omega}}{2(1+\Omega)}. \tag{4.7}$$

At the background level we can continue to treat matter as a perfect fluid; therefore, the energy density and pressure of these components still verify the standard continuity equation given by equation (2.26).

However, if we adopt a fluid-like description for the extra DoF and define a background energy density $\bar{\rho}_{DE}$ and pressure $\bar{p}_{DE}$ for the effective dark fluid as

$$\bar{\rho}_{DE} \equiv 2c - \Lambda - 3m_0^2 H\dot{\Omega}, \tag{4.8}$$

$$\bar{p}_{DE} \equiv \Lambda + m_0^2\left(\ddot{\Omega} + 2H\dot{\Omega}\right), \tag{4.9}$$

the Friedmann equations (4.6) and (4.7) can be re-written in the more familiar fluid form:

$$H^2 = \frac{1}{3m_0^2(1+\Omega)}\left(\bar{\rho}_\gamma + \bar{\rho}_{DE}\right) - \frac{\kappa}{a^2}, \tag{4.10}$$

$$\dot{H} + H^2 = -\frac{1}{6m_0^2(1+\Omega)}\left(\bar{\rho}_\gamma + 3\bar{p}_\gamma + \bar{\rho}_{DE} + 3\bar{p}_{DE}\right) + \frac{\kappa}{a^2}. \tag{4.11}$$

Thus, given the forms of $\bar{\rho}_{DE}$ and $\bar{p}_{DE}$, we verify that in the EFT framework the modifications to the Friedmann equations with respect to those of ΛCDM can be described in terms of the EFT functions. Additionally, by differentiating equation (4.10) with respect to time and then combining it with equations (2.26) and (4.11), one can also obtain a continuity equation for the dark fluid component:

$$\dot{\bar{\rho}}_{DE} + 3H\left(\bar{\rho}_{DE} + p_{DE}\right) = 3m_0^2\dot{\Omega}\left(H^2 + \frac{\kappa}{a^2}\right), \tag{4.12}$$

from which it becomes clear that the energy density $\bar{\rho}_{DE}$ of the dark component will only be conserved when the Ω function is constant.

Moreover, we remember that the EFT of DE/MG provides a model-independent framework for the study of linear cosmological perturbations. When performing such studies it is not uncommon to fix the background history *a priori* and just focus on the dynamics of perturbations.

The background evolution is usually fixed to be equal, or at least close, to that of ΛCDM since the latter remains in very good agreement with cosmological observations. The description of the background dynamics is done by the Friedmann equations in which three unknown EFT functions $\{\Omega, \Lambda, c\}$ and the Hubble parameter H figure. Therefore, to fix the background evolution, two out of these four functions must be fixed, while the other two can then be obtained from the modified Friedmann equations. The common procedure is to choose a form for Ω and an EoS for the dark component w_{DE} to fix the expansion history $H(t)$. After this, the remaining EFT functions, Λ and c, can be obtained from the Friedmann equations through

$$\Lambda(t) = -m_0^2\left(\ddot{\Omega} + 2H\dot{\Omega}\right) - m_0^2(1+\Omega)\left[2\dot{H} + 3H^2 - \frac{\kappa}{a^2}\right] - \bar{p}_\gamma, \tag{4.13}$$

$$c(t) = -\frac{m_0^2\ddot{\Omega}}{2} + \frac{m_0^2 H\dot{\Omega}}{2} + m_0^2(1+\Omega)\left[\frac{2\kappa}{a^2} - \dot{H}\right] - \frac{1}{2}(\bar{\rho}_\gamma + \bar{p}_\gamma). \tag{4.14}$$

4.3 The Stückelberg Trick: Restoring the Full Diffeomorphism Invariance

In Section 4.1 we saw that the EFT action is built in unitary gauge. This allowed the operators to be organized in terms of their order in perturbations, allowing for a simpler identification of which operators contribute at a given level. However, working in unitary gauge also means that the extra scalar DoF of the theory does not explicitly appear in the action.

Since the scalar DoF is not explicitly present, it becomes impossible to find an evolution equation for it, making the unitary gauge unsuitable for a complete study of the evolution of linear perturbations. Nevertheless, it is rather simple to make the scalar DoF reappear by applying the Stückelberg trick [95]. The latter restores the full diffeomorphism invariance by introducing a scalar field π representing the perturbation of the scalar DoF. In practice, this corresponds to performing the following infinitesimal time-coordinate transformations:

$$t \to t + \pi(x^\mu), \qquad x^i \to x^i\ . \tag{4.15}$$

As a result of the previous transformations, terms with π appear in the action in two ways:

- The transformation of time-dependent functions introduces undifferentiated π terms, for example:
$$\Omega(t) \to \Omega(t+\pi) = \Omega(t) + \dot{\Omega}(t)\pi + \frac{1}{2}\ddot{\Omega}(t)\pi^2 + \dots\ , \tag{4.16}$$
where $\Omega(t+\pi)$ is Taylor expanded;

- The transformation of non-scalar quantatites that are not fully diffeomorphism invariant generate terms with derivatives of π, for example [34, 35]:
$$\delta K \to \delta K - 3\dot{H}\pi - \frac{1}{a^2}\nabla^2\pi, \tag{4.17}$$
where $\nabla^2 = \nabla_\mu\nabla^\mu$.

Thus, after applying the Stückelberg trick the action given in equation (4.3) becomes [35]

$$\mathcal{S}=\int d^4x\sqrt{-g}\Bigg[\frac{m_0^2}{2}\left(\Omega(t+\pi)+1\right)R+\Lambda(t+\pi)-c(t+\pi)\Bigg(\delta g^{00}-2\dot{\pi}+2\dot{\pi}\delta g^{00}+2\tilde{\nabla}_i\pi g^{0i}$$
$$-\dot{\pi}^2+\frac{\tilde{g}^{ij}}{a^2}\tilde{\nabla}_i\pi\tilde{\nabla}_j\pi+...\Bigg)+\frac{M_2^4(t+\pi)}{2}\left(\delta g^{00}-2\dot{\pi}+...\right)^2$$
$$-\frac{\bar{M}_1^3(t+\pi)}{2}\left(\delta g^{00}-2\dot{\pi}+...\right)\left(\delta K^{\mu}{}_{\mu}+3\dot{H}\pi+\frac{\tilde{\nabla}^2\pi}{a^2}+...\right)$$
$$-\frac{\bar{M}_2^2(t+\pi)}{2}\left(\delta K^{\mu}{}_{\mu}+3\dot{H}\pi+\frac{\tilde{\nabla}^2\pi}{a^2}+...\right)^2$$
$$-\frac{\bar{M}_3^2(t+\pi)}{2}\left(\delta K^{i}{}_{j}+\dot{H}\pi\delta^i_j+\frac{\tilde{g}^{ik}}{a^2}\tilde{\nabla}_k\tilde{\nabla}_j\pi+...\right)\left(\delta K^{j}{}_{i}+\dot{H}\pi\delta^j_i+\frac{\tilde{g}^{jl}}{a^2}\tilde{\nabla}_l\tilde{\nabla}_i\pi+...\right)$$
$$+\frac{\hat{M}^2(t+\pi)}{2}\left(\delta g^{00}-2\dot{\pi}+...\right)\left(\delta R^{(3)}+4H\frac{\tilde{\nabla}^2\pi}{a^2}+...\right)$$
$$+{m_2}^2(t+\pi)\left(g^{\mu\nu}+n^\mu n^\nu\right)\partial_\mu\left(g^{00}-2\dot{\pi}+...\right)\partial_\nu\left(g^{00}-2\dot{\pi}+...\right)+...\Bigg]+\mathcal{S}_\gamma, \tag{4.18}$$

where we have truncated the contributions up to second order in perturbations and tildes denote quantities associated with the spatial metric. Varying this action with respect to π yields the evolution equation for the extra scalar DoF which can be written as

$$A\ddot{\pi}+B\dot{\pi}+C\pi+k^2D\pi+E=0, \tag{4.19}$$

where the spatial part has been Fourier transformed and A, B, C, D and E are functions of both time and scale whose expressions can be found in [149]. In order to obtain observable predictions, this equation must be solved together with the other perturbative equations obtained from the variation of action (4.18) with respect to the metric components.

4.4 Mapping Procedure

So far we have mainly discussed the model-independent aspect of the EFT formalism. Nevertheless, as we have mentioned before, it is also possible to study specific models by finding the corresponding forms of the EFT functions. The process of finding this correspondence is known as the *mapping procedure*, and it is through it that one can can translate a wide variety of DE/MG models with a single extra scalar DoF into the EFT language.

There are generally two options that one can take when trying to compute the mapping of a certain model. The first one is a more model-specific approach. One starts from the covariant action describing the target model and imposes the unitary gauge. Once this is done, the model's action must be compared to the one for EFT in order to work out the correspondence between the model's terms and the EFT operators. This type of approach involves an individual treatment of each model and can even become quite tricky for the more complex cases.

Alternatively, the second option offers a more general mapping recipe. In this case, the mapping is worked out for a general Lagrangian containing all necessary operators and already

written in unitary gauge. This procedure yields expressions for the EFT functions in terms of the Lagrangian terms. Then, to obtain the mapping for a specific model one just needs to relate its Lagrangian to the one used for the general mapping, in a process that is, in general, simpler. This is the approach that we shall adopt when looking to map our target model, and thus the one we shall explore here by following the procedure as presented in [36].

At the basis of the second mapping procedure rests the Arnowitt-Deser-Misner (ADM) formalism [150]. Similarly to the FLRW metric, the ADM formalism is a $3+1$ decomposition of space-time. In this case, however, the corresponding line element is given by [36]

$$ds^2 = -N^2 dt^2 + h_{ij}\left(dx^i + N^i dt\right)\left(dx^j + N^j dt\right), \tag{4.20}$$

where $N(t,x^i)$ is the lapse function, $N^i(t,x^i)$ is the shift and $h_{ij}(t,x^i)$ is the three-dimensional metric. As shown in [151], it is possible to use the ADM formalism to write a general Lagrangian form describing scalar-tensor theories containing spatial derivatives up to sixth order. For the purpose of this dissertation, however, it is sufficient to consider a general Lagrangian that encompasses the same models as action (4.3). This corresponds to

$$\mathcal{L} = \mathcal{L}\left(N, \mathcal{R}, \mathcal{S}, K, \alpha_1, t\right), \tag{4.21}$$

where the new quantities $\mathcal{S}$ and α_1 figuring above are defined as

$$\mathcal{S} = K_{\mu\nu}K^{\mu\nu} \qquad \text{and} \qquad \alpha_1 = a^i a_i, \tag{4.22}$$

with $a_\nu \equiv n^\mu \nabla_\mu n_\nu$ the acceleration of the normal vector n_μ.

Next we wish to find the mapping of Lagrangian (4.21) into the EFT formalism. To do so, we need to start by expanding the Lagrangian up to second order in perturbations, so as to match the construction of the EFT action. Again taking a FLRW background, the expansion of the quantities featured in the Lagrangian (4.21) yields [36]

$$\begin{aligned} &\delta K = 3H + K, && \delta K_{\mu\nu} = H h_{\mu\nu} + K_{\mu\nu}, \\ &\delta\mathcal{S} = -3H^2 + \mathcal{S} = -2H\delta K + \delta K^\mu_\nu \delta K^\nu_\mu, && \delta\alpha_1 = \partial_i \delta N \partial^i \delta N. \end{aligned} \tag{4.23}$$

Using the previous results, the ADM action, taken up to second order in perturbations only, can be written as [148]:

$$\begin{aligned} \mathcal{S}_{ADM} = \int d^4x\sqrt{-g}\Big[&\bar{\mathcal{L}} + \dot{\mathcal{F}} + 3H\mathcal{F} + \left(\mathcal{L}_N - \dot{\mathcal{F}}\right)\delta N + \left(\dot{\mathcal{F}} + \frac{1}{2}\mathcal{L}_{NN}\right)(\delta N)^2 \\ &+ \mathcal{L}_{\mathcal{S}}\delta K^\nu_\mu \delta K^\mu_\nu + \frac{1}{2}\mathcal{A}(\delta K)^2 + \mathcal{B}\delta N\delta K + \mathcal{C}\delta K\delta\mathcal{R} + \mathcal{L}_{N\mathcal{R}}\delta N\delta\mathcal{R} \\ &+ \mathcal{L}_{\mathcal{R}}\delta R + \frac{1}{2}\mathcal{L}_{\mathcal{R}\mathcal{R}}\delta\mathcal{R}^2 + \mathcal{L}_{\alpha_1}\partial_i\delta N\partial^i\delta N\Big], \end{aligned} \tag{4.24}$$

where $\bar{\mathcal{L}}$ is the Lagrangian evaluated on the background and $\mathcal{L}_X \equiv \partial\mathcal{L}/\partial X$ is the derivative of the Lagrangian with respect to the quantity X. Furthermore, the following definitions have been made:

$$\begin{aligned} &\mathcal{F} = \mathcal{L}_K - 2H\mathcal{L}_{\mathcal{S}}, && \mathcal{A} = \mathcal{L}_{KK} + 4H^2\mathcal{L}_{\mathcal{S}\mathcal{S}} - 4H\mathcal{L}_{\mathcal{S}K}, \\ &\mathcal{B} = \mathcal{L}_{KN} - 2H\mathcal{L}_{\mathcal{S}N}, && \mathcal{C} = \mathcal{L}_{K\mathcal{R}} - 2H\mathcal{L}_{\mathcal{S}\mathcal{R}}. \end{aligned} \tag{4.25}$$

The next step is to write the EFT action in ADM formalism. After this, both actions stand on equal footing and can be directly compared to work out the mapping between them. To achieve this, there are some necessary manipulations of the EFT terms. Firstly, the δg^{00} quantity used in EFT needs to be connected to δN used in ADM formalism. For that we have the following transformation:

$$g^{00} = -\frac{1}{N^2} = -1 + 2\delta N - 3(\delta N)^2 + ... \equiv -1 + \delta g^{00}, \tag{4.26}$$

from which we can conclude that $\left(\delta g^{00}\right)^2 = 4\left(\delta N\right)^2$. Then, the majority of the quantities featured in action (4.3) can easily be converted into the ADM formalism by using the relations given in equation (4.23). The exception is the $(1+\Omega(t))R$ term which requires a more extensive treatment, including the use of the Gauss-Codazzi relation [152], to be translated into ADM notation. For the explicit manipulation of this term we refer the reader to [36]. Here we present the final result of the complete conversion of the EFT action into ADM formalism [36, 148]:

$$\begin{aligned}
\mathcal{S}_{EFT} = \int d^4x\sqrt{-g}\Bigg\{ & \frac{m_0^2}{2}(1+\Omega)\mathcal{R} + 3H^2m_0^2(1+\Omega) + 2\dot{H}m_0^2(1+\Omega) + 2m_0^2H\dot{\Omega} + m_0^2\ddot{\Omega} \\
& + \Lambda + \left[H\dot{\Omega}m_0^2 - 2\dot{H}m_0^2(1+\Omega) - \ddot{\Omega}m_0^2 - 2c\right]\delta N \\
& - \left(m_0^2\dot{\Omega} + \bar{M}_1^3\right)\delta K\delta N + \frac{1}{2}\left[m_0^2(1+\Omega) - \bar{M}_3^2\right]\delta K_\nu^\mu \delta K_\mu^\nu \\
& - \frac{1}{2}\left[m_0^2(1+\Omega) + \bar{M}_2^2\right](\delta K)^2 + \hat{M}^2\delta N\delta\mathcal{R} \\
& + \left[2\dot{H}m_0^2(1+\Omega) + \ddot{\Omega}m_0^2 - Hm_0^2\dot{\Omega} + 3c + 2M_2^4\right](\delta N)^2 \\
& + 4m_2^2h^{\mu\nu}\partial_\mu\delta N\partial_\nu\delta N\Bigg\}.
\end{aligned} \tag{4.27}$$

Finally, to find the mapping between the EFT framework and the Lagrangian in ADM formalism one has to compare actions (4.24) and (4.27), looking to identify the correspondences between the operators. This comparison process yields the following expressions for the EFT functions in terms of the ADM Lagrangian terms:

$$\begin{aligned}
&\Omega(t) + 1 = \frac{2}{m_0^2}\mathcal{L}_R, && c(t) = \frac{1}{2}\left(\dot{\mathcal{F}} - \mathcal{L}_N\right) + \left(H\dot{\mathcal{L}}_\mathcal{R} - \ddot{\mathcal{L}}_\mathcal{R} - 2\mathcal{L}_\mathcal{R}\dot{H}\right), \\
&\Lambda(t) = \bar{\mathcal{L}} + \dot{\mathcal{F}} + 3H\mathcal{F} - 2\left(3H^2\mathcal{L}_\mathcal{R} + \ddot{\mathcal{L}}_\mathcal{R} + 2H\dot{\mathcal{L}}_\mathcal{R} + 2\dot{H}\mathcal{L}_\mathcal{R}\right), \\
&\bar{M}_2^2(t) = -\mathcal{A} - 2\mathcal{L}_\mathcal{R}, && M_2^4(t) = \frac{1}{2}\left(\mathcal{L}_N + \frac{\mathcal{L}_{NN}}{2}\right) - \frac{c}{2}, \\
&\bar{M}_1^3(t) = -\mathcal{B} - 2\dot{\mathcal{L}}_\mathcal{R}, && \bar{M}_3^2(t) = -2\mathcal{L}_\mathcal{S} + 2\mathcal{L}_\mathcal{R}, \\
&m_2^2(t) = \frac{\mathcal{L}_{\alpha_1}}{4}, && \hat{M}^2(t) = \mathcal{L}_{N\mathcal{R}}.
\end{aligned} \tag{4.28}$$

Once equipped with this mapping, one just needs to write the action describing the target model in ADM formalism, without having to perturb it up to second order. After this, the mapping is completely determined by the relations in (4.28).

For the GG class, both the translation of the Galileon action to ADM formalism as well as the corresponding expressions for the EFT functions can be found in [36]. We have retraced the steps followed in the previous reference and obtained the same mapping expressions but, for the purpose of brevity, we shall not reconstruct this process here. Later on, we shall use the

mapping provided in [36] to obtain the specific forms of the EFT functions for the target model of this dissertation.

4.5 Stability Conditions

The fact that EFT is formulated at the action level also offers an important level of control over the theoretical physical stability of the theory. Since the construction of the action is done in a general way, aiming to describe several different theories with an extra scalar DoF, it is possible to obtain a generic model-independent handle on the theoretical viability conditions that ensure the stability of a theory. In fact, it is possible to impose conditions upon the EFT functions, before their functional forms have even been specified, in order to avoid the development of a non-physical behaviour.

The main concerns usually are the ghost, gradient, tachyonic and Jeans instabilities, which are related to the propagation of both scalar and tensor modes. In this case, our concern is with the evolution of the extra scalar DoF - $\pi(x^\mu)$. For the GG model class, a series of field redefinitions can be performed in order to diagonalize the system and de-mix the π field from gravity [34, 153]. Such a procedure yields a quadratic action ruling the propagation of the scalar DoF which can be written as [153]

$$\mathcal{S}_\pi = \int dx^4 a^3 m_0^2 \left[A(t)\dot{\pi}^2 - B(t)\frac{(\nabla\pi)^2}{a^2} \right] + \dots \,, \tag{4.29}$$

where the ellipsis stands for terms that are lower in derivatives and A and B are functions of the EFT functions.

Out of the three instabilities we have mentioned, the ghost and gradient instabilities are the most concerning. We talk about a *ghost instability* when there are modes with negative kinetic energy. They are usually discussed in the context of quantum stability since it is the high energy vacuum that becomes unstable to the production of particles [154]. In the presence of a single field, we deal with this instability by demanding a positive kinetic term which, in terms of action (4.29), translates into the requirement that $A > 0$. On the other hand, *gradient* or *Laplacian instabilities* are characterized by the presence of DoFs propagating with negative speed, i.e. with $c_s^2 < 0$. This results in an exponential destabilisation of the perturbations at small scales, i.e., in the high-k regime. To avoid this instability we must require a positive square of the propagation speed for π. Since the latter corresponds to the ratio of the functions A and B, i.e. $c_s^2 = B/A$, we must impose $B/A > 0$.

Finally, the *tachyonic* and *Jeans instabilities* are the less severe of the group being also the less explored. They are present when the square of the DoF's mass is negative. To prevent this problem, one must consider the bounds of the Hamiltonian of canonical fields $\mathscr{H}(\Phi_i, \dot{\Phi}_i)$ which, for one fluid, is given by [148]

$$\mathscr{H}(\Phi_i, \dot{\Phi}_i) = \frac{a^3}{2}\left[\dot{\Phi}_1^2 + \dot{\Phi}_2^2 + \tilde{\mu}_1(t,k)\Phi_1^2 + \tilde{\mu}_2(t,k)\Phi_2^2 \right], \tag{4.30}$$

where $\tilde{\mu}_1$ and $\tilde{\mu}_2$ are the mass eigenvalues. The instability emerges when the Hamiltonian becomes unbounded from below. One way to make sure this does not happen is to impose that the mass eigenvalues be strictly positive, i.e., $\tilde{\mu}_i > 0$. However, the Jeans instability is needed at

early-time for the process of structure formation, meaning that if we do force $\tilde{\mu}_i$ to be positive at all times we are missing both physics and viable parameter space. In alternative, one can allow $\tilde{\mu}_i$ to be negative at times but require that in such occasions the mass eigenvalues verify $|\tilde{\mu}_i(t,0)| \lesssim H^2$. This condition ensures that the time scale of the evolution of this instability is larger than the Hubble time, so that it does not affect the general stability of the model. For a more complete treatment of this instability in the EFT framework we refer the reader to [155].

In the EFT formalism, it is possible to find the necessary conditions to prevent the appearance of any of these instabilities and ensure the viability of the theory simply by studying the perturbed action. These are then imposed on the EFT functions themselves, independently of their specific forms for particular models. As a matter of fact, it has been found that the enforcement of viability conditions can not only significantly reduce the allowed parameter space [156, 157] of a theory but can even become the dominant constraining contribution, surpassing the constraining power of observational data [42, 158].

4.6 ReParametrized Horndeski: The α-basis

In this Chapter we have been exploring the descriptive and versatile power of EFT. However, it is not the only formulation available to describe DE and MG models. In fact, an alternative parametrization of the EFT action, aiming to describe the phenomenology of Horndeski/GG theory [22, 44, 45], was proposed in [159]. In this parametrization, the evolution of linear perturbations in GG models can be fully described by four time-dependent phenomenological functions: $\alpha_K(t)$, $\alpha_B(t)$, $\alpha_M(t)$ and $\alpha_T(t)$. There have since been generalizations of this α-basis to include GLPV models [144, 145] and higher spatial operators [36], but we shall limit ourselves to the original formulation.

The four α parameters are equivalent to a combination of EFT functions, in fact, the correspondence between the two can be easily obtained by comparing the standard EFT action to the one written in the α-basis. The advantage of the latter, however, rests on the fact that the α functions have a direct relation to the physical effects of the theory, representing a more phenomenological approach. Let us then consider the physical interpretation of the α functions [148, 159]:

- α_K - the *kineticity*: it enters in the definition of the kinetic energy of the scalar mode. Since it affects the speed of propagation of the scalar DoF it consequently has an effect in the no-ghost condition.

- α_B - the *braiding function*: it describes the mixing between the metric and the scalar field. It enters in both the kinetic term and the speed of propagation of the scalar mode, hence affecting the clustering properties of DE.

- α_M - the *running Planck mass*: it describes the time-evolution of the effective Planck mass. The growth of structure is modified when the effective Planck mass is not constant.

- α_T - the *tensor speed excess*: it parametrizes the deviation of the speed of propagation of GWs from the speed of light. It has an impact on the evolution of both scalar gravitational potentials, introducing anisotropic stress. Recent GW observations constrain any existent deviations to be smaller than 10^{-15} [160].

Finally, as stated before, it is fairly easy to obtain the relation between the α-basis and the already presented EFT functions. To be consistent with our chosen form for the EFT action, and all the calculations that ensue, we now present the expressions for the α functions as given in [149]:

$$\alpha_K = \frac{2c+4M_2^4}{H^2M_*^2}, \qquad \alpha_B = \frac{1}{2}\frac{\bar{M}_1^3+m_0^2\dot{\Omega}}{HM_*^2},$$

$$\alpha_M = \frac{a\tilde{M}'}{1+\tilde{M}} = \frac{1}{H}\frac{d\ln M_*^2}{dt}, \qquad \alpha_T = -\frac{\bar{M}_2^2}{M_*^2} \equiv c_t - 1, \tag{4.31}$$

where a prime denotes a derivative with respect to the scale factor a, c_t is the speed of propagation of GWs and M_*^2 is the *effective Planck mass* defined as

$$M_*^2 = m_0^2\left(1+\tilde{M}\right) = m_0^2\left(1+\Omega+\frac{\bar{M}_2^2}{m_0^2}\right). \tag{4.32}$$

4.7 Revisiting the μ, Σ and η Phenomenological Functions

When studying the evolution of linear perturbations in DE and MG models it is common to use a more direct parametrization of the modifications introduced in the evolution equations with respect to their standard GR expressions. As it becomes clear from the forms of equations (3.35)-(3.37), any existing deviations with respect to GR will be described by the three introduced functions: $\mu(k,t)$, $\eta(k,t)$ and $\Sigma(k,t)$. The fact that these three phenomenological functions are related to each other through equation (3.38) means that one only needs to specify two of them in order to solve for the evolution of perturbations. The problem is, it is not generally possible to find exact analytical expressions for them without resorting to the QSA. If one does admit this approximation, functional forms for μ, η and Σ can be obtained for general model classes within the EFT framework. In the literature, the phenomenology of these functions is mainly studied in the context of GG class models [22]. Considering this, and taking into account that the target model of this dissertation also belongs to this class, we shall limit our exploration to this case. For the forms of the phenomenological functions in other model classes and their studies we refer the reader to [121–123, 161, 162].

Under the QSA, the analytical expressions for the phenomenological functions in GG/Horndeski models are given by [32, 148]:

$$\mu = \frac{m_0^2}{M_*^2}\frac{1+M_C^2\left(a^2/k^2\right)}{\left(f_1/2\right)f_3M_*^2+M_C^2\left(1+\alpha_T\right)^{-1}\left(a^2/k^2\right)}, \tag{4.33}$$

$$\eta = \frac{f_5/f_1+M_C^2\left(1+\alpha_T\right)^{-1}\left(a^2/k^2\right)}{1+M_C^2\left(a^2/k^2\right)}, \tag{4.34}$$

$$\Sigma = \frac{m_0^2}{2M_*^2}\frac{1+f_5/f_1+M_C^2\left[1+\left(1+\alpha_T\right)^{-1}\right]\left(a^2/k^2\right)}{\left(f_1/2\right)f_3M_*^2+M_C^2\left(1+\alpha_T\right)^{-1}\left(a^2/k^2\right)}, \tag{4.35}$$

where we recognize the tensor speed excess α_T and both f_i and M_C are dependent on the EFT functions with their explicit expressions given in [32]. Furthermore, we note that M_C marks the transition scale between the screened regime and the regime in which the extra scalar DoF

mediates a fifth force. This transition scale is dependent on the screening mechanism responsible for the suppression of the field on local scales.

Since our interest lies on large-scale modifications of gravity, we shall focus on scales where the scalar DoF is not being screened. In this case, this means we focus on the sub-Compton regime, i.e., $k/a \gg M_C$, which we denote with a "sub" subscript. In this regime, the previous expressions for the phenomenological functions reduce to [32, 148]:

$$\mu_{sub} = \frac{m_0^2}{M_*^2}\left(1+\alpha_T+\beta_\xi^2\right), \tag{4.36}$$

$$\eta_{sub} = \frac{1+\beta_B\beta_\xi/2}{1+\alpha_T+\beta_\xi^2}, \tag{4.37}$$

$$\Sigma_{sub} = \frac{m_0^2}{M_*^2}\left(1+\frac{\alpha_T}{2}+\frac{\beta_\xi^2}{2}+\frac{\beta_B\beta_\xi}{4}\right), \tag{4.38}$$

with

$$\beta_B^2 = \frac{8}{c_s^2\alpha}\alpha_B^2, \tag{4.39}$$

$$\beta_\xi^2 = \frac{2}{c_s^2\alpha}\left[-\alpha_B(1+\alpha_T)+\alpha_M-\alpha_T\right]^2, \tag{4.40}$$

$$\alpha = \alpha_K + 6\alpha_B^2, \tag{4.41}$$

where c_s^2 is the speed of propagation of the scalar mode and α corresponds to the effective no-ghost condition since the original one, given by

$$Q_s = \frac{2M_*^2\alpha}{(2-\alpha_B)^2} > 0, \tag{4.42}$$

can simply be reduced to $\alpha > 0$.

The sub-Compton forms of the phenomenological functions now translate any introduced large-scale deviations from the standard growth scenario. Even being valid only under the QSA, the forms and behaviour of μ, η and Σ can give insight regarding expected modified features appearing on the cosmological observables that we have considered in Section 3.3.3.

4.8 Effective Field Theory for `CAMB`

When studying the dynamics of perturbations in a given model, looking to constrain their parameter spaces or evaluate their impact on cosmological observables, it is very useful to resort to Einstein-Boltzmann solvers. The latter are auxiliary numerical tools capable of evolving the full linear perturbation equations. To maximize the usefulness of these codes, the EFT formalism has been implemented in several of them, resulting in powerful numerical tools for the study of perturbations in DE/MG models. Firstly, thanks to the use of the EFT language the constructed codes become apt to study a large group of models. In fact, when trying to investigate a given model, the user can directly use the perturbation equations for the EFT action that are already implemented in the code rather than having to derive and implement the model's specific perturbation equations. Furthermore, the implementation of the EFT formulation makes

the Einstein-Boltzmann codes capable of supporting not only model-specific studies but model-independent ones as well.

As we saw at the beginning of this Chapter, there are several available Einstein-Boltzmann codes built using the EFT formalism. The one that we chose to work with in this dissertation is the result of implementing the EFT formalism in the publicly available Einstein-Boltzmann solver `CAMB` [37, 39]. The final product, dubbed `EFTCAMB` [40, 41, 149], is capable of evolving the full dynamics of both scalar and tensor perturbations without resorting to any QSA. On one hand, it allows one to fully investigate the impact of the different EFT operators in the perturbation dynamics, without any model specification. Alternatively, one can also explore the characteristic phenomenology of any particular model that can be mapped into the EFT formalism.

Given the available options, it is common to identify two main approaches in which `EFTCAMB` can be employed [41]:

a) The *pure* EFT approach: in which one can study the influence of the different EFT operators on linear perturbations in a completely model-independent way. In this approach one can choose an arbitrary parametrization for the EFT functions.

b) The *mapping* EFT approach: in which one focus on a specific model covered by the EFT framework and explores its perturbation dynamics. In this case, the EFT functions, obtained through the mapping procedure, are determined by the choice of a model.

The two options can also imply a different take on how to deal with the background evolution. In the *pure* EFT approach the background evolution needs to be fixed. This means that the user must specify the desired expansion history by providing the form of the DE equation of state parameter w_{DE} as well as of one of the three background EFT functions $\{\Omega(t), \Lambda(t), c(t)\}$. As we saw in Section 4.2, usually one specifies $\Omega(t)$ and leaves the remaining two functions to be determined using the background equations. For the *mapping* approach, however, one has two choices: the *designer mapping* approach and the *full mapping* approach. In the former, the background history is also fixed, the procedure being the same as for *pure* EFT. On the other hand, in addition to the specific form of the EFT functions, the *full mapping* approach also requires the implementation of a background solver in order to find the expansion history $H(t)$.

An additional attractive feature of `EFTCAMB` is that it has a built-in stability module. This means that the code automatically checks if the theory under investigation remains viable throughout its evolution by imposing physical conditions concerning the ghost, gradient and tachyonic instabilities we discussed in Section 4.5.

4.8.1 The Structure of `EFTCAMB`

The publicly available version of `EFTCAMB` [40] already contains some built-in models. These include, for example, *designer* $f(R)$ [42], minimally coupled Quintessence [149] and low-energy Hořava gravity [158]. Additionally, there are several model-independent parametrizations of the DE equation of state w_{DE} as well as different choices for the functional forms of the EFT functions which are already implemented. It is even possible to use alternative parametrizations of the EFT functions such as the α-basis parametrization of the Horndeski/GG class that we saw in Section 4.6.

Functionally, `EFTCAMB` is organized in a flag structure, shown in Figure 4.1, which allows the user to control the code's behaviour by attributing a number to each flag. The main flag, designated as the `EFTflag`, controls the selection of the desired approach. With `EFTflag`= 0 the code reverts back to original `CAMB`, suited for studying GR only. The selection `EFTflag`= 1 corresponds to the *pure* EFT approach while `EFTflag`= 3 and `EFTflag`= 4 correspond to the *mapping* options: 3 for *designer mapping* and 4 for *full mapping*. Finally, `EFTflag`= 2 is the option for alternative model-independent parametrizations which rely on the EFT functions, where the α-basis parametrization is included. For each of these flags there are other sub-flags designed to control the details of the different approaches. A more detailed description of the `EFTCAMB` structure can be found in [149].

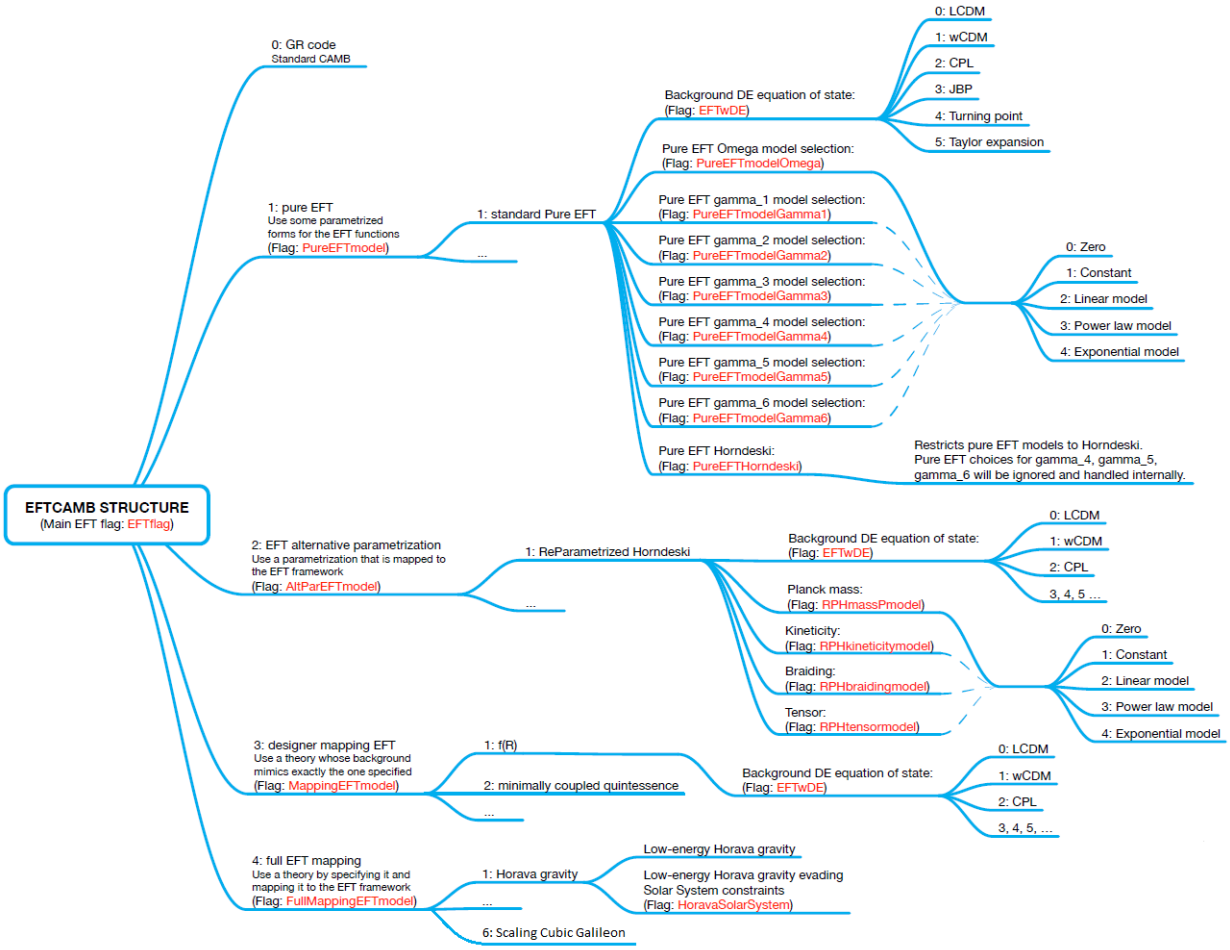

Figure 4.1: Structure of EFTCAMB showing the available flags after the addition of our Scaling Cubic Galileon model.

Since in this dissertation we aim to explore the complete evolution of a specific model, we are interested in using the *full mapping* approach. In practice, this means that we shall add a new sub-flag under `EFTflag`= 4, as we show in Figure 4.1, where we will have to implement a background solver for the target model as well as its mapping.

Finally, we comment on a more technical aspect of the implementation of the EFT functions in `EFTCAMB`. First of all, the code works in conformal time τ, rather than proper time t as we have been mainly doing so far. This means that when implemented, all the EFT functions must be written as functions of the scale factor a. Additionally, all second order EFT functions

are redefined to become dimensionless in order to facilitate their implementation. Thus, we introduce the γ_i functions [149]:

$$\gamma_1 = \frac{M_2^4}{m_0^2 H_0^2}, \qquad \gamma_2 = \frac{\bar{M}_1^3}{m_0^2 H_0}, \qquad \gamma_3 = \frac{\bar{M}_2^2}{m_0^2},$$
$$\gamma_4 = \frac{\bar{M}_3^2}{m_0^2}, \qquad \gamma_5 = \frac{\hat{M}^2}{m_0^2}, \qquad \gamma_6 = \frac{m_2^2}{m_0^2}. \tag{4.43}$$

Regarding the background EFT functions c and Λ, they are usually implemented in the forms ca^2/m_0^2 and $\Lambda a^2/m_0^2$. The Ω function, on the other hand, suffers no redefinitions.

Chapter 5

The Scaling Cubic Galileon

In this Chapter, we shall use all the knowledge gathered through the previous Chapters to perform a detailed analysis of the target model of this dissertation: the SCG. The latter is a MG model belonging to the GG class, discussed in Section 3.2.1, in which the standard gravitational interaction is modified by the addition of the Galileon scalar field ϕ. Since our objective is to obtain a comprehensive understanding of the phenomenology of this model, we set to study both its background evolution and its impact on the cosmological observables.

The SCG model, formally presented in [43], is the product of a collaboration with N. Frusciante, N. Nunes and S. Tsujikawa. The model was proposed as an alternative explanation for the phenomenon of cosmic acceleration and, in particular, as a possibility to obtain new *scaling solutions* [163–173] in the presence of the cubic Horndeski coupling G_3. These solutions are characterized by a constant ratio between the energy density of the matter components and that of the scalar field and can offer the opportunity to alleviate the Coincidence Problem discussed in Section 3.1. They do this by offering the possibility to set the initial conditions based on the model parameters once the scaling solution is found. In this way the initial conditions are no longer completely arbitrary, instead they become determined by the parameter choices.

Scaling solutions had already been found both in the absence and presence of the cubic coupling G_3. In Quintessence models described by the standard $G_2 = X - V(\phi)$ term, scaling solutions were found for the exponential potential $V(\phi) = V_0 e^{-\lambda\phi}$ [163, 164, 166, 168, 174, 175], with V_0 and λ both constants. On the other hand, in K-essence models the scaling behaviour was found for the particular form of $G_2(\phi, X) = Xg(Y)$, where $g(Y)$ is an arbitrary function of $Y = Xe^{\lambda\phi}$ [167, 176]. Then, in generalizations where the cubic term (3.8) is included, scaling solutions were found for $G_3(\phi, X) = a_1 Y + a_2 Y^2$, with a_1 and a_2 constants, together with an exponential potential and a direct coupling between the scalar field and matter [170]. Our objective was to find new scaling solutions in the presence of G_3 while still reproducing a late-time epoch of cosmic acceleration.

Thus, the first step in our project must be to get an understanding on the model's expansion history. To do so, one usually resorts to the tools of dynamical analysis [57, 58]. The model's background equations are converted into an autonomous system of first order differential equations from which the cosmological dynamics is then ascertained by studying the evolution around the critical points. Of course, as we have discussed in previous Chapters, the background history alone is not sufficient to establish a model as a viable cosmological option or to distinguish it from other proposed alternatives. A complete study of any model must also include a detailed analysis of the dynamics of perturbation growth and its impact on cosmological observables.

For this purpose, we can employ the EFT formalism reviewed in Chapter 4 and then resort to an Einstein-Boltzmann solver such as `EFTCAMB`.

Keeping our objective in mind, this Chapter is organized as follows. The model's construction and background analysis, which were the subject of a publication in Physical Review D [43], are reviewed in Sections 5.1 and 5.2. In them we discuss the choice of Lagrangian terms and their ability to reproduce the target cosmological evolution as well as the imposed viability requirements. Then, to complement the preliminary study of modifications in the growth of perturbations that we performed in [43], we compute the mapping of the model into the EFT formalism, implement it in `EFTCAMB` and examine its impact on the cosmological observables introduced in Section 3.3.3. We present these steps and their results in Section 5.3. Specifically, in Section 5.3.1 we show the mapping of the SCG model and in Section 5.3.2 we briefly explain the process of implementing it in `EFTCAMB`. Finally, in Section 5.3.3 we investigate the evolution of perturbations in the SCG model and discuss its effects on the LSS observables that are obtained as output of the code.

5.1 The Foundations of the SCG Model

To achieve our objective of obtaining new scaling solutions in the presence of cubic interactions while still reproducing a viable epoch of accelerated expansion, we employ the following action:

$$\mathcal{S} = \int d^4x\sqrt{-g}\left[\frac{m_0^2}{2}R + G_2(\phi, X) - G_3(\phi, X)\Box\phi\right] + \mathcal{S}_\gamma, \tag{5.1}$$

where S_γ is the matter action accounting for the presence of matter perfect fluids. In relation to the general action for the GG class, which is given in equation (3.6), this means that we have set $G_4 = (m_0^2/2)$ and $G_5 = 0$. These choices are done in accordance to the constraints [160] placed on the GG model class by the recently detected GW event GW170817 [177, 178].

To derive and study the background equations for the SCG model we adopt the flat ($\kappa = 0$) FLRW metric given by equation (2.18) and, for simplification purposes, use the units $8\pi G_N = 1$. Then, by varying action (5.1) with respect to the metric, we obtain the modified Friedmann equations

$$3H^2 = \rho_\gamma + \rho_\phi, \tag{5.2}$$

$$2\dot{H} + 3H^2 = -\left(p_\gamma + p_\phi\right), \tag{5.3}$$

where ρ_γ and p_γ are the energy density and pressure of the matter fluids, related through the barotropic equation of state (2.27), and ρ_ϕ and p_ϕ are the energy density and pressure of the scalar field which are given by

$$\rho_\phi = 2XG_{2,X} - G_2 + 6X\dot{\phi}HG_{3,X} - 2XG_{3,\phi}, \tag{5.4}$$

$$p_\phi = G_2 - 2X\left(G_{3,\phi} + \ddot{\phi}G_{3,X}\right), \tag{5.5}$$

with $X = \dot{\phi}^2/2$. On the other hand, the variation of the action with respect to ϕ yields the equation of motion for the scalar field:

$$\frac{1}{a^3}\frac{d}{dt}\left[a^3\left(\dot{\phi}G_{2,X} + 6HXG_{3,X} - 2\dot{\phi}G_{3,\phi}\right)\right] = G_{2,\phi} - 2X\left(G_{3,\phi\phi} + \ddot{\phi}G_{3,\phi X}\right). \tag{5.6}$$

The derived equations of motion still remain somewhat general, since so far only the forms of G_4 and G_5 have been specified. In the case of the SCG model, the choice of forms for G_2 and G_3 is then motivated by a necessity to close the autonomous system constructed from the background equations as well as to obtain an expansion history with an early scaling era followed by a period of late-time acceleration. Taking these requirements into account, we start by considering the quadratic Lagrangian $G_2(\phi, X)$ of a standard canonical scalar field, i.e.

$$G_2(\phi, X) = X - V(\phi) \tag{5.7}$$

where X is the standard kinetic term and $V(\phi)$ is the scalar potential, together with the following general form for the cubic coupling:

$$G_3(\phi, X) = g(Y), \qquad Y = Xe^{\lambda\phi}, \tag{5.8}$$

where g is an arbitrary function of Y and λ is a constant. Thanks to the latter definition, the derivatives of G_3 with respect to ϕ and X can be expressed as

$$\begin{aligned} G_{3,\phi} = \lambda Y g_{,Y}, \quad G_{3,X} = \frac{Y g_{,Y}}{X}, \quad G_{3,XX} = \frac{Y^2 g_{,YY}}{X}, \\ G_{3,\phi\phi} = (g_{,Y} + Y g_{,YY})\,\lambda^2 Y, \quad G_{3,\phi X} = G_{3,X\phi} = (g_{,Y} + Y g_{,YY})\,\lambda \frac{Y}{X}. \end{aligned} \tag{5.9}$$

To finally determine the forms of $V(\phi)$ and $g(Y)$ we must consider the model's corresponding dynamical system and its evolution, to which we dedicate the following Section. As we will see moving forward, it took us two attempts at choosing the forms of the missing functions before we were in fact capable of obtaining a model presenting both scaling solutions and a viable late-time period of cosmic acceleration.

5.2 Background Dynamics

The cosmological evolution of a model can be ascertained by converting its background equations into an autonomous system and then investigating its behaviour around the corresponding critical points. A critical point, or fixed point, of a system is a point where the latter is in equilibrium. Whether this steady state is then maintained after the system reaches the critical point depends on its stability with respect to small perturbations. To determine the stability of a fixed point, the autonomous equations are linearized around it, as we explicitly show in Appendix A, and the signs of the real part of eigenvalues of the associated Jacobian matrix are then analysed. For a 2D system, a critical point is said stable when both eigenvalues have negative real parts, being also referred to as an *attractor*, it is said unstable when the real parts of both eigenvalues are positive and, finally, when one of them is positive and the other negative it is said to be a saddle point. This dynamical analysis proves most useful since it allows us to confirm if we do obtain an expansion history with both a scaling era and a period of late-time acceleration. For a detailed review on dynamical analysis and its applications in Cosmology we refer the reader to [57, 58].

5.2.1 Dynamical Analysis: Single Exponential Potential

In our first attempt at reproducing an expansion history in which an early scaling radiation/matter era is followed by a period of late-time acceleration, we consider a single exponential potential of the form

$$V(\phi) = V_0 e^{-\beta\phi}, \tag{5.10}$$

where V_0 and β are constants. Following this choice, we define the following set of dimensionless variables to help us with the study of the background cosmological dynamics:

$$x = \frac{\dot{\phi}}{\sqrt{6}H}, \qquad y = \frac{\sqrt{V}}{\sqrt{3}H}, \qquad \Omega_\gamma = \frac{\rho_\gamma}{3H^2}. \tag{5.11}$$

Equipped with the previous definitions, we can use equations (5.4)-(5.6) together with the derivative forms presented in (5.9) to obtain the following dynamical system:

$$x' = \frac{1}{\sqrt{6}} f(x,y) - h(x,y)x, \tag{5.12}$$

$$y' = -\sqrt{\frac{3}{2}}\beta xy - h(x,y)y, \tag{5.13}$$

where a prime denotes a derivative with respect to $\ln a$ and we have defined

$$f(x,y) \equiv \frac{\ddot{\phi}}{H^2} = s(x,y)\Bigg\{ -3\sqrt{6}x + 3\beta y^2 - 6\lambda x\left(Yg_{,Y} + Y^2 g_{,YY}\right)\left(\sqrt{6} - \lambda x\right) \\ - 6Yg_{,Y}\left[3 - 3x^2 - \sqrt{6}\lambda x - \frac{3}{2}\gamma\Omega_\gamma + 3xYg_{,Y}\left(2\lambda x - \sqrt{6}\right)\right]\Bigg\} \tag{5.14}$$

with

$$s(x,y)^{-1} \equiv 1 + 2\left(Yg_{,Y} + Y^2 g_{,YY}\right)\left(\frac{\sqrt{6}}{x} - \lambda\right) + 2Yg_{,Y}\left(3Yg_{,Y} - \lambda\right), \tag{5.15}$$

and

$$h(x,y) \equiv \frac{\dot{H}}{H^2} = Yg_{,Y} f(x,y) - \frac{3}{2}\gamma\Omega_\gamma + 3xYg_{,Y}\left(2\lambda x - \sqrt{6}\right) - 3x^2. \tag{5.16}$$

Furthermore, the introduction of the dimensionless variables also allows us to re-write the Friedmann constraint given in equation (5.4) as

$$\Omega_\gamma = 1 - \Omega_\phi, \tag{5.17}$$

where Ω_γ and Ω_ϕ are the total fluid density parameter and the scalar field density parameter, respectively, with the latter being given by

$$\Omega_\phi = x^2 + y^2 + 2xYg_{,Y}\left(\sqrt{6} - \lambda x\right). \tag{5.18}$$

According to the constraint equation (5.17), if the fluid density is positively defined, i.e., if $\Omega_\gamma \geq 0$, the field density parameter has an upper bound: $\Omega_\phi \leq 1$. This is one of the constraints that we shall impose when exploring the viable parameter region of our model. We also introduce the specific contribution of the cubic coupling G_3 to the energy density, which can be translated

by

$$\Omega_{G_3} = 2xYg_{,Y}\left(\sqrt{6}-\lambda x\right). \tag{5.19}$$

Finally, let us define the scalar field EoS parameter:

$$w_\phi \equiv \frac{p_\phi}{\rho_\phi} = \frac{x^2-y^2-2Yg_{,Y}\left(f/3+\lambda x^2\right)}{x^2+y^2+2Yg_{,Y}\left(\sqrt{6}x-\lambda x^2\right)}. \tag{5.20}$$

When the scalar field is the dominant component in the Universe, the condition $w_\phi < -1/3$ is sufficient to realize the cosmic acceleration. Outside of this situation, however, we must impose $w_{\text{eff}} < -1/3$, where $w_{\text{eff}} = -1-(2/3)h$ is the effective EoS parameter.

Following the previous considerations regarding the bound on Ω_ϕ and the realization of cosmic acceleration, this is probably an appropriate point to discuss the issue of model viability. As we have mentioned several times so far, being able to achieve a cosmological evolution with an early scaling regime followed by a late-time period of accelerated expansion is, obviously, a critical requirement that we impose on our model. However, one must not forget that moving on we will also be interested in the perturbation dynamics. In light of this, our viability concerns must also extend to the perturbative level accounting, for example, for the ghost and Laplacian instabilities discussed in Section 4.5. Therefore, looking to ensure the reproduction of a correct background history as well as a stable evolution of perturbations, we impose some theoretical conditions. Starting at the background level, we enforce the following:

- Existence condition: the system's critical points must be real;
- Stability of the critical points: to realize the desired expansion history we must, first of all, find critical points that we can identify as responsible for radiation and matter eras and for the late-time cosmic acceleration period. Then, from a cosmological point of view, we need the critical points of radiation and matter eras to be either unstable or saddle points so that the system can later exit them to approach a scalar field dominated late-time attractor. Furthermore, since the scalar field must be able to drive an accelerated expansion we also impose that the corresponding solution verifies $w_\phi < -1/3$;
- Phase-space constraint: following the Friedmann constraint, we impose the previously mentioned upper bound for the scalar field density parameter: $\Omega_\phi \leq 1$.

In addition to the previous background viability requirements, there are also theoretical stability conditions to be imposed in order to avoid the development of the ghost and Laplacian instabilities during the evolution of perturbations. Since we chose the Lagrangian form of our model to be in accordance with the GWs' placed constraints [160], there are no modifications in the tensor perturbation sector with respect to GR. Thus, there are neither ghost nor Laplacian instabilities plaguing the tensor sector of our model. The scalar sector, however, is modified by the presence of the cubic coupling. In this case, the conditions for the absence of ghost and Laplacian instabilities in the small-scale limit are respectively given by [179]

$$Q_s \equiv \frac{4w_3+9w_2^2}{3w_2^2} > 0 \tag{5.21}$$

$$c_s^2 \equiv \frac{2\left(Hw_2-\dot{w}_2-\gamma\rho_\gamma\right)-w_2^2}{w_2^2 Q_s} > 0, \tag{5.22}$$

where

$$w_2 = 2H\left(1 - Yg_{,Y}\sqrt{6}x\right), \tag{5.23}$$

$$w_3 = 9H^2\left[x^2\left(1 - 2\lambda Y^2 g_{,YY} - 4\lambda Y g_{,Y}\right) + 2\sqrt{6}x\left(2Yg_{,Y} + Y^2 g_{,YY}\right) - 1\right]. \tag{5.24}$$

As we shall clearly see further ahead, it is the enforcement of the above conditions that defines the viable parameter space for our model.

In order to proceed with our analysis we are now only missing a form for the cubic coupling $G_3 = g(Y)$. In the end, this choice comes down to the necessity of closing the constructed autonomous system. Considering equations (5.12)-(5.13) together with the expressions of f and h, we find that the dynamical system is closed when the form of $g(Y)$ verifies that both $Yg_{,Y}$ and $Y^2 g_{,YY}$ are constants. Bearing this in mind, we select the following form for the cubic coupling:

$$G_3(\phi, X) = A\ln(Y), \tag{5.25}$$

where A is a constant and we consequently verify that

$$Yg_{,Y} = -Y^2 g_{,YY} = A = \text{constant}. \tag{5.26}$$

The critical points (x_c, y_c) can finally be found by setting $x' = y' = 0$ in equations (5.12) and (5.13). In Table 5.1, we present the critical points found for the current choices of potential and cubic coupling, given by equations (5.10) and (5.25) respectively, together with the corresponding values of Ω_ϕ and w_ϕ. Additionally, the perturbative viability conditions (5.21) and (5.22) which, for the cubic coupling form given in equation (5.25), reduce to

$$Q_s = \frac{3x^2\left(1 - 2A\lambda + 6A^2\right)}{\left(1 - \sqrt{6}Ax\right)^2} > 0, \tag{5.27}$$

$$c_s^2 = \frac{3x\left(1 - 2A\lambda - 2A^2\right) + 4\sqrt{6}A}{3x\left(1 - 2A\lambda + 6A^2\right)} > 0, \tag{5.28}$$

are also computed and presented in Table 5.1 for each critical point. Let us also note that in the limit $A \to 0$ we have $Q_s = 3x^2$ and $c_s^2 = 1$, so the conditions above are automatically satisfied. When the cubic coupling is present, and thus $A \neq 0$, the parameters A and λ are constrained to verify the conditions (5.27) and (5.28).

For our current selections of $V(\phi)$ and G_3 we find a total of five critical points. In what follows, we shall discuss their stability following the previously stated viability criteria and explore their cosmological interest. In order to determine the stability of the critical points we present the corresponding eigenvalues of the Jacobian matrix associated with the linearization of our system in Appendix A. Let us then consider

- Point (a) – Scaling Solution: This point corresponds to

$$x_c = \sqrt{\frac{3}{2}}\frac{\gamma}{\beta}, \qquad y_c = \sqrt{\frac{3\left(2-\gamma\right)}{2\beta^2}\left[\gamma + 2A\left(\beta - \gamma\lambda\right)\right]}\,, \tag{5.29}$$

	x_c	y_c^2	Ω_ϕ	w_ϕ	Q_s	c_s^2
(a)	$\sqrt{\frac{3}{2}}\frac{\gamma}{\beta}$	$\frac{3(2-\gamma)}{2\beta^2}[\gamma+2A(\beta-\gamma\lambda)]$	Eq. (5.30)	$\gamma-1$	$\frac{9\gamma^2}{2}\frac{1+2A(3A-\lambda)}{(\beta-3A\gamma)^2}$	$1+\frac{8A}{3\gamma}\frac{\beta-3A\gamma}{1+2A(3A-\lambda)}$
(b)	$\frac{\beta-6A}{\sqrt{6}[1+A(\beta-2\lambda)]}$	$\frac{[1+2A(3A-\lambda)][6-\beta^2+12A(\beta-\lambda)]}{6[1+A(\beta-2\lambda)]^2}$	1	$-1+\frac{\beta(\beta-6A)}{3[1+A(\beta-2\lambda)]}$	$\frac{(\beta-6A)^2}{2[1+2A(3A-\lambda)]}$	$1+\frac{8A}{\beta-6A}$
(c)	$\frac{\sqrt{6}A}{2A\lambda-1}$	0	$\frac{6A^2}{2A\lambda-1}$	$\gamma-1$	$\frac{18A^2}{1+2A(3A-\lambda)}$	$-\frac{1}{3}$
(d1)	$\frac{\sqrt{6}A-\sqrt{1+2A(3A-\lambda)}}{2A\lambda-1}$	0	1	1	3	$1+\frac{4\sqrt{6}A}{3\sqrt{1+2A(3A-\lambda)}}$
(d2)	$\frac{\sqrt{6}A+\sqrt{1+2A(3A-\lambda)}}{2A\lambda-1}$	0	1	1	3	$1-\frac{4\sqrt{6}A}{3\sqrt{1+2A(3A-\lambda)}}$

Table 5.1: Table I in [43]. Critical points (x_c, y_c^2) of the dynamical system (5.12)-(5.13) for the model given by the functions $G_2 = X - V_0 e^{-\beta\phi}$ and $G_3 = A\ln Y$ with $Y = Xe^{\lambda\phi}$, in the presence of a barotropic perfect fluid with the equation of state $\gamma - 1$. For each critical point, we also show the values of Ω_ϕ, w_ϕ, Q_s, and c_s^2 defined, respectively, in equations (5.18), (5.20), (5.21) and (5.22).

with $w_\phi = w_{\text{eff}} = \gamma - 1$ and

$$\Omega_\phi = \frac{3}{\beta^2}\Big[\gamma + A\Big(\gamma\,(\beta - 2\lambda) + 2\beta\Big)\Big]. \tag{5.30}$$

Given that $\Omega_\gamma = 1 - \Omega_\phi$, we can easily identify this as the *scaling solution*, verifying that the scalar field and fluid energy densities maintain a constant ratio, i.e., $\Omega_\phi/\Omega_\gamma = \text{constant}$, which is only dependent on the values of parameters A, β, λ and γ. Additionally, since the scalar field EoS is equivalent to that of the fluid components, $w_\phi = \gamma - 1$, the energy densities of the two components scale together regardless of the value of γ. Let us note that in the limit $A \to 0$, our critical point (a) reduces to the scaling solution found in [163] for a canonical scalar field with the exponential potential (5.10). However, the presence of G_3 in our case modifies the scaling ratio $\Omega_\phi/\Omega_\gamma$. Furthermore, this cubic coupling provides an important contribution to the field density (5.30), which is given by

$$\Omega_{G_3} = \frac{3}{\beta^2} A\gamma\,(2\beta - \gamma\lambda)\,. \tag{5.31}$$

Focusing now on the viability of the point, the existence condition dictates that y_c must be real, therefore we must verify

$$\gamma + 2A\,(\beta - \gamma\lambda) \geq 0. \tag{5.32}$$

On the other hand, the absence of ghost and Laplacian instabilities is ensured under the following conditions:

$$1 + 2A\,(3A - \lambda) > 0, \tag{5.33}$$

$$8A\beta + 3\gamma\Big[1 - 2A\,(A + \lambda)\Big] > 0. \tag{5.34}$$

Finally, for determining the stability of point (a), we consider the corresponding eigenvalues given by equation (A.4) in Appendix A. By combining conditions (5.32), (5.33), $0 < \gamma < 2$ and $\Omega_\phi \leq 1$ we verify that neither of the two eigenvalues can be positive. The direct conclusion is that point (a) is always stable under the imposed viability conditions. Most importantly, however, is the cosmological implication of this result. The fact that (a) is always stable means that if it is used to realize the scaling radiation and matter eras, we need to consider an additional mechanism for the solutions to exit from this regime into

an epoch of cosmic acceleration. In the absence of such extra mechanism the solutions remain trapped in the scaling regime.

- Point (b) – Scalar Field Dominated Solution: For this point we have

$$x_c = \frac{\beta - 6A}{\sqrt{6}\big[1 + A(\beta - 2\lambda)\big]}, \qquad y_c = \sqrt{\frac{\big[1 + 2A(3A - \lambda)\big]\big[6 - \beta^2 + 12A(\beta - \lambda)\big]}{6\big[1 + A(\beta - 2\lambda)\big]^2}}\,, \tag{5.35}$$

with $\Omega_\phi = 1$ and

$$w_\phi = w_{\text{eff}} = -1 + \frac{\beta(\beta - 6A)}{3\big[1 + A(\beta - 2\lambda)\big]}. \tag{5.36}$$

Since $\Omega_\phi = 1$ it is straightforward to identify this as a *scalar field dominated* point. This is also the point that we can use for a late-time epoch of accelerated expansion by imposing $w_\phi < -1/3$, which in this case translates into the condition

$$\frac{\beta(\beta - 6A)}{1 + A(\beta - 2\lambda)} < 2. \tag{5.37}$$

Once again considering the imposed viability conditions, we can conclude from the values of Q_s and c_s^2 presented in Table 5.1 that ghost and Laplacian instabilities are avoided for

$$1 + 2A(3A - \lambda) > 0, \tag{5.38}$$

$$(\beta + 2A)(\beta - 6A) > 0. \tag{5.39}$$

The previous absence of ghosts condition also helps in reducing the existence condition, which imposes that y_c must be real. The latter is now given by

$$6 - \beta^2 + 12A(\beta - \lambda) \geq 0. \tag{5.40}$$

Additionally, if we wish point (b) to be the one responsible for cosmic acceleration we need it to correspond to a late-time attractor. For that purpose, both of its associated eigenvalues given by equations (A.5) and (A.6) must be negative. Thus, we need to verify

$$\mu_1 = \frac{\beta(\beta - 6A)}{1 + A(\beta - 2\lambda)} - 3 < 0, \tag{5.41}$$

$$\mu_2 = \frac{\beta^2 - 6 + 12A(\lambda - \beta)}{2\big[1 + A(\beta - 2\lambda)\big]} < 0, \tag{5.42}$$

where we have set $\gamma = 1$ since at late-time the greatest contribution to the Universe's energy density between non-relativistic matter and radiation comes from the first. If we consider the limit $A \to 0$, conditions (5.38) and (5.39) are automatically satisfied whereas the remaining conditions are verified for $\beta^2 < 2$. In our case, the presence of the cubic coupling term modifies the upper bound on β. Moreover, from equation (5.36) we find that we can have $w_\phi \simeq -1$ for values of A close to $\beta/6$. However, the absence of Laplacian instabilities condition given in equation (5.39) constrains the value of A to be in the range

$$-\frac{\beta}{6} < A < \frac{\beta}{6}, \tag{5.43}$$

when considering positive values of β only. Finally, the density parameter (5.19) of the cubic coupling associated with point (b) is given by

$$\Omega_{G_3} = \frac{A(\beta - 6A)\left[6 + 6A(\beta - \lambda) - \beta\lambda\right]}{3\left[1 + A(\beta - 2\lambda)\right]^2}, \tag{5.44}$$

which means that for $A \approx \beta/6$ both Ω_{G_3} and x_c are brought close to 0 and the potential becomes the dominant contribution to the field's energy density.

- Point (c) – Kinetic Scaling Solution: For this point we find $y_c = 0$ and $w_\phi = \gamma - 1$, thus we can identify it as a *kinetic scaling solution* which only exists for $A \neq 0$. We can confirm the scaling nature of this point by considering the corresponding value of Ω_ϕ, given in Table 5.1, which we again find to be a constant only dependent on the model parameters. However, as we can also find in Table 5.1, the square of the speed of propagation for this point is negative: $c_s^2 = -1/3$. This means that the physical viability condition (5.22) is never satisfied for $A \neq 0$. This makes point (c) non-viable to take part in the cosmological evolution.

  Nevertheless, if we do take the limit $A \to 0$, this point becomes fluid dominated, i.e., $\Omega_\gamma = 1$, and the eigenvalues given in (A.7) and (A.8) verify $\mu_1 < 0$ and $\mu_2 > 0$. Thus, the point becomes a saddle node which can be used to realize radiation or matter eras.

- Points (d1) and (d2) – Kinetic Dominated Scalar Field Solutions: Since these points are characterized by $y_c = 0$ and $\Omega_\phi = 1$, we identify them as *kinetically dominated* scalar field solutions. One of their eigenvalues, $\mu_1 = 3(2 - \gamma)$ is guaranteed to be positive thanks to the condition $0 < \gamma < 2$, which means that they are either saddles or unstable nodes. Additionally, both of them have $w_\phi = w_{\text{eff}} = 1$ and $\Omega_\phi = 1$, rendering them incapable of driving a period of accelerated expansion and of describing radiation or matter eras.

In summary, by choosing the forms of the potential $V(\phi)$ and of the cubic coupling G_3 according to equations (5.10) and (5.25), respectively, we obtain five critical points. Out of these five, we find that points (c), (d1) and (d2) are not suited to describe a viable expansion history after the onset of the radiation-dominated era. In addition to this, we find that we can realize scaling radiation/matter eras and a period of cosmic acceleration separately by using critical points (a) and (b), respectively. However, since point (a) revealed itself as always stable when under the imposed viability conditions, the solutions do not exit from the matter scaling regime to a period of late-time accelerated expansion without the introduction of an additional mechanism. Alternatively, if we set the parameters so that the solutions approach (b) at late times, we lose the scaling behaviour at early times. Thus, we can conclude that the choices made in this Subsection do not allow us to realize both an early scaling regime and a late-time period of cosmic acceleration. In the following Subsection we shall try to solve this by adding a second exponential term to the potential.

5.2.2 The SCG Model: Double Exponential Potential

The model we built in the previous Section failed in realizing the proper expansion history with a matter/radiation scaling regime followed by a period of late-time accelerated expansion. However, we would like to maintain the scaling behaviour since, as we have discussed, it offers

a possibility to alleviate the Coincidence Problem. Therefore, we try to construct a model capable of retaining the features associated with both critical points (a) and (b) by adding a second exponential term to the potential similarly to what was done in [174].

Thus, following the mentioned example, we decide to keep the form of the G_3 coupling as given in equation (5.25) and consider:

$$V(\phi) = V_1 e^{-\beta_1 \phi} + V_2 e^{-\beta_2 \phi}, \tag{5.45}$$

where V_1, V_2, β_1 and β_2 are positive constants and the latter two parameters are chosen so that $\beta_1 \gg \mathcal{O}(1)$ whereas $\beta_2 \lesssim \mathcal{O}(1)$. With this setup, the first potential $V_1 e^{-\beta_1 \phi}$ gives rise to critical point (a) with $\beta = \beta_1$ while the second potential $V_2 e^{-\beta_2 \phi}$ leads to point (b) with $\beta = \beta_2$. Therefore, the first potential contributes to the scaling eras while the second potential provides the exiting mechanism into the period of late-time cosmic acceleration.

To study the background dynamics of this model we follow the same procedure of last Section. This time we explicitly consider contributions from radiation and non-relativistic matter for the matter sector, denoting the related quantities with the subscripts r and m, respectively. Then, we define the following partially new set of dimensionless variables:

$$x = \frac{\dot{\phi}}{\sqrt{6}H}, \quad y_1 = \frac{\sqrt{V_1 e^{-\beta_1 \phi}}}{\sqrt{3}H}, \quad y_2 = \frac{\sqrt{V_2 e^{-\beta_2 \phi}}}{\sqrt{3}H}, \quad \Omega_r = \frac{\rho_r}{3H^2}, \quad \Omega_m = \frac{\rho_m}{3H^2}, \tag{5.46}$$

where we have kept the definition of x. With these definitions, the Friedmann constraint (5.4) can once again be re-written as

$$\Omega_m = 1 - \Omega_r - \Omega_\phi, \tag{5.47}$$

where the field density parameter Ω_ϕ is now given by

$$\Omega_\phi = x^2 + y_1^2 + y_2^2 + 2xA\left(\sqrt{6} - \lambda x\right). \tag{5.48}$$

Moreover, from the background equations (5.4)-(5.6) we now obtain the following autonomous system:

$$x' = \frac{1}{\sqrt{6}}\tilde{f}(x, y_1, y_2) - \tilde{h}(x, y_1, y_2)x, \tag{5.49}$$

$$y_i' = -\sqrt{\frac{3}{2}}\beta_i x y_i - \tilde{h}(x, y_1, y_2)y_i, \tag{5.50}$$

$$\Omega_r' = -4\Omega_r - 2\tilde{h}(x, y_1, y_2)\Omega_r, \tag{5.51}$$

where $i = 1, 2$. The function $\tilde{f}(x, y_1, y_2)$ is obtained from expression (5.14) by using equation (5.26) and performing the following substitutions: $\beta y^2 \to \beta_1 y_1^2 + \beta_2 y_2^2$ and $\gamma\Omega_\gamma \to \Omega_m + (4/3)\Omega_r$. In a similar way, $\tilde{h}(x, y_1, y_2)$ is obtained from equation (5.16) with the replacements $\gamma\Omega_\gamma \to \Omega_m + (4/3)\Omega_r$ and $Y g_{,Y} = A$. Since these expressions are quite long, we choose to present their final forms in Appendix B. The scalar field EoS parameter, on the other hand, is quite simply given by

$$w_\phi = \frac{x^2 - y_1^2 - y_2^2 - 2A\left(\tilde{f}/3 + \lambda x^2\right)}{x^2 + y_1^2 + y_2^2 + 2A\left(\sqrt{6}x - \lambda x^2\right)}. \tag{5.52}$$

The critical points of our new model can also be obtained from the ones found in the previous Subsection by performing the necessary substitutions. Specifically, we find:

- (a1) - Radiation Scaling Point:

$$(x, y_1, y_2, \Omega_m) = \left(\frac{2\sqrt{6}}{3\beta_1}, \frac{\sqrt{12+6A\,(3\beta_1-4\lambda)}}{3\beta_1}, 0, 0 \right), \tag{5.53}$$

  and $\Omega_r = 1-\Omega_\phi$ with $\Omega_\phi = \left[4+2A\,(5\beta_1-4\lambda)\right]/\beta_1^2$.

- (a2) - Matter Scaling Point:

$$(x, y_1, y_2, \Omega_r) = \left(\sqrt{\frac{3}{2}}\frac{1}{\beta_1}, \frac{\sqrt{6+12A\,(\beta_1-\lambda)}}{2\beta_1}, 0, 0 \right), \tag{5.54}$$

  and $\Omega_m = 1-\Omega_\phi$ with $\Omega_\phi = 3\left(1+A\,(3\beta_1-2\lambda)\right)/\beta_1^2$.

- (b) - Scalar Field Dominated Point:

$$x = \frac{\beta_2-6A}{\sqrt{6}\left[1+A\,(\beta_2-2\lambda)\right]}, \qquad y_1 = 0, \qquad y_2 = \sqrt{\frac{\left[1+2A\,(3A-\lambda)\right]\left[6-\beta_2^2+12A\,(\beta_2-\lambda)\right]}{6\left[1+A\,(\beta_2-2\lambda)\right]^2}}, \tag{5.55}$$

  with $\Omega_r = \Omega_m = 0$ and $\Omega_\phi = 1$.

Once again, it is quite straightforward to identify the last of these three points as the scalar field dominated one since it verifies $\Omega_\phi = 1$. For the identified radiation and matter scaling points, we verify $\Omega_\phi/\Omega_r = \text{constant}$ and $\Omega_\phi/\Omega_m = \text{constant}$, respectively, as a result of Ω_ϕ being constant and of the relation between the density parameters for the field and the fluid components. Additionally, we point out that we can now explicitly see the first potential term contributing exclusively to the scaling solutions (a1) and (a2) while the second potential term is singularly responsible for driving the solutions to the scalar field dominated point (b).

At this point, we are left with a model with a set of four free parameters $\{\beta_1, \beta_2, A, \lambda\}$. To ensure that during our investigation we are working with a stable model, we choose to fix two out of our four parameters and then constrain the values of the remaining two using the theoretically consistent viability conditions discussed in Section 5.2.1. This means that for points (a1) and (a2) we must enforce the conditions (5.32)-(5.34) with the replacement $\beta \to \beta_1$ as well as $\gamma = 4/3$ for (a1) and $\gamma = 1$ for (a2). Then, for the critical point (b), we require that the conditions (5.37)-(5.42) hold after the substitution $\beta \to \beta_2$.

In this case, we opt to fix β_1 and β_2 and constrain the allowed parameter space for A and λ, doing so for two cases: (i) $\beta_1 = 100$, $\beta_2 = 0.7$ and (ii) $\beta_1 = 100$, $\beta_2 = 2.5$. In Figure 5.1 we plot the found viable parameter regions (in light blue) of the (λ, A) plane for cases (i) (left panel) and (ii) (right panel). In addition to the already discussed viability requirements, there are two additional observational bounds plotted in Figure 5.1 which, we stress, are not imposed but simply considered. The first one is an extra constraint arising from BBN [164], which bounds the scalar field density parameter in the scaling radiation regime $\Omega_\phi^{(r)}$ to be [180]

$$\Omega_\phi^{(r)} = \frac{4}{\beta_1^2}\left[1+\frac{A}{2}\,(5\beta_1-4\lambda)\right] < 0.045. \tag{5.56}$$

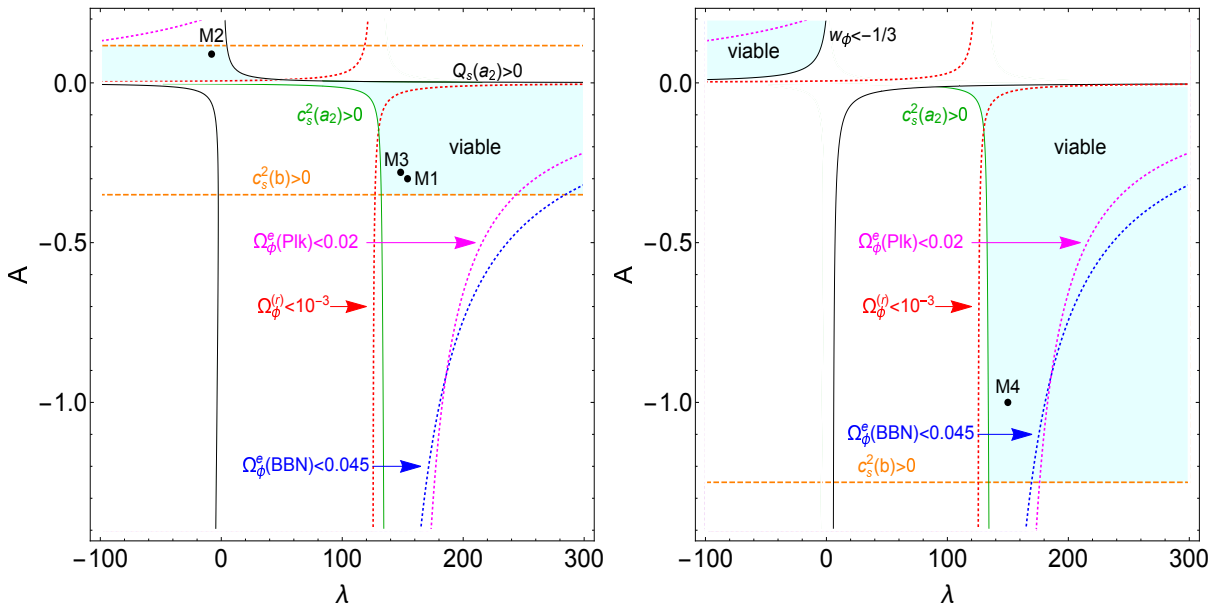

Figure 5.1: Figure 1 in Ref. [43]. Viable model parameter spaces (light blue) in the (λ, A) plane for the two cases: (i) $\beta_1 = 100$, $\beta_2 = 0.7$ (left) and (ii) $\beta_1 = 100$, $\beta_2 = 2.5$ (right). Each boundary is obtained by imposing the viability conditions discussed in Section 5.2.1. We also plot the observational bounds (5.56) and (5.57), together with the region where $\Omega_\phi^{(r)} < 10^{-3}$. The labels M1, M2, M3 and M4 correspond to the toy models presented in Table 5.2.

The second observational bound comes from CMB measurements provided by the *Planck* team [128]. According to these, the scalar field density parameter verifies: $\Omega_\phi < 0.02$ (95% C.L.) at redshift $z \approx 50$. Therefore, if the solution is in the scaling regime during the matter era, the scalar field density parameter $\Omega_\phi^{(m)}$ is constrained to be

$$\Omega_\phi^{(m)} = \frac{3}{\beta_1^2}\left[1 + A\left(3\beta_1 - 2\lambda\right)\right] < 0.02. \tag{5.57}$$

Finally, we also include the condition $\Omega_\phi^{(r)} < 10^{-3}$ without imposing it, simply to understand in which region of the (λ, A) plane the primordial value of Ω_ϕ is small.

The enforcement of the previous ensemble of conditions determines the regions inside of which we can pick our parameter values while being sure that the system is stable at the critical points. However, the imposed conditions do not guarantee the stability of our system during its entire evolution, which instead needs to be confirmed. We did so for several combinations of parameters inside the allowed regions and found that the system remains stable at any time. Regarding the observational bounds, we can see that in the first case (left plot) they only exclude a small region of the viable parameter space whereas for the second case (right plot) the excluded region is larger. In either case, however, we note that it is always possible to select a set of parameters lying inside the theoretically viable parameter region while still meeting the observational bounds. In fact, from this point forward we select four sets of such parameters that we shall use to investigate the cosmological evolution of the SCG model. These correspond to the four toy models {M1, M2, M3, M4} that are depicted in Figure 5.1, for which the corresponding parameter choices are shown in Table 5.2. Additionally, we also consider a standard Quintessence model (QE1) which we can easily reproduce simply by setting $A = 0$. The latter is also listed in Table 5.2.

The first test that we can perform regarding our model, is to numerically verify if the

Model	β_2	A	λ	$w_\phi^{(0)}$	$w_{\rm eff}^{(0)}$	$\Omega_\phi(z=50)$
M1	0.7	-0.3	154	-0.993	-0.675	1.0×10^{-3}
M2	0.7	0.09	-8	-0.988	-0.672	8.9×10^{-3}
M3	0.7	-0.28	148.3	-0.993	-0.675	4.3×10^{-5}
M4	2.5	-1	150	-0.975	-0.663	3.6×10^{-4}
QE1	0.7	0	0	-0.927	-0.630	3.2×10^{-4}

Table 5.2: Model parameters β_2, A and λ that characterize our research toy models M1-M4 and QE1. All of these models have $\beta_1 = 100$. In addition to the parameter values, we also show today's dark energy equation of state $w_\phi^{(0)}$, today's effective equation of state $w_{\rm eff}^{(0)}$ and the dark energy density parameter Ω_ϕ at the redshift $z = 50$. All of the presented models give rise to the cosmic acceleration today, i.e., they verify $w_{\rm eff}^{(0)} < -1/3$.

background solutions do in fact go through early-time scaling radiation and matter eras and then later approach the scalar field attractor and enter a period of cosmic acceleration. For the purpose of this test and that of all of the numerical simulations presented in this Subsection, we select the initial conditions for x an y_1 corresponding to critical point (a1). This fixes the start of the background evolution in the scaling radiation era. Additionally, the initial conditions for y_2 and Ω_r are chosen in order to guarantee that at present time we have the observationally consistent values: $\Omega_\phi^{(0)} = 0.68$ and $\Omega_r^{(0)} = 10^{-4}$. We also choose to start integrating our system from the initial redshift $z_i = 10^{10}$.

In Figure 5.2, the evolution of the total fluid density $\rho_m + \rho_r$ is plotted together with the evolution of the scalar field energy densities for models M1 and QE1. The scaling behaviour is evident at early times (large z), where we can see that the fluid and field densities maintain a constant ratio between them ($\rho_\phi \propto \rho_m + \rho_r$). At later times (small z), the solutions then exit the scaling regime, ρ_ϕ becomes dominant and the Universe enters the period of accelerated expansion. This simulation, together with similar ones for the other M models, allows us to conclude that our model with two exponential terms of the form (5.45) and with the cubic coupling $G_3 = A\ln Y$ is indeed capable of reproducing the desired expansion history.

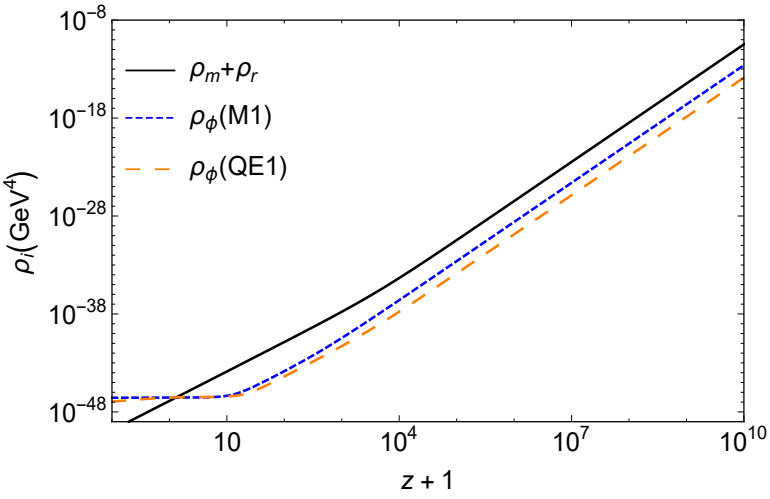

Figure 5.2: Evolution of the total fluid density $\rho_m + \rho_r$ (solid black line) and scalar field density ρ_ϕ for models M1 (dashed blue line) and QE1 (long-dashed orange line) as a function of redshift $z+1$. The corresponding model parameters are given in Table 5.2. The initial conditions for x and y_1 are chosen to match critical point (a1) whereas those for y_2 and Ω_r are chosen to realize today's density parameters $\Omega_\phi^{(0)} = 0.68$ and $\Omega_r^{(0)} = 10^{-4}$.

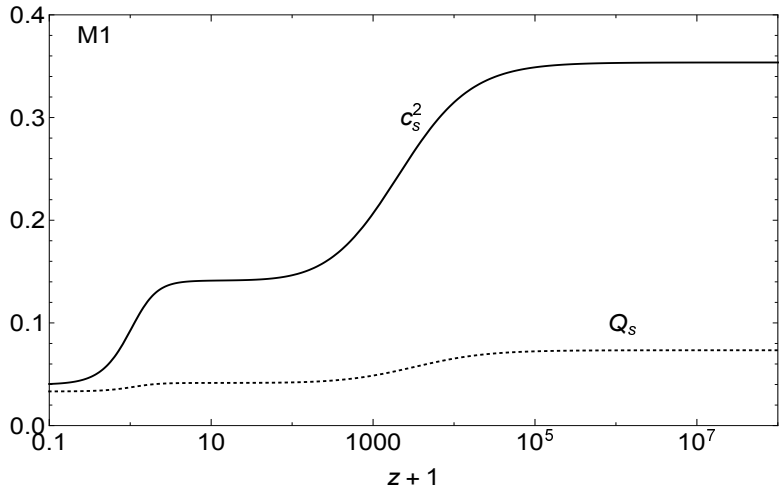

Figure 5.3: Figure 3 in Ref. [43]. Evolution of the square of the propagation speed c_s^2 (solid line) and of the kinetic term Q_s (dotted line) as a function of redshift $z+1$ for model M1 of Table 5.2.

As we previously mentioned, the viability conditions applied to find the allowed parameter space for A and λ only guarantee the stability of the evolution around the critical points. Thus, another fundamental preliminary test is that of verifying if this stability is in fact maintained throughout the entire evolution so that the system avoids the appearance of ghost and Laplacian instabilities. To that purpose, we check if the kinetic term Q_s and the square of the propagation speed c_s^2, given by equations (5.27) and (5.28), remain positive during the system's evolution. In Figure 5.3, we plot the evolution of the previous quantities for model M1. As we can observe, both c_s^2 and Q_s remain positive at all times, meaning that the model is not plagued by either ghost or Laplacian instabilities during its entire cosmological evolution. We have verified that this is the case for all the models featured in Table 5.2.

In Figure 5.4, we plot the evolution of the density parameters for the M2 model of Table 5.2. In general, we can observe the usual succession of cosmological eras: first the dominant contribution comes from radiation, then we have a matter-dominated period and finally DE, or in this case the scalar field, takes over. Furthermore, we observe that the density contribution

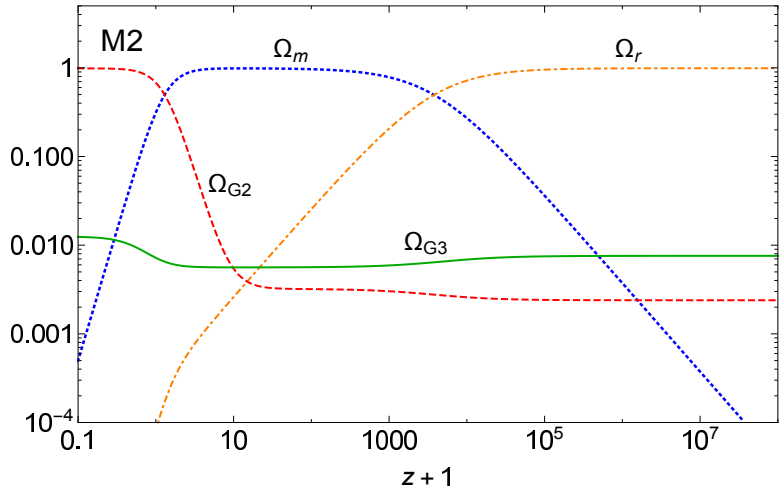

Figure 5.4: Figure 4 in Ref. [43]. Evolution of the density parameters Ω_r (dot-dashed orange line), Ω_m (dotted blue line), Ω_{G_2} (dashed red line) and Ω_{G_3} (solid green line) for the model M2. The density parameters Ω_{G_2} and Ω_{G_3} arise from the contributions of the Lagrangian terms G_2 and $-G_3\Box\phi$, respectively.

from the cubic coupling G_3, i.e., Ω_{G_3}, dominates over the quadratic Lagrangian's contribution Ω_{G_2} at early times. However, at more recent times ($z \lesssim 10$), Ω_{G_2} becomes the main contribution to Ω_ϕ. This serves to prove that the cubic coupling can be the dominant contribution to the scalar field density during the scaling eras but then be suppressed at low redshifts.

Finally, let us consider the evolution of the scalar field EoS parameter for our models, which we present in Figure 5.5. For models M1 and M2 we can clearly see a scaling radiation epoch ($w_\phi \simeq 1/3$) followed by a matter scaling epoch ($w_\phi \simeq 0$). On the other hand, in models M3 and M4 the matter scaling epoch seems almost completely absent. This is a reflection of the fact that both of these models present a much smaller value of Ω_ϕ at point (a2) than at point (a1). For example, for M3 we verify that $\Omega_\phi(a1) = 5.6 \times 10^{-3}$ while $\Omega_\phi(a2) = 1.4 \times 10^{-5}$. In these cases, the matter-dominated epoch is simply a transient period between critical points (a1) and (b), as we can see by the more sudden drops of the EoS parameter from $w_\phi \simeq 1/3$ to $w_\phi \simeq -1$. Additionally, let us note that all of the M toy models give rise to $w_\phi^{(0)}$ closer to -1 than QE1, as we can also conclude from the respective column of Table 5.2. This is an attractive feature since it shows better agreement with current observational constraints [3, 12, 14, 181] in comparison to Quintessence.

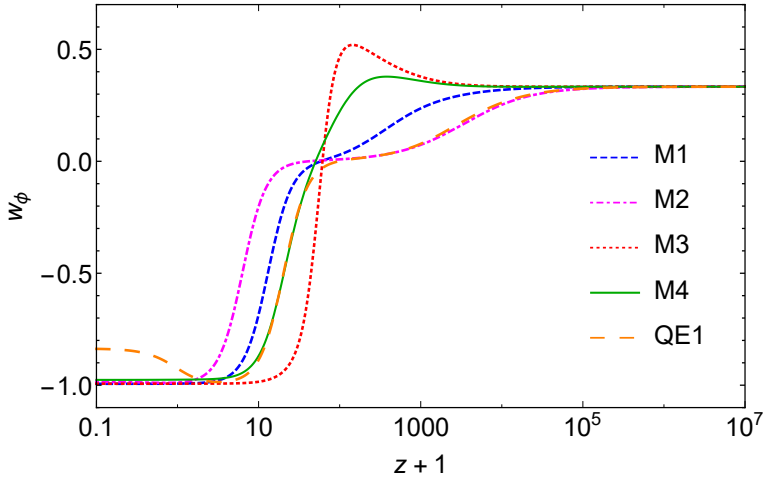

Figure 5.5: Evolution of the scalar field equation of state parameter w_ϕ for the models of Table 5.2, specifically: QE1 (long dashed orange line), M1 (dashed blue line), M2 (dot-dashed magenta line), M3 (dotted red line) and M4 (solid green line).

5.3 Cosmology of Linear Scales

Our next objective is to study the evolution of linear scalar perturbations in the constructed SCG model and analyse its impact on the cosmological observables. To do this, we will use the EFT formalism discussed in Chapter 4. Therefore, we need to start by computing the mapping of the model into the EFT language, i.e., we need to specify the forms of the EFT functions for the SCG model so that we can then implement it in the Einstein-Boltzmann solver `EFTCAMB` and use it to evolve the perturbation equations and study the effects on the cosmological observables.

5.3.1 Mapping in the EFT Language

To find the corresponding expressions of the EFT functions we resort to the mapping procedure we have reviewed in Section 4.4. Thus, we start by translating the SCG action (5.1)

into the ADM formalism by following the procedure provided in [36]. Once this is done, we use the mapping relations given in (4.28) to finally compute the EFT functions. At the end of this procedure, and keeping consistent with `EFTCAMB`'s notation, we find:

$$\frac{ca^2}{m_0^2} = 3\mathcal{H}^2x^2 + A\mathcal{H}^2\left[3\sqrt{6}x - 6\lambda x^2 - \sqrt{6}\left(x' + \tilde{h}x\right)\right], \tag{5.58}$$

$$\frac{\Lambda a^2}{m_0^2} = 3\mathcal{H}^2\left(x^2 - y_1^2 - y_2^2\right) - 2A\mathcal{H}^2\left[3\lambda x^2 + \sqrt{6}\left(x' + \tilde{h}x\right)\right], \tag{5.59}$$

$$\gamma_1 = \sqrt{\frac{3}{2}}\frac{A\mathcal{H}^2}{a^2H_0^2}\left(\tilde{h}x - 3x + x'\right), \tag{5.60}$$

$$\gamma_2 = -\frac{2\sqrt{6}A\mathcal{H}}{aH_0}x, \tag{5.61}$$

together with $\gamma_i = 0$ for $i = 3, 4, 5, 6$. We note that the EFT functions are completely expressed in terms of the model's parameters and variables. As a result, the code can use the evolution of the latter, obtained through an implemented background solver, to find the evolution of the EFT functions and proceed with solving the already implemented perturbation equations.

The forms of our EFT functions do, however, already reveal some information regarding the expected effects of the model parameters. Since we know that the γ_1 and γ_2 functions are going to be the ones with the most impact on the perturbative sector, we can expect that modifications in the growth of perturbations will arise when the parameter A, present in both (5.60) and (5.61), is non-zero. On the other hand, λ will propagate its effect through the background evolution since it enters in the expressions for the background EFT functions c and Λ.

Additionally, now that we have the expressions for the EFT functions we can also compute the SCG's parametrization in terms of the α-basis we introduced in Section 4.6. To do this, we only need to substitute the obtained EFT functions in equations (4.31) and (4.32), leaving us with:

$$M_*^2 = m_0^2, \quad \alpha_K = 6x^2\left(1 - 2A\lambda\right), \quad \alpha_B = -\sqrt{6}Ax, \quad \alpha_M = 0, \quad \alpha_T = 0. \tag{5.62}$$

In particular, from the form of α_B we can note that having $A \neq 0$ traduces a braiding effect where the kinetic terms of the metric and the scalar field become mixed.

5.3.2 Implementation in `EFTCAMB`

Finally, to proceed with the perturbative analysis of the SCG model we implement it on the Einstein-Boltzmann solver `EFTCAMB`. Since our aim is to investigate the full evolution of linear scalar perturbations, we implement the model using the *full mapping* approach. As we have previously discussed, this involves providing the code with a background solver as well as with the EFT functions corresponding to the SCG model. The former will be responsible for computing all the necessary information to finally evolve the full general linear perturbation equations which are already implemented in `EFTCAMB`. In practice, the background solver consists on a:

- routine to solve the background field equations which includes a bisection algorithm;
- routine to compute the Hubble parameter in conformal time $\mathcal{H}$ and its derivatives;

- routine to compute the evolution of the EFT functions and its derivatives.

Thus, once everything is implemented, the code starts by employing the background solver to determine the previous information before using it to evolve the perturbation equations and compute the output quantities.

To add the SCG model to `EFTCAMB` we created a new file (`10p6_Scaling_Cubic.f90`) where we implemented the autonomous system given by equations (5.49)-(5.50) so that we could solve for the model's background evolution. These were, of course, accompanied by the expressions of the featuring functions $\tilde{f}$ and $\tilde{h}$ which are given by equations (B.1) and (B.2) of Appendix B. Once the background system is solved and, consequently, the evolution of the variables $\{x, y_i\}$ have been found, the Hubble parameter in conformal time $\mathcal{H} \equiv d\ln a/d\tau$ and its derivatives can be computed through:

$$\mathcal{H}^2 = H^2 a^2 = \frac{8\pi G_N}{3\left(1-\Omega_\phi\right)}\left(\frac{\rho_{r,0}}{a^4}+\frac{\rho_{m,0}}{a^3}\right)a^2 \ , \tag{5.63}$$

$$\dot{\mathcal{H}} = \mathcal{H}^2\left(1+\tilde{h}\right), \tag{5.64}$$

$$\ddot{\mathcal{H}} = 2\mathcal{H}\dot{\mathcal{H}}\left(1+\tilde{h}\right)+\mathcal{H}^3\tilde{h}', \tag{5.65}$$

where the dot and prime superscripts represent derivatives with respect to the conformal time τ and $\ln a$, respectively, the 0 subscript denotes a quantity evaluated at present time and Ω_ϕ is given in terms of the model's variables following equation (5.48). Equations (5.63)-(5.65) also had to be implemented in the code.

Regarding the background solver, let us point out that we are intentionally leaving out of the implementation the differential equation pertaining the radiation density parameter Ω_r, i.e., we are leaving out equation (5.51). To understand why, we start by noting that by choosing to write the Hubble parameter as in equation (5.63) one is automatically fixing $H(t)$ at any t simply through Ω_ϕ and, consequently, the x and y_i variables that enter in the expression of this density parameter. Then, since the radiation density parameter can be written as

$$\Omega_r = \frac{8\pi G_N \rho_{r,0}}{3H^2 a^4}, \tag{5.66}$$

its value at a certain time is fixed alongside that of H^2 through x and y_i. As a result, we only need to provide initial conditions for x and y_i, i.e., we only need to give the set $\{x(t_i), y_1(t_i), y_2(t_i)\}$, to automatically fix $H(t_i)$ and $\Omega_r(t_i)$ as well.

The issue of initial conditions did merit some special consideration in the model's implementation. Similarly to what we did during the background study of our model in Section 5.2.2, the initial conditions for x and y_1 are selected to correspond to the critical point for radiation scaling (a1). This means that $x(t_i)$ and $y_1(t_i)$ are set to be exactly the ones given in (5.53), ensuring that our solutions start in the radiation scaling regime. The choice of initial condition for y_2 is still motivated by the need to recover a chosen value for the present time ($a = 1$) density parameters. In this case, it is important that today's value of the scalar field density parameter $\Omega_{\phi,0}$ verifies:

$$\Omega_{\phi,0} = x_{,0}^2 + y_{1,0}^2 + y_{2,0}^2 + 2x_{,0}A\left(\sqrt{6}-\lambda x_{,0}\right) = 1 - \frac{8\pi G_N\left(\rho_{r,0}+\rho_{m,0}\right)}{3H_0^2}, \tag{5.67}$$

where the values of $\rho_{m,0}$ and $\rho_{r,0}$ are inputs of `EFTCAMB` itself. To achieve this, we used a

bisection algorithm to tune the value of $y_2(t_i)$ until the previous condition is verified. This implies solving the background equations repeatedly using different initial values for y_2 until the calculated value of $\Omega_{\phi,0}$ is deemed close enough to the one fixed in `EFTCAMB`'s input parameters file. Numerically, this is done using a `while` cycle that calls on the background solver for three values of $y_2(t_i)$ in each iteration: a lower limit value, a higher limit value and a third one inside their interval. Once the background evolution is determined, the tolerance which is defined as

$$\mathrm{tol} = \frac{\left[\mathrm{x}_{,0}^2 + \mathrm{y}_{1,0}^2 + \mathrm{y}_{2,0}^2 + 2\mathrm{x}_{,0}\mathrm{A}\left(\sqrt{6} - \lambda \mathrm{x}_{,0}\right)\right] - \left[1 - 8\pi \mathrm{G_N}\left(\rho_{\mathrm{r},0} + \rho_{\mathrm{m},0}\right) / \left(3\mathrm{H}_0^2\right)\right]}{\left[1 - 8\pi \mathrm{G_N}\left(\rho_{\mathrm{r},0} + \rho_{\mathrm{m},0}\right) / \left(3\mathrm{H}_0^2\right)\right]}, \tag{5.68}$$

is computed for each of the $y_2(t_i)$ values. By comparing the sign of the intermediate value's tolerance with those of the lower and higher limits and moving the intermediate one accordingly, the allowed interval for $y_2(t_i)$ is successively shortened. Once the tolerance drops below the imposed limit of 10^{-6}, the cycle ends and the code moves on using the value found for $y_2(t_i)$ and the corresponding background solution.

In addition to the autonomous system equations which seed the background solver, we also implemented the EFT functions for the SCG model, given in Section 5.3.1, together with their derivatives: $\dot{c}a^2/m_0^2$, $\dot{\Lambda}a^2/m_0^2$, $d\gamma_1/da$ and $d\gamma_2/da$, so that the code can then evolve the perturbation equations which depend on them. Furthermore, since the latter depends on derivatives of $\tilde{h}$ and $\tilde{f}$, they are also included in the code. The expressions for all of the needed derivatives are explicitly given in Appendix B.

During the implementation process, efforts were also made to try to identify and dispose of any existing typos and to ensure the code was working correctly. For this purpose, several aspects of the `EFTCAMB` output were compared to the results obtained by explicitly implementing the SCG model in the numerical tool `Wolfram Mathematica`. This included background tests such as comparing the evolution of the Hubble parameter H and of the density parameters Ω_i, as well as a verification of the obtained evolution for the EFT functions. This crosscheck allowed us to test different parts of our code and helped in pinning down the source of any possible problem.

Once all is implemented and we become confident that the code is working properly, the SCG model can be studied using the `EFTCAMB` solver by selecting `EFTflag`$= 4$ together with `FullMappingEFTModel`$= 6$. The SCG flag was added in the `params_EFT.ini` file, being the command responsible for telling the code to select and run our model file. Additionally, in this file we also included a section where the values of our model parameters $\{\beta_1, \beta_2, A, \lambda\}$ can be set. These were left unspecified during the implementation and in this way they can be chosen at the beginning of each run of the model, allowing the user to easily study different combinations without having to alter the implementation file. Lastly, we note that even though so far the code remains private, we shall publicly release it on `http://eftcamb.org` once our work is completed.

5.3.3 Results on the Phenomenology of Cosmological Observables

In this section, we study the dynamics of scalar cosmological perturbations in the SCG model. To this purpose, we consider the perturbed FLRW line element given by equation (3.28)

and, making use of the phenomenological functions μ, Σ and η together with the `EFTCAMB` solver, analyse the evolution of linear perturbations in our model as well as its impact on the related cosmological observables.

Phenomenology of μ, Σ and c_s^2. As we saw in Section 3.3.2, the introduction of the phenomenological functions $\mu(k,t)$, $\Sigma(k,t)$ and $\eta(k,t)$ offers a practical way to study the evolution of perturbations in a certain model and especially its deviation from the standard growth behaviour of GR. By introducing them as we did in equations (3.35)-(3.37), these functions translate any existent departures from GR. The drawback is, however, that in general we can only find analytic expressions for μ, η and Σ under the QSA regime. For the GG class specifically, we presented the corresponding expressions which, we stress, are only found under the QSA, in equations (4.36)-(4.38).

Given the fact that the analytic forms for μ, η and Σ are expressed in terms of the EFT functions and α-basis parameters, we need both in order to compute their specific expressions in a given model. Since we have already worked out the mapping of our model and subsequently computed the α_i parameters, we just need to use the results of Section 5.3.1 in equations (4.36)-(4.38) to find that in the SCG model:

$$\eta = 1, \qquad \mu = \Sigma = 1 + \frac{2\alpha_B^2}{c_s^2 \alpha} = 1 + \frac{6A^2 x}{3x\left(1 - 2A\lambda - 2A^2\right) + 4\sqrt{6}A}, \tag{5.69}$$

where we have also used the speed of sound expression given in equation (5.28). From the above expressions, we start by noting that while there is no gravitational slip and the two potentials remain equal ($\Phi = \Psi$), the presence of the cubic coupling G_3 introduces modifications on both the structure growth ($\mu \neq 1$) and the evolution of the weak lensing potential ($\Sigma \neq 1$) for all non-zero values of A. Moreover, we can also infer that under the stability requirements of the absence of ghosts ($\alpha > 0$) and Laplacian instabilities ($c_s^2 > 0$) we have $\mu = \Sigma > 1$. As a consequence, we should expect enhancements of the growth of structure and gravitational lensing with respect to ΛCDM. We must remember, however, that all of this has been done under the QSA whereas in what follows we shall evolve the full perturbation equations using `EFTCAMB`. Nevertheless, the results obtained so far offer a good starting point for the following discussion.

To study the dynamics of perturbations in the SCG model, including understanding the effects caused by its different parameters, we consider the same four cases (M1, M2, M3, M4) that we used for the background analysis in Section 5.2.2 and that, we remember, are listed in Table 5.2. All M models share the same values of β_1 and β_2 with the exception of M4 which has a different value of β_2. Thus, their biggest differences reside in the choices of A and λ which, according to the expressions in equation (5.69), are the two parameters directly involved in the modifications of the evolution of perturbations. Nonetheless, it is still possible for β_1 and β_2 to have some effect through their impact on the background evolution.

We start by considering Figure 5.6 in which we plot the evolution of $\mu - 1$ for all M models. As we can see, this quantity increases in time for all cases, even if only slightly for M2. Then, the present time ($z + 1 = 1$) deviation of μ from 1 is of about 2% for both M1 and M3, 0.08% for M2 and 8% for M4. As one expected from equation (5.69), the largest deviation from GR arises for the model with the largest value of A^2, i.e., for M4. Simultaneously, the M2 model, which is the one with the lowest magnitudes of both A and λ, presents the smallest deviation in Figure 5.6. Alternatively, the small magnitude of $\mu - 1$ for M2 in comparison to the other

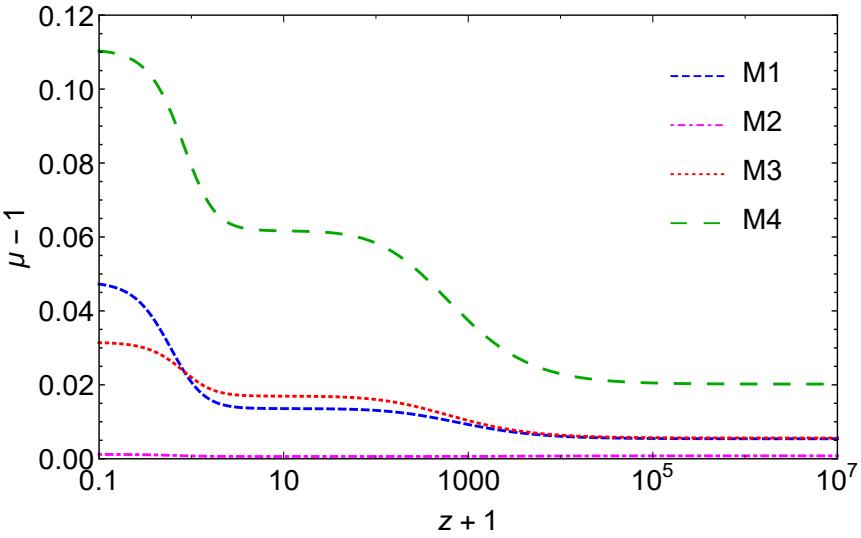

Figure 5.6: Evolution $\mu - 1$ versus $z + 1$ for the four M models of Table 5.2, specifically: M1 (dashed blue line), M2 (dot-dashed magenta line), M3 (dotted red line) and M4 (long dashed green line).

models can be clearly understood by considering their respective evolution of the square of the speed of propagation, c_s^2. We present the latter in Figure 5.7, where we observe that c_s^2 for M2 is considerably larger than those of the other three models. Thus, since c_s^2 appears in the denominator of μ's deviation from 1, the larger its magnitude the smaller the deviation is.

We note that since in our case $\mu = \Sigma$, the previous discussion directly translates to the behaviour of Σ. Consequently, the results of Figure 5.6, once again, lead us to expect enhancements of both the growth of structure and the gravitational lensing effect with respect to ΛCDM, with the departures being proportional to A^2.

Evolution of the gravitational potentials Ψ and Φ. Let us now focus on the output of `EFTCAMB`. This includes the full evolution of the metric potentials, Ψ and Φ, obtained, as we have stated before, without resorting to any approximation. However, we chose to compute this quantity at the wavenumber $k = 0.01$ Mpc^{-1} which is well within the range of the QSA, and therefore can be compared with the results at the beginning of this Subsection. On the top

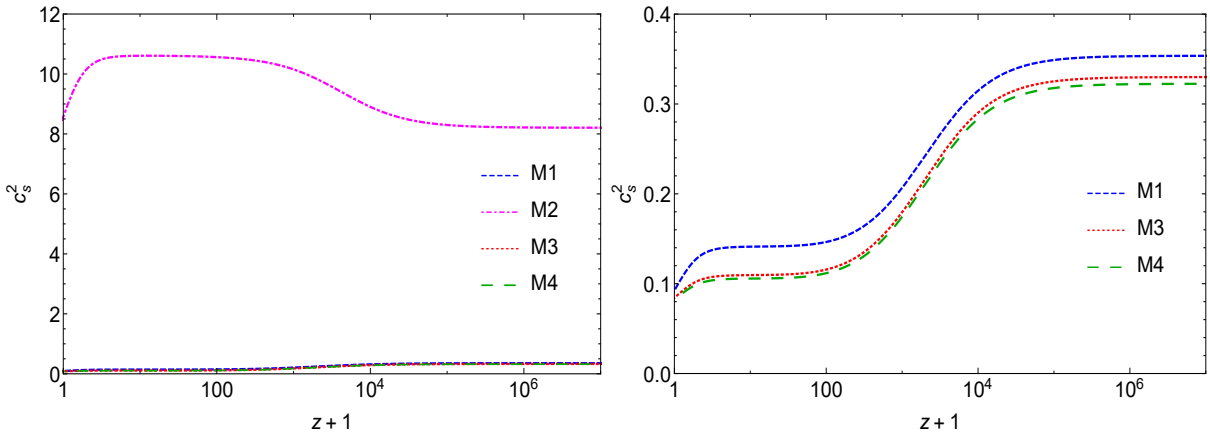

Figure 5.7: (Left panel) Evolution of the square of the propagation speed of the scalar modes c_s^2 versus $z + 1$ for the four M models of Table 5.2, specifically: M1 (dashed blue line), M2 (dot-dashed magenta line), M3 (dotted red line) and M4 (long dashed green line). (Right panel) Zoom on the three models with lower c_s^2, i.e., M1, M3 and M4, maintaining the same representation scheme.

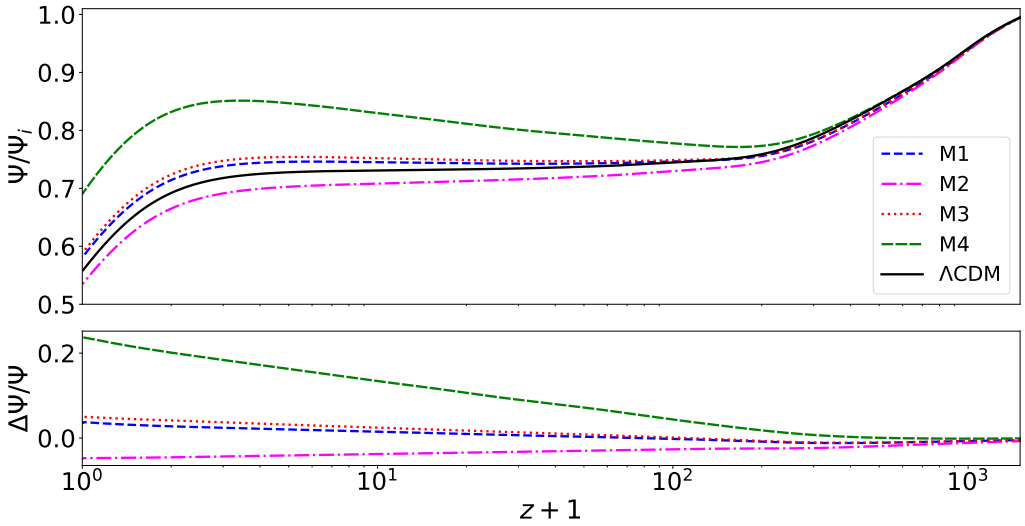

Figure 5.8: (Top) Evolution of the metric potential Ψ normalized by its initial value Ψ_i as a function of redshift $z+1$ for the wavenumber $k = 0.01$ Mpc^{-1}. This evolution is presented for the four M models listed on Table 5.2 and for ΛCDM (solid black line). (Bottom) Percentage relative difference of the models' Ψ in relation to its value in ΛCDM.

panel of Figure 5.8 we plot the evolution of Ψ normalized by its initial value Ψ_i for the M models and ΛCDM. On the bottom panel, we show the percentage difference for Ψ between each of the models and ΛCDM. Although here we only show Ψ, the evolution of Φ was confirmed to be the same as for the first potential, hence verifying $\Psi = \Phi$. Regarding Figure 5.8, we find that at late-time the gravitational potentials for models M1, M3 and M4 are enhanced with respect to ΛCDM. The largest deviation verified is of about $\sim 24\%$ at present time and it arises for M4, a fact that is consistent with our early estimation of the deviation being mostly influenced by the value A^2. Following only this logic, and taking into account the values of A presented in Table 5.2, the growing order in deviation should be M3, M1, M4. However, in Figure 5.8 we can see M3 coming slightly above M1, inverting their expected order. This can be attributed to the combination of these models' values for A and λ. In fact, the A parameters of the two models are very close whereas M3's value for λ is noticeably smaller than that of M1. Since the latter parameter features in the denominator for the deviation of μ, the existent difference in λ combined with the close proximity of the values of A is sufficient to raise M3 slightly above M1. We can also look at this effect through the models' speeds of propagation c_s^2. Focusing on the right panel of Figure 5.7, we can see that the propagation speed for M1 is always slightly larger than that of M3. Since c_s^2 appears in the denominator for μ's deviation from unity in equation (5.69), we can again understand why for similar values of A the M3 model ends up above M1.

For M2, however, we observe a late-time suppression of Ψ with respect to ΛCDM. To try to understand this behaviour, let us start by remembering that our model verifies $\Psi = \Phi$ and as such we can re-write the Poisson equation (3.35) using Ψ instead of Φ:

$$-\frac{k^2}{a^2}\Psi = 4\pi G_N \mu \rho \Delta. \tag{5.70}$$

This means that the evolution of the gravitational potential is connected to μ but also to the scale k and to the density contrast δ through the comoving density contrast Δ. Since in this

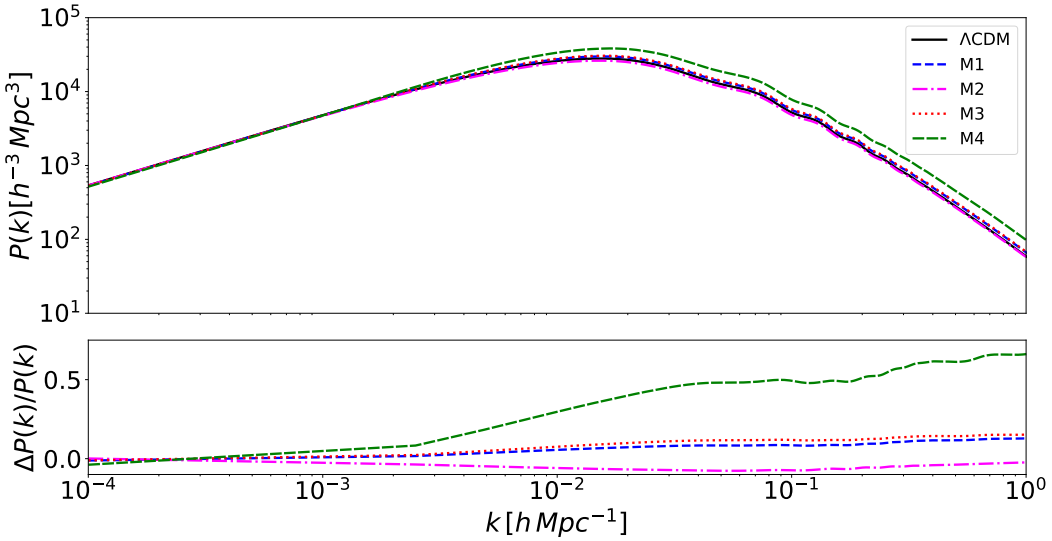

Figure 5.9: (Top) Matter power spectra $P(k)$ for ΛCDM (solid black line) and the four M models of Table 5.2, specifically: M1 (dashed blue line), M2 (dot-dashed magenta line), M3 (dotted red line) and M4 (long dashed green line). (Bottom) Percentage relative difference of the matter power spectra computed with respect to ΛCDM.

case we are considering the evolution of Ψ for a fixed k, this leaves μ and δ as the possible culprits for the observed suppression. However, as we have seen through the expression for μ and can also observe in Figure 5.6, μ is expected to be above 1 for M2, even if only slightly. So we also cannot explain M2's suppression from the behaviour of μ, meaning that it should be δ to be suppressed and lead Ψ to the same result. To test the validity of this hypothesis, we analysed the matter power spectrum $P(k)$, defined in (3.42) and presented in Figure 5.9 for all M models. By considering this figure, we do verify that the matter power spectrum of M2 is suppressed with respect to ΛCDM at $k = 0.01$ Mpc^{-1}, meaning that at this scale the growth of matter density perturbations, i.e., of δ, is suppressed in relation to that of the standard model. This in turn seems to lead to a suppression of Ψ as well.

The matter power spectrum $P(k)$. Now, turning our complete attention to the matter power spectra presented on the top panel of Figure 5.9, we see that all the M models seem to closely follow the behaviour of ΛCDM at large scales ($k < 10^{-3}$ hMpc^{-1}), with M4 showing only a slight suppression according to the difference plot on the figure's bottom panel. The more noticeable deviations from the matter power spectrum of ΛCDM start to appear around $k = 10^{-3}$ hMpc^{-1}. Below that scale, we can see an enhancement of the growth of structure with respect to ΛCDM for models M1, M3 and M4, as well as the already reported suppression in the case of M2. The noted enhancements are in agreement with the observed behaviour of μ, again verifying that the largest deviation, which reaches about 66% at present time, arises for M4, the model with the greatest value of A^2. The models M1 and M3 remain very close to one another and follow the same order as in Ψ/Ψ_i.

To try to gain some insight into the behaviour of M2, which appears suppressed in relation to ΛCDM, we recall the linear growth equation (3.39), introduced in Section 3.3.2. We can look at this equation much like as an harmonic oscillator equation. In this light, the second term, which involves the background history $H(t)$, can be considered as a friction term hindering

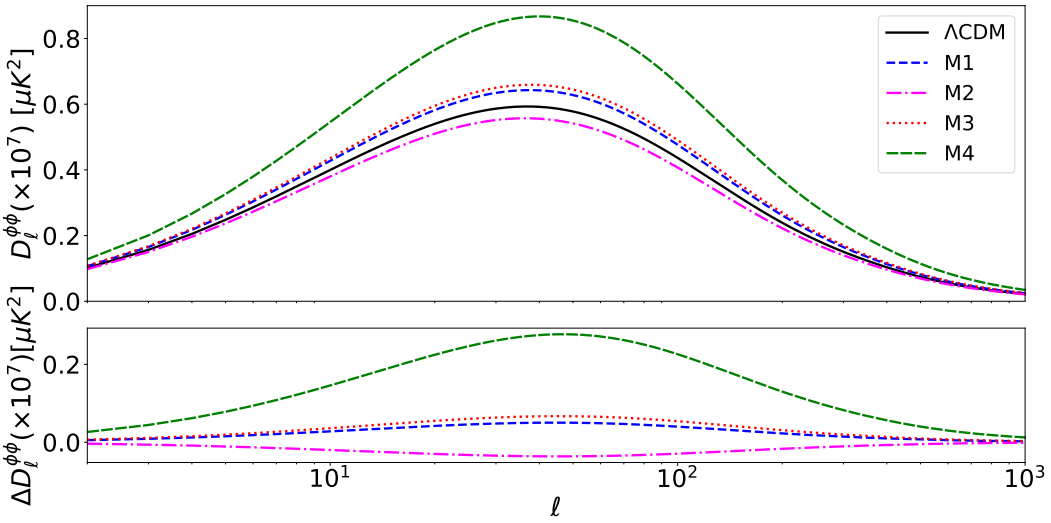

Figure 5.10: (Top) Lensing angular power spectra $D_\ell^{\phi\phi} = \ell(\ell+1)C_\ell^{\phi\phi}/(2\pi)$ for ΛCDM (solid black line) and the four M models of Table 5.2, namely: M1 (dashed blue line), M2 (dot-dashed magenta line), M3 (dotted red line) and M4 (long dashed green line). (Bottom) Difference between the lensing power spectra of each of the M models and that of ΛCDM.

the growth of matter perturbations whereas the third term can be taken as the forcing term promoting their growth. Therefore, the growth of δ is determined by the balance between the two contributions. Now, according to Figure 5.6, the deviation of μ from 1 in the M2 case is almost null. As a result, we expect a very small additional contribution coming from the forcing term. Given this, the friction term has the opportunity to provoke a suppression of the structure growth caused by the background dynamics acting through $H(t)$. If the background effect is in fact significant, M2's small value of A may not be capable of compensating for it and the matter power spectrum falls below the one of ΛCDM. This effect has previously been observed for Quintessence [182] and is also maintained in models where A is very small and, as we have stated before, its magnitude becomes incapable of compensating for the background effect. This feature might also prove very attractive since it offers an opportunity to alleviate the existent tension regarding $\sigma_{8,0}$, i.e., the present day value of the matter power spectrum at $8h^{-1}$ Mpc. A discordance of about 2.3σ on $\sigma_{8,0}$ can be spotted between the Weak Lensing Kilo-Degree Survey (KiDS) [183] and *Planck*'s CMB data [183–187], with the former predicting a smaller amplitude for $\sigma_{8,0}$. Thus, our model might show a better agreement with KiDS data and possibly offer an opportunity to alleviate the discordance between the two data sets. This will be the subject of a future study.

Lensing potential and power spectrum. Regarding the effects of the SCG model on gravitational lensing, we expect the Weyl potential $\phi_{len} = (\Phi + \Psi)/2$ to present a similar behaviour to that of the gravitational potential Ψ since there is no gravitational slip. To analyse this, we consider the lensing angular power spectrum $C_\ell^{\phi\phi}$ which we have defined in equation (3.50) and plot on the top panel of Figure 5.10 under the redefinition $D_\ell^{\phi\phi} = \ell(\ell+1)C_\ell^{\phi\phi}/(2\pi)$. Again, for models M1, M3 and M4 we verify an enhancement with respect to ΛCDM, following the same order as for Ψ and the matter power spectra, and reflecting the fact that $\Sigma = \mu > 1$. Furthermore, similarly to what we observed in the previous two situations, M2 is the only model

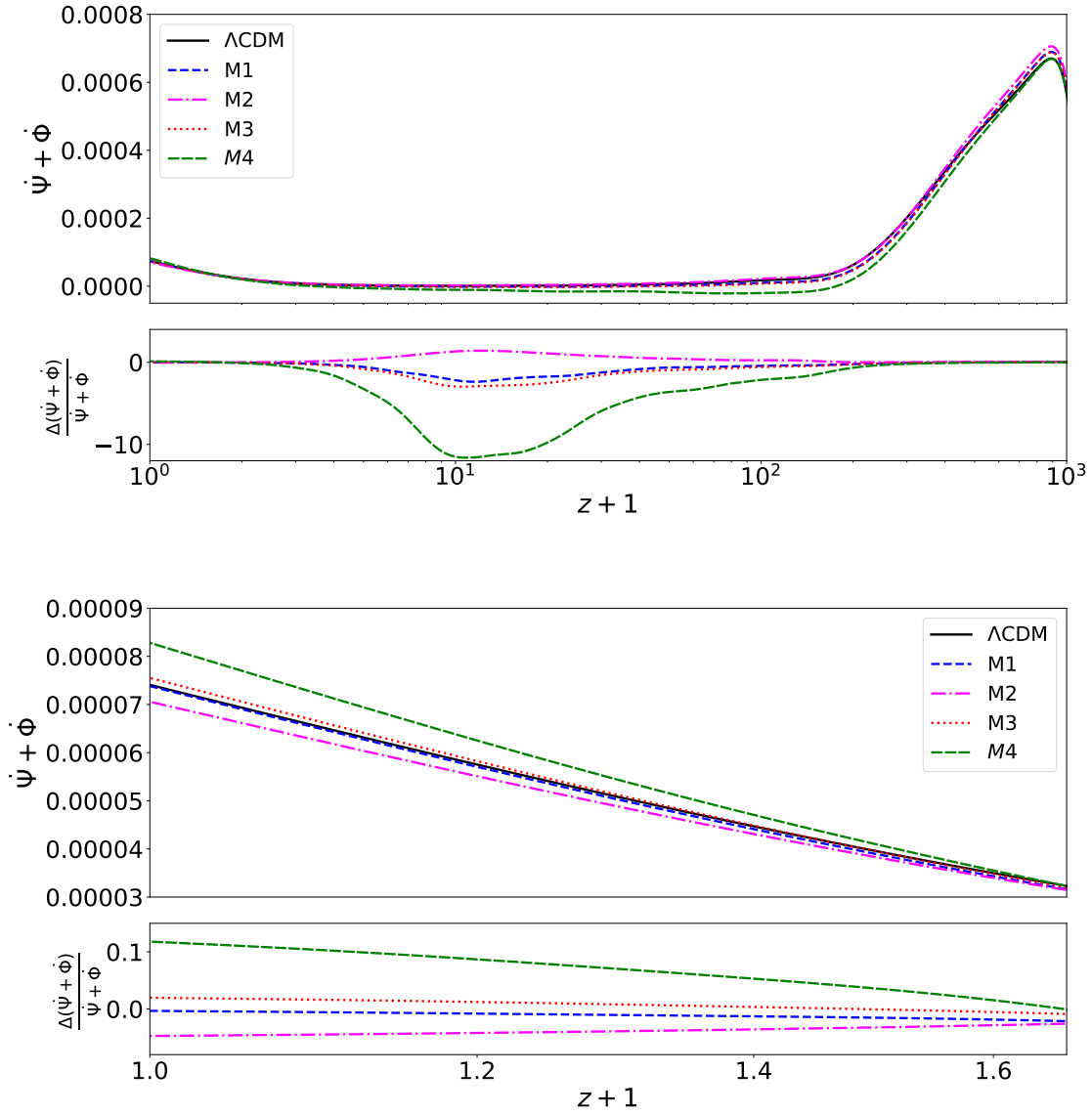

Figure 5.11: Complete evolution (top plot) and late-time zoom (bottom plot) of the time derivative of $\Psi+\Phi$, computed at $k=0.01$ Mpc^{-1}, for ΛCDM (black solid line) and the four M models of Table 5.2, namely: M1 (dashed blue line), M2 (dot-dashed magenta line), M3 (dotted red line) and M4 (long dashed green line). Both plots are accompanied by a bottom panel displaying the percentage relative difference of the M models' $\dot{\Psi}+\dot{\Phi}$ computed with respect to ΛCDM.

for which we register a suppression of the lensing potential with respect to the standard model. This is connected with the model's weaker ability to produce structure, due to the suppressed matter power spectrum, which in turn leads to a smaller lensing effect.

ISW effect and CMB TT power spectrum. Next, we study the impact of our SCG model on the CMB temperature anisotropies. As we saw in Section 3.3.3, the small temperature fluctuations around the CMB's mean temperature can be described by the temperature-temperature (TT) angular power spectrum C_ℓ^{TT} which can be computed using equation (3.47). Thus, we shall consider Figures 5.12 and 5.13 in which we plot the CMB TT power spectra as $D_\ell^{TT}=\ell(\ell+1)C_\ell^{TT}/(2\pi)$, first at large angular scales ($\ell\lesssim 50$) and then for a wider range of scales. To help with the discussion of these plots, we also present the evolution of the time

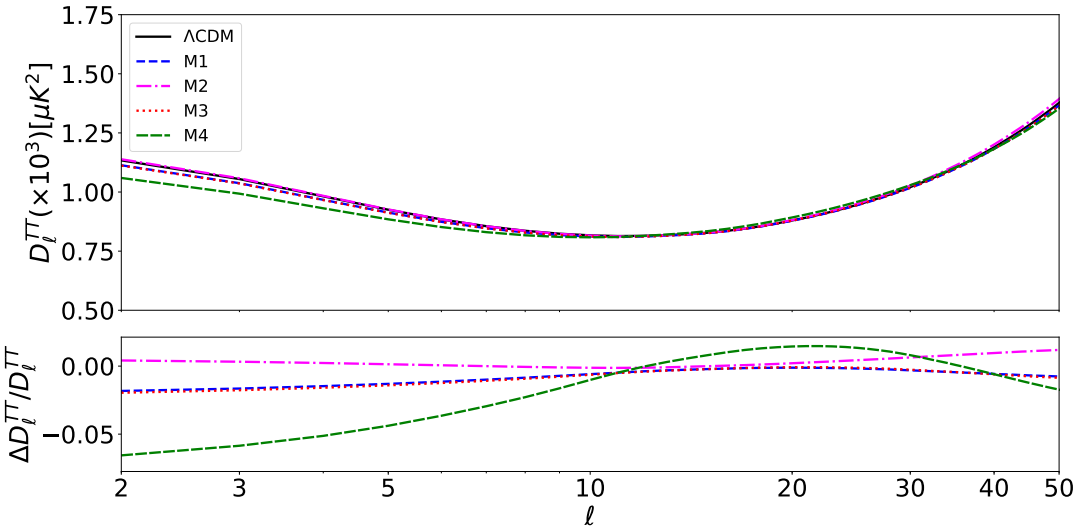

Figure 5.12: (Top) CMB temperature-temperature (TT) angular power spectra $D_\ell^{TT} = \ell(\ell+1)C_\ell^{TT}/(2\pi)$ at large angular scales for ΛCDM (solid black line) and the four M models of Table 5.2, namely: M1 (dashed blue line), M2 (dot-dashed magenta line), M3 (dotted red line) and M4 (long dashed green line). (Bottom) Percentage relative difference of the M models' TT power spectra with respect to ΛCDM.

derivative of $\Psi + \Phi$ in Figure 5.11. As we saw in Section 3.3.3, this derivative serves as the source for the ISW effect which contributes to the shape of the TT power spectrum. Since the power spectra plots are all computed at present time ($z = 0$), Figure 5.11 includes a zoom of the ISW source on this time frame.

Focusing first on the spectra at large angular scales, and thus on Figure 5.12, we find that the large-scale ISW tails for models M1, M3 and M4 are suppressed with respect to ΛCDM while M2's is slightly enhanced but in general very close to the latter. Since modifications on this end of the spectra are attributed to the late-time ISW effect, we turn to the bottom plot of Figure 5.11 to try to understand the observed behaviour. By doing so, we see that M4 again presents the largest deviation from ΛCDM, which was to be expected since it is the model where Σ most departs from unity. The observed enhancement of $\dot{\Psi} + \dot{\Phi}$ with respect to the standard model, which reaches about 12% at present time, offers a significant contribution to C_ℓ^{TT} in such a way that it leads to a noticeable suppressed ISW tail in Figure 5.12. For both M1 and M3, the smaller deviations of Σ from 1 are translated to similarly small present time deviations of the ISW source from that of ΛCDM: 0.3% and 2%, respectively. These small changes on the ISW contribution work only to slightly suppress the models' low-ℓ TT power spectra. Finally, for M2 we find the smallest magnitude of Σ is still capable of originating a $\sim 5\%$ suppression of $\dot{\Psi} + \dot{\Phi}$ in relation to the standard model. This decrease in the contribution from the late-time ISW effect results in a small enhancement of M2's ISW tail, most noticeable in the difference plot presented on the bottom panel of Figure 5.12.

Then, considering the high-ℓ (or small angular scales) CMB TT power spectra plotted in Figure 5.13, we remember our discussion in Section 3.3.4 and look for two main modified features regarding the acoustic peaks: changes in their positions and/or in their amplitudes. The first is usually attributed to modifications of the expansion history, i.e., of $H(t)$, with respect to ΛCDM. In Figure 5.13, we do not note any significant peak shifting for any of the M models.

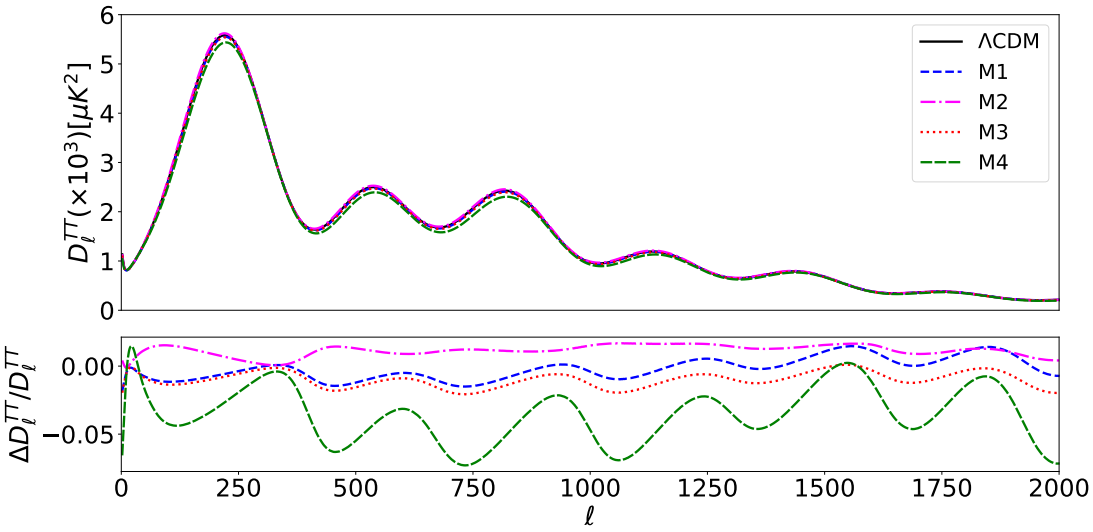

Figure 5.13: (Top) CMB temperature-temperature (TT) angular power spectra $D_\ell^{TT} = \ell(\ell+1)C_\ell^{TT}/(2\pi)$ for ΛCDM (black solid line) and the four M models of Table 5.2, namely: M1 (dashed blue line), M2 (dot-dashed magenta line), M3 (dotted red line) and M4 (long dashed green line). (Bottom) Percentage relative difference of the M models' TT power spectra with respect to ΛCDM.

However, to confirm this impression we plot the difference of the Hubble parameter H in relation to the standard model as a function of redshift $z+1$ in Figure 5.14. In the latter, we do not find any significant modifications that would justify large changes in the peak positions. The largest deviations verified, which happen for M2 at early-time and M4 at late-time, are always smaller than 1%. This justifies the absence of any visible shifting of the acoustic peaks.

On the other hand, we observe a difference in height between the peaks of M4's power spectrum and those of ΛCDM, with the former coming up below the standard model. The peak amplitude is known to be altered in models that show early-time modifications of gravity [188, 189]. To try to understand why this modification is only present in the case of M4, we can consider the contribution arising from the y_1 variable since, as we have previously discussed, the first potential is the one that is active on the concerning evolution period. Even though it does not enter directly in the perturbation equations, y_1 modifies the early-time expansion history. Therefore, it impacts the evolution of the gravitational potentials and consequently modifies the early-ISW effect as well. In Figure 5.15, we present the evolution of y_1 for all M models, where we can verify that M4 is in fact the one receiving the largest contribution from y_1 at all times. Furthermore, according to the top plot of Figure 5.11, we also find that out of the four considered models, M4 is the one with the smallest early-time ISW contribution, which has a role in the peak suppression of M4.

In summary, we find that the SCG model has a measurable impact on different cosmological observables, offering many testable features for present and future observational surveys. Additionally, the model's possibility to reproduce a matter power spectrum with lower amplitude with respect to ΛCDM, a feature supported by some Weak Lensing observational data, might represent an important advantage over the standard model. The next step in testing the SCG model shall be to directly connect it with available observational data in order to constrain its parameter space. This involves performing a Markov-Chain Monte-Carlo (MCMC) analysis

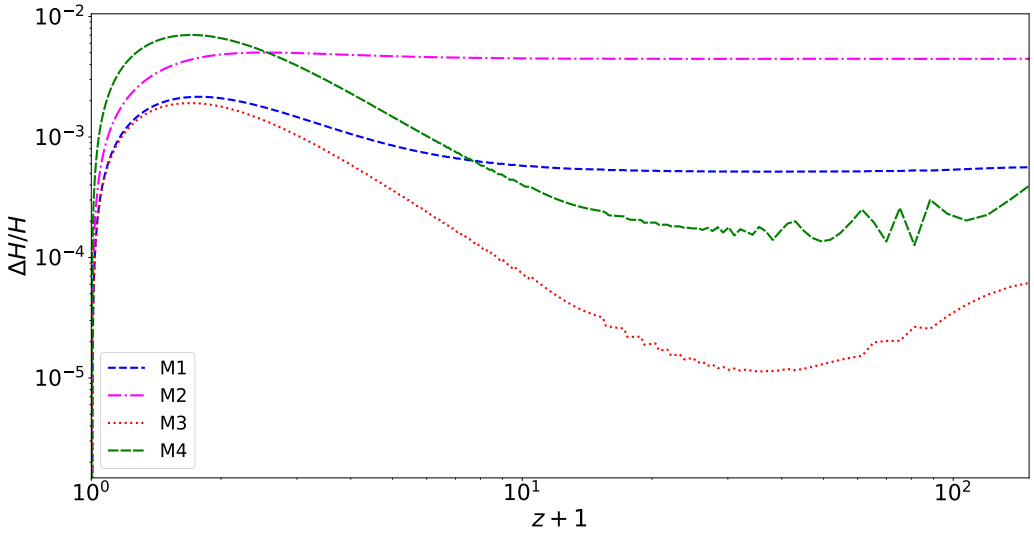

Figure 5.14: Evolution of the relative difference of the Hubble parameter H in the M models in relation to ΛCDM.

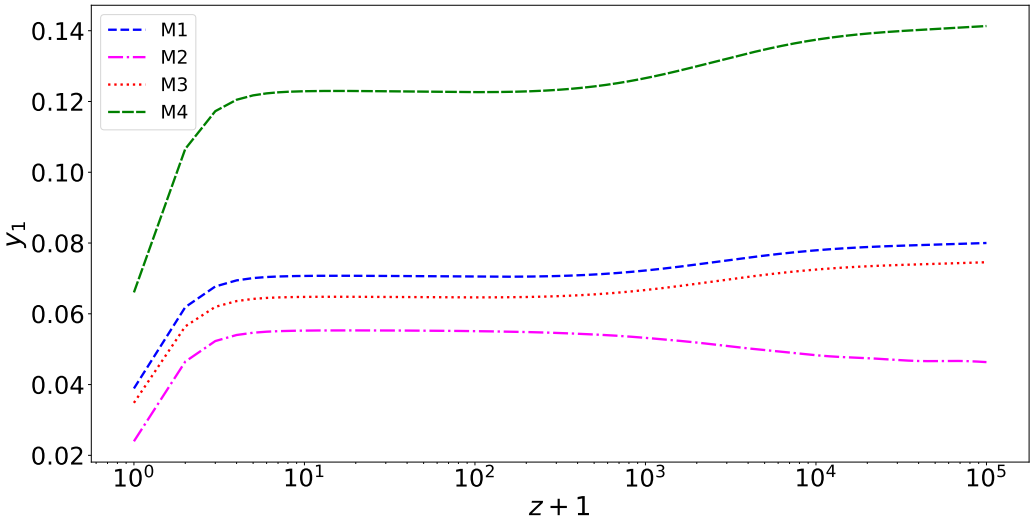

Figure 5.15: Evolution of the y_1 variable for the models M1 (dashed blue line), M2 (dot-dashed magenta line), M3 (dotted red line) and M4 (long dashed green line).

using a selection of data sets to constrain the model parameters. We leave this study for future work. Given the promising features of our model, specifically, the lower ISW tails and the suppressed matter power spectrum, we believe it can be of interest to be further investigated by the Euclid space mission [190, 191] of the European Space Agency (ESA).

Chapter 6

Final Remarks

In this dissertation we have investigated the background and perturbative phenomenology of the SCG model. The latter is a MG model belonging to the GG class in which the Galileon scalar field ϕ modifies the standard gravitational action. The model itself was first presented in [43] as the result of a collaboration with N. Frusciante, N. J. Nunes and S. Tsujikawa. In the present dissertation, we have reviewed the model's construction and background analysis which had been previously performed in [43], learning about its expansion history with the help of dynamical analysis tools. Following this, we used SPT, the EFT formalism and the `EFTCAMB` solver to study the evolution of perturbations in our model and discuss its impact on the cosmological observables.

The model was proposed as a viable framework for cosmic acceleration where new scaling solutions in cubic Horndeski theories could be obtained. We employed a cubic Horndeski coupling of the form $G_3 = g(Y)$, with $Y = Xe^{\lambda\phi}$, in addition to the standard scalar field kinetic term $G_2 = X - V(\phi)$ with two exponential potentials $V(\phi) = V_1 e^{-\beta_1\phi} + V_2 e^{-\beta_2\phi}$. Searching for scaling solutions as a way of alleviating the Coincidence Problem, we considered a yet unexplored form for the cubic coupling, specifically, $G_3 = A \ln Y$, and thus found a new type of scaling solutions.

We performed a dynamical analysis of the SCG model where we transformed the background equations into an autonomous system and determined the correspondent critical points. We found early scaling radiation and matter eras, followed by a late-time period of accelerated expansion. In this case, the first potential $V_1 e^{-\beta_1\phi}$ is responsible for the scaling radiation and matter critical points (see equations (5.53) and (5.54)), whereas the second potential $V_2 e^{-\beta_2\phi}$ gives rise to the scalar-field dominated point (equation (5.55)) which is the one responsible for cosmic acceleration.

The model is characterized by four free parameters: β_1, β_2, λ and A. In order to choose their values in such a way that they are consistent with the viability of our model, we applied a set of theoretical viability conditions. Additionally, we also verified that it is possible to find SCG models respecting the early-time BBN and CMB constraints on the scalar field density parameter Ω_ϕ. Moving forward, we selected four sets of parameters inside the determined viable region, which we designated as M models. Using these toy models, we numerically solved the background equations and plotted the corresponding expansion history, verifying the absence of the ghost and gradient instabilities during the complete model evolution and found that while G_3 can provide the dominant contribution to Ω_ϕ during the scaling eras, it tends to be suppressed at low redshifts. Furthermore, we also found that all M models show a present value of the scalar field equation of state parameter $w_\phi^{(0)}$ closer to -1 than that of Quintessence. Thus, in

this aspect the SCG model proves to be in better agreement with recent observational data.

Following this, we studied the evolution of perturbations in the SCG model and investigated its impact on the cosmological observables. For that purpose, we started by mapping the model into the EFT language, finding the corresponding forms of the EFT functions. Then, we implemented our model in the `EFTCAMB` solver using a full mapping approach. This entailed creating a new patch where we implemented a background solver as well as the forms of the EFT functions. Additionally, we added a new `FullMappingEFTModel` flag responsible for the selection of our model. We proceeded with a preliminary analysis of the perturbative behaviour done under the QSA and using the μ, η and Σ parametrization. This revealed the model parameter A as the one with most relevance in the introduction of modifications with respect to GR and ΛCDM. It also revealed an expected enhancement of both the growth of structure and the lensing potential, which can reach 8% at present time.

Finally, thanks to the modifications we implemented on `EFTCAMB` we were able to obtain the main cosmological observables, namely the matter, lensing and CMB TT power spectra, for the SCG model as well as ΛCDM, which we used as reference. The analysis of these observables, for which we used the same four toy models selected during the dynamical analysis, revealed several observational features that distinguish the SCG model from ΛCDM. In general, we found the behaviour of the majority of the toy models to be in accordance with our preliminary analysis, presenting enhancements of the gravitational potentials and the matter and lensing power spectra. Furthermore, the scale of the enhancements registered for each of the toy models confirmed the important impact of the A parameter on the modifications. In fact, the larger modifications with respect to ΛCDM, which can even reach 24% for the gravitational potential Ψ, 66% for the matter power spectra and 46% for the lensing power spectra, were verified for the case with the largest value of A. However, we also found that our model offers the possibility of having suppressed lensing and matter power spectra. This peculiar feature was attributed to a strong background effect which small values of A are incapable of compensating for as it happens on the other cases. Moreover, the noted lower amplitude of the matter power spectrum with respect to ΛCDM could prove a valuable advantage over the standard model. Indeed, it might show a better agreement with the results of Weak Lensing surveys which predict a lower amplitude (with respect to ΛCDM) for the matter power spectrum at the scale of $8h^{-1}$ Mpc. Lastly, regarding the CMB TT power spectra, we found that our model in general leads to a suppressed ISW tail and does not produce any significant peak shifting. Nevertheless, we did find that when the early-time modifications of gravity in our model are large enough, we can verify an alteration in the height of the CMB peaks.

In the future we aim to complete the study of the SCG model. To do so, our next step must be to fit it directly against cosmological data in order to constrain its parameter space. This means performing a MCMC analysis using cosmological data from CMB, BAO, Redshift-Space Distortions (RSD) and Type Ia Supernovae to determine the best fit values of the model parameters. For this purpose, we plan to use `EFTCosmoMC` [42], a public patch for the Cosmological Monte-Carlo (`CosmoMC`) engine [192] that allows the statistical study of DE/MG models using the EFT formalism. The phenomenological analysis and the results of the MCMC constraints will be collected in a paper and submitted to an high impact journal. After that, the new `EFTCAMB` patch will be publicly released on `http://eftcamb.org`. Our ultimate goal is to propose the SCG model to be included in the group of proposals that will be investigated by ESA's space mission Euclid [190, 191].

Bibliography

[1] A. Einstein. The Foundation of the General Theory of Relativity. *Annalen Phys.*, 49(7): 769–822, 1916. [Annalen Phys.354,no.7,769(1916)].

[2] B. P. Abbott et al. Observation of Gravitational Waves from a Binary Black Hole Merger. *Phys. Rev. Lett.*, 116(6):061102, 2016.

[3] T. M. C. Abbott et al. Dark Energy Survey year 1 results: Cosmological constraints from galaxy clustering and weak lensing. *Phys. Rev.*, D98(4):043526, 2018.

[4] K. Akiyama et al. First M87 Event Horizon Telescope Results. VI. The Shadow and Mass of the Central Black Hole. *Astrophys. J.*, 875(1):L6, 2019.

[5] A. G. Riess et al. Observational evidence from supernovae for an accelerating universe and a cosmological constant. *Astron. J.*, 116:1009–1038, 1998.

[6] S. Perlmutter et al. Measurements of Ω and Λ from 42 high redshift supernovae. *Astrophys. J.*, 517:565–586, 1999.

[7] F. Zwicky. Die Rotverschiebung von extragalaktischen Nebeln. *Helvetica Physica Acta*, 6: 110–127, 1933.

[8] I. Tkachev. Cosmology and Dark Matter. In *Proceedings, 2016 European School of High-Energy Physics (ESHEP2016): Skeikampen, Norway, June 15-28 2016*, volume 5, pages 259–294, 2017.

[9] M. Drees. Dark Matter Theory. *PoS*, ICHEP2018:730, 2019.

[10] V. C. Rubin, W. K. Ford, Jr., and N. Thonnard. Rotational properties of 21 SC galaxies with a large range of luminosities and radii, from NGC 4605 (R = 4kpc) to UGC 2885 (R = 122 kpc). *Astrophys. J.*, 238:471–487, June 1980.

[11] E. Battaner and E. Florido. The Rotation curve of spiral galaxies and its cosmological implications. *Fund. Cosmic Phys.*, 21:1–154, 2000.

[12] N. Aghanim et al. Planck 2018 results. VI. Cosmological parameters. 2018.

[13] R. Massey, T. Kitching, and J. Richard. The dark matter of gravitational lensing. *Rept. Prog. Phys.*, 73:086901, 2010.

[14] P. A. R. Ade et al. Planck 2015 results. XIII. Cosmological parameters. *Astron. Astrophys.*, 594:A13, 2016.

[15] S. Weinberg. The Cosmological constant problems. In *Sources and detection of dark matter and dark energy in the universe. Proceedings, 4th International Symposium, DM 2000, Marina del Rey, USA, February 23-25, 2000*, pages 18–26, 2000.

[16] M. Chevallier and D. Polarski. Accelerating universes with scaling dark matter. *Int. J. Mod. Phys.*, D10:213–224, 2001.

[17] E. V. Linder. Exploring the expansion history of the universe. *Phys. Rev. Lett.*, 90:091301, 2003.

[18] E. J. Copeland, M. Sami, and S. Tsujikawa. Dynamics of dark energy. *Int. J. Mod. Phys.*, D15:1753–1936, 2006.

[19] D. K. Hazra, S. Majumdar, S. Pal, S. Panda, and A. A. Sen. Post-Planck Dark Energy Constraints. *Phys. Rev.*, D91:083005, 2015.

[20] S. Tsujikawa. Modified gravity models of dark energy. *Lect. Notes Phys.*, 800:99–145, 2010.

[21] T. Clifton, P. G. Ferreira, A. Padilla, and C. Skordis. Modified Gravity and Cosmology. *Phys. Rept.*, 513:1–189, 2012.

[22] G. W. Horndeski. Second-order scalar-tensor field equations in a four-dimensional space. *Int. J. Theor. Phys.*, 10:363–384, 1974.

[23] A. Nicolis, R. Rattazzi, and E. Trincherini. The Galileon as a local modification of gravity. *Phys. Rev.*, D79:064036, 2009.

[24] T. P. Sotiriou and V. Faraoni. f(R) Theories Of Gravity. *Rev. Mod. Phys.*, 82:451–497, 2010.

[25] H. Kodama and M. Sasaki. Cosmological Perturbation Theory. *Prog. Theor. Phys. Suppl.*, 78:1–166, 1984.

[26] S. Carroll. *Spacetime and Geometry: An Introduction to General Relativity*. Pearson Education Limited, 2014.

[27] S. Weinberg. *Cosmology*. Oxford University Press, USA, oup edition, 2008.

[28] D. Baumann. Cosmology: Part III mathematical tripos. `http://theory.uchicago.edu/~liantaow/my-teaching/dark-matter-472/lectures.pdf`. Accessed: 31.08.2019.

[29] R. Bean and M. Tangmatitham. Current constraints on the cosmic growth history. *Phys. Rev.*, D81(8):083534, 2010.

[30] A. Silvestri, L. Pogosian, and R. V. Buniy. Practical approach to cosmological perturbations in modified gravity. *Phys. Rev.*, D87(10):104015, 2013.

[31] L. Pogosian, A. Silvestri, K. Koyama, and G.-B. Zhao. How to optimally parametrize deviations from general relativity in the evolution of cosmological perturbations. *Phys. Rev.*, D81(10):104023, May 2010.

[32] L. Pogosian and A. Silvestri. What can cosmology tell us about gravity? Constraining Horndeski gravity with Σ and μ. *Phys. Rev.*, D94(10):104014, 2016.

[33] T. Baker, P. G. Ferreira, and C. Skordis. The Parameterized Post-Friedmann framework for theories of modified gravity: concepts, formalism and examples. *Phys. Rev.*, D87(2): 024015, 2013.

[34] G. Gubitosi, F. Piazza, and F. Vernizzi. The Effective Field Theory of Dark Energy. *JCAP*, 1302:032, 2013. [JCAP1302,032(2013)].

[35] J. K. Bloomfield, E. E. Flanagan, M. Park, and S. Watson. Dark energy or modified gravity? An effective field theory approach. *JCAP*, 1308:010, 2013.

[36] N. Frusciante, G. Papadomanolakis, and A. Silvestri. An Extended action for the effective field theory of dark energy: a stability analysis and a complete guide to the mapping at the basis of EFTCAMB. *JCAP*, 1607(07):018, 2016.

[37] A. Lewis and A. Challinor. Code for anisotropies in the microwave background. `https://camb.info/`.

[38] J. Lesgourgues and T. Tram. Cosmic linear anisotropy solving system. `http://class-code.net/`.

[39] A. Lewis, A. Challinor, and A. Lasenby. Efficient computation of CMB anisotropies in closed FRW models. *Astrophys. J.*, 538:473–476, 2000.

[40] B. Hu, M. Raveri, N. Frusciante, and A. Silvestri. Effective Field Theory for CAMB. http://eftcamb.org/.

[41] B. Hu, M. Raveri, N. Frusciante, and A. Silvestri. Effective Field Theory of Cosmic Acceleration: an implementation in CAMB. *Phys. Rev.*, D89(10):103530, 2014.

[42] M. Raveri, B. Hu, N. Frusciante, and A. Silvestri. Effective Field Theory of Cosmic Acceleration: constraining dark energy with CMB data. *Phys. Rev.*, D90(4):043513, 2014.

[43] I. S. Albuquerque, N. Frusciante, N. J. Nunes, and S. Tsujikawa. New scaling solutions in cubic Horndeski theories. *Phys. Rev.*, D98(6):064038, 2018.

[44] C. Deffayet, S. Deser, and G. Esposito-Farese. Generalized Galileons: All scalar models whose curved background extensions maintain second-order field equations and stress-tensors. *Phys. Rev.*, D80:064015, 2009.

[45] C. Deffayet, X. Gao, D. A. Steer, and G. Zahariade. From k-essence to generalised Galileons. *Phys. Rev.*, D84:064039, 2011.

[46] P. Creminelli, A. Nicolis, and E. Trincherini. Galilean Genesis: An Alternative to inflation. *JCAP*, 1011:021, 2010.

[47] C. Burrage, C. de Rham, D. Seery, and A. J. Tolley. Galileon inflation. *JCAP*, 1101:014, 2011.

[48] T. Kobayashi, M. Yamaguchi, and J. Yokoyama. Generalized G-inflation: Inflation with the most general second-order field equations. *Prog. Theor. Phys.*, 126:511–529, 2011.

[49] F. P. Silva and K. Koyama. Self-Accelerating Universe in Galileon Cosmology. *Phys. Rev.*, D80:121301, 2009.

[50] T. Kobayashi, H. Tashiro, and D. Suzuki. Evolution of linear cosmological perturbations and its observational implications in Galileon-type modified gravity. *Phys. Rev.*, D81: 063513, 2010.

[51] T. Kobayashi. Cosmic expansion and growth histories in Galileon scalar-tensor models of dark energy. *Phys. Rev.*, D81:103533, 2010.

[52] A. De Felice and S. Tsujikawa. Cosmology of a covariant Galileon field. *Phys. Rev. Lett.*, 105:111301, 2010.

[53] R. Gannouji and M. Sami. Galileon gravity and its relevance to late time cosmic acceleration. *Phys. Rev.*, D82:024011, 2010.

[54] A. Ali, R. Gannouji, and M. Sami. Modified gravity a la Galileon: Late time cosmic acceleration and observational constraints. *Phys. Rev.*, D82:103015, 2010.

[55] D. F. Mota, M. Sandstad, and T. Zlosnik. Cosmology of the selfaccelerating third order Galileon. *JHEP*, 12:051, 2010.

[56] H. E. S. Velten, R. F. vom Marttens, and W. Zimdahl. Aspects of the cosmological "coincidence problem". *Eur. Phys. J.*, C74(11):3160, 2014.

[57] G. F. R. E. J. Wainwright. *Dynamical Systems in Cosmology.* Cambridge University Press, 2005.

[58] S. Bahamonde, C. G. Böhmer, S. Carloni, E. J. Copeland, W. Fang, and N. Tamanini. Dynamical systems applied to cosmology: dark energy and modified gravity. *Phys. Rept.*, 775-777:1–122, 2018.

[59] A. Einstein. On the electrodynamics of moving bodies. *Annalen Phys.*, 17:891–921, 1905. [Annalen Phys.14,194(2005)].

[60] C. M. Will. The Confrontation between General Relativity and Experiment. *Living Rev. Rel.*, 17:4, 2014.

[61] E. Asmodelle. Tests of General Relativity: A Review. Master's thesis, Central Lancashire U., 2017.

[62] F. W. Dyson, A. S. Eddington, and C. Davidson. A Determination of the Deflection of Light by the Sun's Gravitational Field, from Observations Made at the Total Eclipse of May 29, 1919. *Phil. Trans. Roy. Soc. Lond.*, A220:291–333, 1920.

[63] R. d'Inverno. *Introducing Einstein's Relativity.* Clarendon Press; Oxford University Press, 1992.

[64] C. W. Misner, K. S. Thorne, and J. A. Wheeler. *Gravitation*. San Francisco, W.H. Freeman, 1973.

[65] D. Lovelock. The Einstein tensor and its generalizations. *J. Math. Phys.*, 12:498–501, 1971.

[66] D. Lovelock. The Four-Dimensionality of Space and the Einstein Tensor. *Journal of Mathematical Physics*, 13:874–876, June 1972.

[67] A. Einstein. Cosmological Considerations in the General Theory of Relativity. *Sitzungsber. Preuss. Akad. Wiss. Berlin (Math. Phys.)*, 1917:142–152, 1917.

[68] A. S. Eddington. On the instability of Einstein's spherical world. *MNRAS*, 90:668–678, May 1930.

[69] E. Hubble. A relation between distance and radial velocity among extra-galactic nebulae. *Proc. Nat. Acad. Sci.*, 15:168–173, 1929.

[70] A. A. Penzias and R. W. Wilson. A Measurement of excess antenna temperature at 4080-Mc/s. *Astrophys. J.*, 142:419–421, 1965.

[71] A. Friedman. Über die krümmung des raumes. *Zeitschrift für Physik*, 10(1):377–386, Dec 1922.

[72] G. Lemaître. L'Univers en expansion. *Annales de la Société Scientifique de Bruxelles*, 53, 1933.

[73] A. G. Walker. On Milne's Theory of World-Structure. *Proceedings of the London Mathematical Society, (Series 2) volume 42, p. 90-127*, 42:90–127, 1937.

[74] S. Weinberg. The Cosmological Constant Problem. *Rev. Mod. Phys.*, 61:1–23, 1989.

[75] S. M. Carroll. The Cosmological constant. *Living Rev. Rel.*, 4:1, 2001.

[76] J. D. Barrow and D. J. Shaw. The Value of the Cosmological Constant. *Gen. Rel. Grav.*, 43:2555–2560, 2011. [Int. J. Mod. Phys.D20,2875(2011)].

[77] J. Martin. Everything You Always Wanted To Know About The Cosmological Constant Problem (But Were Afraid To Ask). *Comptes Rendus Physique*, 13:566–665, 2012.

[78] A. Padilla. Lectures on the Cosmological Constant Problem, 2015.

[79] S. E. Rugh and H. Zinkernagel. The Quantum vacuum and the cosmological constant problem. *Stud. Hist. Phil. Sci.*, B33:663–705, 2002.

[80] A. H. Guth. Inflationary universe: A possible solution to the horizon and flatness problems. *Phys. Rev. D*, 23:347–356, Jan. 1981.

[81] A. D. Linde. A New Inflationary Universe Scenario: A Possible Solution of the Horizon, Flatness, Homogeneity, Isotropy and Primordial Monopole Problems. *Phys. Lett.*, 108B: 389–393, 1982. [Adv. Ser. Astrophys. Cosmol.3,149(1987)].

[82] A. D. Linde. Particle physics and inflationary cosmology. *Contemp. Concepts Phys.*, 5: 1–362, 1990.

[83] A. H. Guth. Inflation and eternal inflation. *Phys. Rept.*, 333:555–574, 2000.

[84] A. Joyce, B. Jain, J. Khoury, and M. Trodden. Beyond the Cosmological Standard Model. *Phys. Rept.*, 568:1–98, 2015.

[85] T. Jacobson and D. Mattingly. Gravity with a dynamical preferred frame. *Phys. Rev.*, D64:024028, 2001.

[86] N. Arkani-Hamed, H. Georgi, and M. D. Schwartz. Effective field theory for massive gravitons and gravity in theory space. *Annals Phys.*, 305:96–118, 2003.

[87] S. Tsujikawa. Quintessence: A Review. *Class. Quant. Grav.*, 30:214003, 2013.

[88] C. Brans and R. H. Dicke. Mach's principle and a relativistic theory of gravitation. *Phys. Rev.*, 124:925–935, 1961. [,142(1961)].

[89] C. Deffayet, G. Esposito-Farese, and A. Vikman. Covariant Galileon. *Phys. Rev.*, D79: 084003, 2009.

[90] M. Ostrogradsky. Mémoires sur les équations différentielles, relatives au problème des isopérimètres. *Mem. Acad. St. Petersbourg*, 6(4):385–517, 1850.

[91] V. Faraoni. de Sitter space and the equivalence between f(R) and scalar-tensor gravity. *Phys. Rev.*, D75:067302, 2007.

[92] T. Kaluza. Zum Unitätsproblem der Physik. *Sitzungsber. Preuss. Akad. Wiss. Berlin (Math. Phys.)*, 1921:966–972, 1921. [Int. J. Mod. Phys.D27,no.14,1870001(2018)].

[93] G. R. Dvali, G. Gabadadze, and M. Porrati. 4-D gravity on a brane in 5-D Minkowski space. *Phys. Lett.*, B485:208–214, 2000.

[94] K. Hinterbichler, M. Trodden, and D. Wesley. Multi-field galileons and higher co-dimension branes. *Phys. Rev.*, D82:124018, 2010.

[95] H. Ruegg and M. Ruiz-Altaba. The Stueckelberg field. *Int. J. Mod. Phys.*, A19:3265–3348, 2004.

[96] A. Silvestri and M. Trodden. Approaches to Understanding Cosmic Acceleration. *Rept. Prog. Phys.*, 72:096901, 2009.

[97] S. Capozziello and M. De Laurentis. Extended Theories of Gravity. *Phys. Rept.*, 509: 167–321, 2011.

[98] P. Avelino et al. Unveiling the Dynamics of the Universe. *Symmetry*, 8(8):70, 2016.

[99] A. Joyce, L. Lombriser, and F. Schmidt. Dark Energy Versus Modified Gravity. *Ann. Rev. Nucl. Part. Sci.*, 66:95–122, 2016.

[100] P. G. Ferreira. Cosmological Tests of Gravity. 2019.

[101] T. Kobayashi. Horndeski theory and beyond: a review. *Rept. Prog. Phys.*, 82(8):086901, 2019.

[102] A. Lue, R. Scoccimarro, and G. D. Starkman. Probing Newton's constant on vast scales: DGP gravity, cosmic acceleration and large scale structure. *Phys. Rev.*, D69:124015, 2004.

[103] K. Koyama. Cosmological Tests of Modified Gravity. *Rept. Prog. Phys.*, 79(4):046902, 2016.

[104] J. Khoury and A. Weltman. Chameleon fields: Awaiting surprises for tests of gravity in space. *Phys. Rev. Lett.*, 93:171104, 2004.

[105] J. Khoury and A. Weltman. Chameleon cosmology. *Phys. Rev.*, D69:044026, 2004.

[106] P. Brax, C. van de Bruck, A.-C. Davis, J. Khoury, and A. Weltman. Detecting dark energy in orbit: The cosmological chameleon. *Phys. Rev.*, D70:123518, 2004.

[107] P. Brax, C. van de Bruck, A. C. Davis, J. Khoury, and A. Weltman. Chameleon dark energy. *AIP Conf. Proc.*, 736(1):105–110, 2004.

[108] K. Hinterbichler and J. Khoury. Symmetron Fields: Screening Long-Range Forces Through Local Symmetry Restoration. *Phys. Rev. Lett.*, 104:231301, 2010.

[109] K. A. Olive and M. Pospelov. Environmental dependence of masses and coupling constants. *Phys. Rev.*, D77:043524, 2008.

[110] E. Babichev, C. Deffayet, and R. Ziour. k-Mouflage gravity. *Int. J. Mod. Phys.*, D18: 2147–2154, 2009.

[111] A. I. Vainshtein. To the problem of nonvanishing gravitation mass. *Phys. Lett.*, 39B: 393–394, 1972.

[112] R. Kimura, T. Kobayashi, and K. Yamamoto. Vainshtein screening in a cosmological background in the most general second-order scalar-tensor theory. *Phys. Rev.*, D85:024023, 2012.

[113] Y.-S. Song, H. Peiris, and W. Hu. Cosmological Constraints on f(R) Acceleration Models. *Phys. Rev.*, D76:063517, 2007.

[114] Y.-S. Song, W. Hu, and I. Sawicki. The Large Scale Structure of f(R) Gravity. *Phys. Rev.*, D75:044004, 2007.

[115] T. Giannantonio, M. Martinelli, A. Silvestri, and A. Melchiorri. New constraints on parametrised modified gravity from correlations of the CMB with large scale structure. *Journal of Cosmology and Astroparticle Physics*, 2010(4):030, Apr 2010.

[116] G.-B. Zhao, T. Giannantonio, L. Pogosian, A. Silvestri, D. J. Bacon, K. Koyama, R. C. Nichol, and Y.-S. Song. Probing modifications of General Relativity using current cosmological observations. *Phys. Rev.*, D81:103510, 2010.

[117] E. Lifshitz. Republication of: On the gravitational stability of the expanding universe. *J. Phys.(USSR)*, 10:116, 1946. [Gen. Rel. Grav.49,no.2,18(2017)].

[118] J. M. Bardeen. Gauge Invariant Cosmological Perturbations. *Phys. Rev.*, D22:1882–1905, 1980.

[119] D. Baumann. Inflation. In *Physics of the large and the small, TASI 09, proceedings of the Theoretical Advanced Study Institute in Elementary Particle Physics, Boulder, Colorado, USA, 1-26 June 2009*, pages 523–686, 2011.

[120] S. Dodelson. *Modern Cosmology*. Academic Press, Amsterdam, 2003.

[121] J. Gleyzes, D. Langlois, M. Mancarella, and F. Vernizzi. Effective Theory of Interacting Dark Energy. *JCAP*, 1508(08):054, 2015.

[122] G. D'Amico, Z. Huang, M. Mancarella, and F. Vernizzi. Weakening Gravity on Redshift-Survey Scales with Kinetic Matter Mixing. *JCAP*, 1702:014, 2017.

[123] D. Traykova, E. Bellini, and P. G. Ferreira. The phenomenology of beyond Horndeski gravity. *JCAP*, 2019(08):035, 2019.

[124] G. F. Smoot et al. Structure in the COBE differential microwave radiometer first year maps. *Astrophys. J.*, 396:L1–L5, 1992.

[125] `https://map.gsfc.nasa.gov/`.

[126] `https://www.cosmos.esa.int/web/planck`.

[127] R. K. Sachs and A. M. Wolfe. Perturbations of a cosmological model and angular variations of the microwave background. *Astrophys. J.*, 147:73–90, 1967. [Gen. Rel. Grav.39,1929(2007)].

[128] P. A. R. Ade et al. Planck 2015 results. XIV. Dark energy and modified gravity. *Astron. Astrophys.*, 594:A14, 2016.

[129] M. Kunz, P.-S. Corasaniti, D. Parkinson, and E. J. Copeland. Model-independent dark energy test with sigma(8) using results from the Wilkinson microwave anisotropy probe. *Phys. Rev.*, D70:041301, 2004.

[130] M. Baldi and V. Pettorino. High-z massive clusters as a test for dynamical coupled dark energy. *Monthly Notices of the Royal Astronomical Society: Letters*, 412(1):L1–L5, Mar 2011.

[131] W. Hu and M. J. White. Acoustic signatures in the cosmic microwave background. *Astrophys. J.*, 471:30–51, 1996.

[132] C. L. Reichardt, R. de Putter, O. Zahn, and Z. Hou. New Limits on Early Dark Energy from the South Pole Telescope. *The Astrophysical Journal Letters*, 749(1):L9, Apr 2012.

[133] L. Amendola, V. Pettorino, C. Quercellini, and A. Vollmer. Testing coupled dark energy with next-generation large-scale observations. *Physical Review D*, 85(10):103008, May 2012.

[134] V. Acquaviva and C. Baccigalupi. Dark energy records in lensed cosmic microwave background. *Phys. Rev.*, D74:103510, 2006.

[135] C. Carbone, M. Baldi, V. Pettorino, and C. Baccigalupi. Maps of CMB lensing deflection from N-body simulations in Coupled Dark Energy Cosmologies. *JCAP*, 1309:004, 2013.

[136] S. Weinberg. Effective Field Theory for Inflation. *Phys. Rev.*, D77:123541, 2008.

[137] C. Cheung, P. Creminelli, A. L. Fitzpatrick, J. Kaplan, and L. Senatore. The Effective Field Theory of Inflation. *JHEP*, 03:014, 2008.

[138] N. Frusciante, S. Peirone, S. Casas, and N. A. Lima. Cosmology of surviving Horndeski theory: The road ahead. *Phys. Rev.*, D99(6):063538, 2019.

[139] S. Peirone, G. Benevento, N. Frusciante, and S. Tsujikawa. Cosmological constraints and phenomenology of a beyond-Horndeski model. *Phys. Rev.*, D100(6):063509, 2019.

[140] J. Lesgourgues. The Cosmic Linear Anisotropy Solving System (CLASS) I: Overview. *arXiv e-prints*, art. arXiv:1104.2932, Apr 2011.

[141] M. Zumalacárregui, E. Bellini, I. Sawicki, J. Lesgourgues, and P. G. Ferreira. `hi_class`: Horndeski in the Cosmic Linear Anisotropy Solving System. *JCAP*, 1708(08):019, 2017.

[142] Z. Huang. Observational effects of a running Planck mass. *Phys. Rev.*, D93(4):043538, 2016.

[143] F. Pace, R. A. Battye, B. Bolliet, and D. Trinh. Dark sector evolution in Horndeski models. 2019.

[144] J. Gleyzes, D. Langlois, F. Piazza, and F. Vernizzi. Exploring gravitational theories beyond Horndeski. *JCAP*, 1502:018, 2015.

[145] J. Gleyzes, D. Langlois, and F. Vernizzi. A unifying description of dark energy. *Int. J. Mod. Phys.*, D23(13):1443010, 2015.

[146] P. Horava. Membranes at Quantum Criticality. *JHEP*, 03:020, 2009.

[147] P. Horava. Quantum Gravity at a Lifshitz Point. *Phys. Rev.*, D79:084008, 2009.

[148] N. Frusciante and L. Perenon. Effective Field Theory of Dark Energy: a Review. 2019.

[149] B. Hu, M. Raveri, N. Frusciante, and A. Silvestri. EFTCAMB/EFTCosmoMC: Numerical Notes v3.0. 2014.

[150] R. L. Arnowitt, S. Deser, and C. W. Misner. Dynamical Structure and Definition of Energy in General Relativity. *Phys. Rev.*, 116:1322–1330, 1959.

[151] R. Kase and S. Tsujikawa. Effective field theory approach to modified gravity including Horndeski theory and Hořava–Lifshitz gravity. *Int. J. Mod. Phys.*, D23(13):1443008, 2015.

[152] E. Gourgoulhon. 3+1 formalism and bases of numerical relativity. 2007.

[153] F. Piazza, H. Steigerwald, and C. Marinoni. Phenomenology of dark energy: exploring the space of theories with future redshift surveys. *JCAP*, 1405:043, 2014.

[154] J. M. Cline, S. Jeon, and G. D. Moore. The Phantom menaced: Constraints on low-energy effective ghosts. *Phys. Rev.*, D70:043543, 2004.

[155] A. De Felice, N. Frusciante, and G. Papadomanolakis. On the stability conditions for theories of modified gravity in the presence of matter fields. *JCAP*, 1703(03):027, 2017.

[156] V. Salvatelli, F. Piazza, and C. Marinoni. Constraints on modified gravity from Planck 2015: when the health of your theory makes the difference. *JCAP*, 1609(09):027, 2016.

[157] S. Peirone, M. Martinelli, M. Raveri, and A. Silvestri. Impact of theoretical priors in cosmological analyses: the case of single field quintessence. *Phys. Rev.*, D96(6):063524, 2017.

[158] N. Frusciante, M. Raveri, D. Vernieri, B. Hu, and A. Silvestri. Hořava Gravity in the Effective Field Theory formalism: From cosmology to observational constraints. *Phys. Dark Univ.*, 13:7–24, 2016.

[159] E. Bellini and I. Sawicki. Maximal freedom at minimum cost: linear large-scale structure in general modifications of gravity. *JCAP*, 1407:050, 2014.

[160] P. Creminelli and F. Vernizzi. Dark Energy after GW170817 and GRB170817A. *Phys. Rev. Lett.*, 119(25):251302, 2017.

[161] D. Langlois, M. Mancarella, K. Noui, and F. Vernizzi. Effective Description of Higher-Order Scalar-Tensor Theories. *JCAP*, 1705(05):033, 2017.

[162] G. Cusin, M. Lewandowski, and F. Vernizzi. Nonlinear Effective Theory of Dark Energy. *JCAP*, 1804(04):061, 2018.

[163] E. J. Copeland, A. R. Liddle, and D. Wands. Exponential potentials and cosmological scaling solutions. *Phys. Rev.*, D57:4686–4690, 1998.

[164] P. G. Ferreira and M. Joyce. Cosmology with a primordial scaling field. *Phys. Rev.*, D58: 023503, 1998.

[165] A. R. Liddle and R. J. Scherrer. A Classification of scalar field potentials with cosmological scaling solutions. *Phys. Rev.*, D59:023509, 1999.

[166] Z.-K. Guo, Y.-S. Piao, R.-G. Cai, and Y.-Z. Zhang. Cosmological scaling solutions and cross coupling exponential potential. *Phys. Lett.*, B576:12–17, 2003.

[167] S. Tsujikawa and M. Sami. A Unified approach to scaling solutions in a general cosmological background. *Phys. Lett.*, B603:113–123, 2004.

[168] Z. K. Guo, Y.-S. Piao, and Y.-Z. Zhang. Cosmological scaling solutions and multiple exponential potentials. *Phys. Lett.*, B568:1–7, 2003.

[169] L. Amendola, M. Quartin, S. Tsujikawa, and I. Waga. Challenges for scaling cosmologies. *Phys. Rev.*, D74:023525, 2006.

[170] A. R. Gomes and L. Amendola. Towards scaling cosmological solutions with full coupled Horndeski Lagrangian: the KGB model. *JCAP*, 1403:041, 2014.

[171] V. Pettorino, C. Baccigalupi, and F. Perrotta. Scaling solutions in scalar-tensor cosmologies. *JCAP*, 0512:003, 2005.

[172] J. Ohashi and S. Tsujikawa. Assisted dark energy. *Phys. Rev.*, D80:103513, 2009.

[173] T. Chiba, A. De Felice, and S. Tsujikawa. Cosmological Scaling Solutions for Multiple Scalar Fields. *Phys. Rev.*, D90(2):023516, 2014.

[174] T. Barreiro, E. J. Copeland, and N. J. Nunes. Quintessence arising from exponential potentials. *Phys. Rev.*, D61:127301, 2000.

[175] L. Amendola, T. Barreiro, and N. J. Nunes. Multifield coupled quintessence. *Phys. Rev.*, D90(8):083508, 2014.

[176] F. Piazza and S. Tsujikawa. Dilatonic ghost condensate as dark energy. *JCAP*, 0407:004, 2004.

[177] B. P. Abbott et al. GW170817: Observation of Gravitational Waves from a Binary Neutron Star Inspiral. *Phys. Rev. Lett.*, 119(16):161101, 2017.

[178] B. P. Abbott et al. Gravitational Waves and Gamma-rays from a Binary Neutron Star Merger: GW170817 and GRB 170817A. *Astrophys. J.*, 848(2):L13, 2017.

[179] A. De Felice and S. Tsujikawa. Conditions for the cosmological viability of the most general scalar-tensor theories and their applications to extended Galileon dark energy models. *JCAP*, 1202:007, 2012.

[180] R. Bean, S. H. Hansen, and A. Melchiorri. Early universe constraints on a primordial scaling field. *Phys. Rev.*, D64:103508, 2001.

[181] M. A. Troxel et al. Dark Energy Survey Year 1 results: Cosmological constraints from cosmic shear. *Phys. Rev.*, D98(4):043528, 2018.

[182] J. M. Alimi, A. Füzfa, V. Boucher, Y. Rasera, J. Courtin, and P. S. Corasaniti. Imprints of dark energy on cosmic structure formation - I. Realistic quintessence models and the non-linear matter power spectrum. *Monthly Notices of the Royal Astronomical Society*, 401(2):775–790, Jan 2010.

[183] J. T. A. de Jong et al. The first and second data releases of the Kilo-Degree Survey. *Astron. Astrophys.*, 582:A62, 2015.

[184] H. Hildebrandt et al. KiDS-450: Cosmological parameter constraints from tomographic weak gravitational lensing. *Mon. Not. Roy. Astron. Soc.*, 465:1454, 2017.

[185] K. Kuijken et al. Gravitational Lensing Analysis of the Kilo Degree Survey. *Mon. Not. Roy. Astron. Soc.*, 454(4):3500–3532, 2015.

[186] I. Fenech Conti, R. Herbonnet, H. Hoekstra, J. Merten, L. Miller, and M. Viola. Calibration of weak-lensing shear in the Kilo-Degree Survey. *Mon. Not. Roy. Astron. Soc.*, 467 (2):1627–1651, 2017.

[187] S. Joudaki et al. KiDS+VIKING-450 and DES-Y1 combined: Cosmology with cosmic shear. 2019.

[188] M.-X. Lin, M. Raveri, and W. Hu. Phenomenology of Modified Gravity at Recombination. *Phys. Rev.*, D99(4):043514, 2019.

[189] G. Benevento, M. Raveri, A. Lazanu, N. Bartolo, M. Liguori, P. Brax, and P. Valageas. K-mouflage Imprints on Cosmological Observables and Data Constraints. *JCAP*, 1905 (05):027, 2019.

[190] `https://www.cosmos.esa.int/web/euclid`, .

[191] `https://www.euclid-ec.org`, .

[192] A. Lewis and S. Bridle. Cosmological parameters from CMB and other data: A Monte Carlo approach. *Phys. Rev.*, D66:103511, 2002.

Appendix A

Dynamical Analysis: Eigenvalues of the Critical Points

The stability of the critical points (x_c, y_c) presented in Table 5.1 can be determined by considering homogeneous perturbations $(\delta x, \delta y)$ around them, such that

$$x = x_c + \delta x, \qquad y = y_c + \delta y. \tag{A.1}$$

If we substitute these expressions into equations (5.12) and (5.13), the perturbations will, at linear order, obey the following differential equation:

$$\frac{d}{dN}\begin{pmatrix}\delta x\\ \delta y\end{pmatrix} = \mathcal{M}\begin{pmatrix}\delta x\\ \delta y\end{pmatrix}, \tag{A.2}$$

where the Jacobian matrix $\mathcal{M}$ is given by

$$\mathcal{M} = \begin{pmatrix}\frac{\partial x'}{\partial x} & \frac{\partial x'}{\partial y}\\ \frac{\partial y'}{\partial x} & \frac{\partial y'}{\partial y}\end{pmatrix}_{(x=x_c, y=y_c)}. \tag{A.3}$$

The general solutions to δx and δy can then be expressed as linear combinations of two terms: $e^{\mu_1 N}$ and $e^{\mu_2 N}$, where μ_1 and μ_2 are the eigenvalues of $\mathcal{M}$. As we briefly explain in Section 5.2, it is the signs of the real parts of μ_1 and μ_2 that determine the stability of a given critical point. For two negative real parts of the eigenvalues we have a stable point, for two positive ones the point is said unstable and for eigenvalues with real parts of opposite signs we have a saddle point.

For the critical points presented in Table 5.1, we obtain the following eigenvalues:

- Point (a):

$$\mu_{\frac{1}{2}} = \frac{3}{4}(\gamma - 2)\left[1 \pm \sqrt{1 - \frac{8(1-\Omega_\phi)[\gamma + 2A(\beta - \gamma\lambda)]}{(2-\gamma)[1 + 2A(3A - \lambda)]}}\right], \tag{A.4}$$

  where Ω_ϕ is given by equation (5.30).

- Point (b):

$$\mu_1 = -3\gamma + \frac{\beta(\beta - 6A)}{1 + A(\beta - 2\lambda)}, \tag{A.5}$$

$$\mu_2 = \frac{\beta^2 - 6 + 12A(\lambda - \beta)}{2[1 + A(\beta - 2\lambda)]}. \tag{A.6}$$

- Point (c):

$$\mu_1 = -\frac{3}{2}(2 - \gamma), \tag{A.7}$$

$$\mu_2 = \frac{3\gamma}{2} + \frac{3A\beta}{1 - 2A\lambda}. \tag{A.8}$$

- Points (d1) and (d2):

$$\mu_1 = 3(2 - \gamma), \tag{A.9}$$

$$\mu_2 = \frac{6 + 6A(\beta - 2\lambda) \mp \sqrt{6}\beta\sqrt{1 + 2A(3A - \lambda)}}{2(1 - 2A\lambda)}, \tag{A.10}$$

  where the $(-)$ and $(+)$ signs of μ_2 correspond to critical points (d1) and (d2), respectively.

Appendix B

Implementation in EFTCAMB: Background Equations

One of the advantages of working with EFTCAMB to study a specific model is that one does not need to go through the lengthy and complicated process of deriving and then implementing the specific perturbation equations for that model. Instead, one just needs to find its mapping into the EFT formalism and implement the latter, together with the background evolution, into the solver. The code will then proceed by using the general perturbation equations derived for the EFT action which are already implemented.

As we discussed in Section 5.3.2, the implementation of a background solver for the SCG model consists in implementing the autonomous system (5.49)-(5.50) together with the expressions for the Hubble parameter, its derivatives and the expressions of the EFT functions. Any other necessary auxiliary quantities must also be provided for the code to run. In this case, this implies the following functions:

$$\tilde{f}(x,y_1,y_2) \equiv \frac{\ddot{\phi}}{H^2} = \Bigg\{ -3\sqrt{6}x + 3\left(\beta_1 y_1^2 + \beta_2 y_2^2\right) - 6A\Bigg[3 - 3x^2 - \sqrt{6}\lambda x - \frac{3}{2}\Omega_m - 2\Omega_r + 3xA\left(2\lambda x - \sqrt{6}\right)\Bigg]\Bigg\} \Bigg/ \Big[1 + 2A\left(3A - \lambda\right)\Big] \tag{B.1}$$

and

$$\tilde{h}(x,y_1,y_2) \equiv \frac{\dot{H}}{H^2} = A\tilde{f}(x,y_1,y_2) - 2\Omega_r - \frac{3}{2}\Omega_m + 3xA\left(2\lambda x - \sqrt{6}\right) - 3x^2. \tag{B.2}$$

Both $\tilde{f}$ and $\tilde{h}$ can be further simplified by removing their dependence on Ω_m. To do this, we use constraint equation (5.47) to re-write Ω_m in terms of x, y_i and Ω_r and leave $\tilde{f}$ and $\tilde{h}$ also completely written in terms of the latter variables.

Besides the background system, we must also provide the code with the expressions of the EFT functions in our model. These shall be used together with the expansion history to evolve the already implemented perturbation equations of EFTCAMB. However, these equations not only depend on the EFT functions but also on some of their derivatives which, consequently, we must provide. Here we present the explicit expressions for the necessary EFT functions' derivatives

in the case of the SCG model:

$$\frac{\dot{c}a^2}{m_0^2} = -\mathcal{H}^3\Bigg[2\sqrt{6}A\tilde{h}^2x + \tilde{h}\left(-6\sqrt{6}Ax + 6\left(2A\lambda-1\right)x^2 + 3\sqrt{6}Ax'\right) + \sqrt{6}A\left(-3x' + x''\right) + x\left(\sqrt{6}A\tilde{h}' + 6\left(2A\lambda-1\right)x'\right)\Bigg], \tag{B.3}$$

$$\frac{\dot{\Lambda}a^2}{m_0^2} = -2\mathcal{H}^3\Bigg[2\sqrt{6}A\tilde{h}^2x + 3\tilde{h}\left(\left(2A\lambda-1\right)x^2 + y_1^2 + y_2^2 + \sqrt{6}Ax'\right) + 3y_1y_1' + 3y_2y_2' + x\left(\sqrt{6}A\tilde{h}' + 3\left(2A\lambda-1\right)x'\right) + \sqrt{6}Ax''\Bigg], \tag{B.4}$$

$$\frac{d\gamma_1}{da} = \frac{\sqrt{3/2}A\mathcal{H}^2\left(2\tilde{h}^2x + x\tilde{h}' - 3x' + \tilde{h}\left(-6x + 3x'\right) + x''\right)}{a^3H_0^2}, \tag{B.5}$$

$$\frac{d\gamma_2}{da} = \frac{-2\sqrt{6}A\mathcal{H}\left(\tilde{h}x + x'\right)}{a^2H_0}. \tag{B.6}$$

Because the above expressions include $\tilde{f}'$, $\tilde{h}'$ and x'' we also implement their expressions in `EFTCAMB`. These are given by:

$$x'' = \frac{1}{\sqrt{6}}\tilde{f}' - \tilde{h}'x - \tilde{h}x', \tag{B.7}$$

with

$$\tilde{h}' = \Bigg[\frac{1}{2}\Omega_r'\left(2A\lambda-1\right) + 3\Bigg(\left(2A\lambda-1\right)\left(\sqrt{6}A + x - 2A\lambda x\right)x' + \left(1-2A\lambda+2A\beta_1\right)y_1y_1' + \left(1-2A\lambda+2A\beta_2\right)y_2y_2'\Bigg)\Bigg] \Bigg/ \left(1+6A^2-2A\lambda\right) \tag{B.8}$$

and finally

$$\tilde{f}' = \Bigg[-3\Bigg(-A\Omega_r' + \left(2A\lambda-1\right)\left(6Ax - \sqrt{6}\right)x' + 2\left(3A-\beta_1\right)y_1y_1' + 2\left(3A-\beta_2\right)y_2y_2'\Bigg)\Bigg] \Bigg/ \left(1+6A^2-2A\lambda\right). \tag{B.9}$$

Finally, we note that the code is capable of computing numerical derivatives. However, we chose to include the numerical expressions of the necessary derivatives because it helps to speed up the code and reduce numerical errors.